Mon. Not. R. Astron. Soc. **355,** 553–584 (2004) doi:10.1111/j.1365-2966.2004.08340.x

Long-term monitoring of 6.7-GHz methanol masers

S. Goedhart,[1,2]★ M. J. Gaylard[1] and D. J. van der Walt[2]

[1]*Hartebeesthoek Radio Astronomy Observatory, PO Box 443, Krugersdorp, 1740, South Africa*
[2]*Space Research Unit, Physics Department, NorthWest University, Private Bag X6001, Potchefstroom, 2520, South Africa*

Accepted 2004 August 19. Received 2004 August 13; in original form 2004 April 22

ABSTRACT

A sample of 54 6.7-GHz methanol masers was monitored using the Hartebeesthoek 26-m telescope during the period 1999 January – 2003 March. The observations were taken at 1–2 week intervals, with daily observations when possible if a source was seen to be varying rapidly. It was found that the majority of the sources display a significant level of variability. The time-range of variations range from a few days up to several years. The types of behaviour observed included non-varying, monotonic increases or decreases, as well as aperiodic, quasi-periodic and periodic variations. Seven sources show clear evidence of periodicity, with periods ranging from 132 d up to 520 d.

Key words: masers – stars: formation – ISM: clouds – H II regions – radio lines: ISM.

1 INTRODUCTION

High-mass stars in their early evolutionary phases are deeply embedded in their natal molecular cloud, making it impossible to observe them directly at optical wavelengths. Class II methanol masers appear to be closely associated with newly formed massive stars (Menten 2002; Minier et al. 2003, and references therein) and are potentially powerful tools for studying conditions in these regions. At present, the exact location of these masers relative to the (proto)star is unknown. High-resolution imaging has shown that some sources have maser spots in linear or arc-like structures with velocity gradients characteristic of Keplerian rotation (Norris et al. 1998), implying that these masers may be in circumstellar discs, but there are many sources which do not have such structure (Walsh et al. 1998). It was speculated that some sources may be associated with outflows or expanding H II regions (Minier et al. 2002).

A number of methanol masers have been found to be variable at 6.7 GHz (Caswell, Vaile & Ellingsen 1995; MacLeod & Gaylard 1996) and 12.2 GHz (Moscadelli & Catarzi 1996; MacLeod & Gaylard 1993). The variability of the masers can be used to examine changing conditions in the star formation region. The study by Caswell et al. (1995) followed the variability of a small sample of masers for a short time, with intervals between observations of the order of three months. However, observations of G351.78–0.54 show rapid variations on a time-scale of weeks when the maser is in an active phase (MacLeod & Gaylard 1996). On the other hand, other masers appear to be non-varying over the same time-scales. Regular monitoring of a large sample of methanol masers will be able to quantify the nature of the variability and the time-scales over which it occurs. The range of behaviour we might expect to find in well-sampled time-series of sufficient duration are: non-varying; monotonic increase or decrease; and fluctuations which may be aperiodic, quasi-periodic or periodic. No results of a multi-year monitoring programme on a large sample of class II methanol masers have been published to date.

It is relevant to widen the scope to consider other maser species in star-forming regions. Little long-term monitoring of ground state hydroxyl masers has been reported for many years; for example Sullivan & Kerstholt (1976) monitored 11 sources at typically 10 epochs over five years. Most the maser peaks showed slow secular changes in amplitude, while one, the $+0.6$ km s^{-1} feature in W75S, was noted to show 'semi-periodicity', but the light curve is very undersampled. Similarly, Lekht (1974) showed that there were long-term changes in NGC6334 A and B and W75S with six or seven measurements over 6 yr. Weaver, Dieter & Williams (1968) found that several maser peaks in NGC6334 varied over a two month period in 1965, but with no discernable periodicity. Excited state hydroxyl masers were monitored at 4.765 GHz by Smits (1997), Smits, Cohen & Hutawarakorn (1998) and Smits (2003). These revealed non-varying and aperiodic variable masers.

Water masers at 22 GHz in star-forming regions have been subject to a number of monitoring programmes, which revealed a high level of variability and large amplitude flaring. Most recently, Brand et al. (2003) analysed 14 star-forming regions monitored once every 2–3 months for up to 13 yr. They describe 'a periodic long-term variation in several sources. This may be a consequence of periodic variations in the wind/jets from the exciting YSO (young stellar object).' This is based on data covering two cycles in Sh2-269 and Sh2-184, with a repeat time of about 2000 d. Lekht & Krasnov (2000) find an 11.5-yr period in the masers in W75N, based on 20 yr of data, which also corresponds to about two cycles. White & MacDonald (1979) monitored 14 sources for 2.5 yr; no periodic variations were reported. Trinidad et al. (2003), monitoring 11 sources, found no periodic variations over 8 months.

★E-mail: sharmila@hartrao.ac.za

Long term monitoring data can ultimately be used to test maser models and to probe the maser environment. Variations in maser flux density could be as a result of turbulent motions in the cloud with subsequent changes in maser path length, the passage of shocks, changes in the intrinsic brightness of the star or the radiation reaching the masing region, or partial quenching of the maser region. Some of the variations may be extrinsic to the maser source, e.g. interstellar scintillation. Drifts in the maser velocity would give an indication of motion in the masers, as seen for water masers entrained in outflows (Liljeström et al. 1989; Brand et al. 2003). Thus the sensitivity of methanol masers to changes in their environment make them a sensitive probe of changing conditions at small angular scales.

A programme to monitor the variability of a large sample of 6.7-GHz methanol masers was started in 1999 January. The details of the observing and calibrations are given in Section 2. The source selection process is noted in Section 3. Section 4 discusses the quantification of variability and illustrates and describes the behaviour of each source. The results are summarized in Section 5.

2 OBSERVATIONS

The monitoring programme used the 26-m telescope at HartRAO. All observations were made using left circular polarization. The sources were observed at intervals of 1–2 weeks, with observations at 2–3 d intervals when a source was seen to be varying rapidly. The observing parameters are summarized in Table 1. Two different bandwidths were used. The 0.32-MHz bandwidth spectra provide the better velocity resolution, but have half the velocity range obtained with 0.64-MHz bandwidth spectroscopy, which had to be used for some sources.

Pointing corrections were calculated by taking observations offset by half a beamwidth to the north, south, east and west of the source position. These observations were done on the stronger sources in the sample and applied to nearby weaker sources. The pointing corrections at 6.7 GHz are on average less than 5 per cent, therefore it is not a dominant factor in the calibrations.

Since 2000 April the telescope surface, comprising perforated aluminium panels, has been progressively replaced with new high-accuracy solid panels. The point source sensitivity (PSS) of the telescope was regularly measured by observing 3C123, 3C218 and 3C274. Prior to the upgrade the PSS was found to be 15.7 Jy K^{-1} at 6.7 GHz, based on the Ott et al. (1994) flux scale. During the upgrade period regular calibrations were made using precision Dicke radiometry at 4.9 and 8.6 GHz. Changes relative to the pre-upgrade values for the PSS at 6.7 GHz were obtained by interpolating the PSS measured at these two wavelengths. The corrections obtained are believed to be accurate to 5 per cent or better.

The validity of the corrections was tested by applying them to a number of maser features in different sources in the monitoring sample that appeared to be non-varying. The strongest peaks in the

Table 1. Observing parameters for sources with large and small velocity ranges.

Rest frequency (MHz)	6668.518	
System temperature (K)	50	
Half Power Beamwidth (°)	0.133	
Number of spectral channels	256	
Correlator bandwidth (MHz)	0.64	0.32
Velocity range (km s^{-1})	28	14
Correlator resolution (km s^{-1})	0.112	0.056

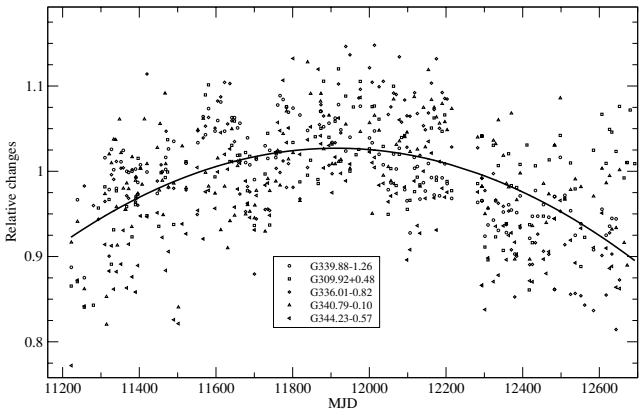

Figure 1. Normalized time-series for maser features showing strongly correlated variations. The solid line shows a third-order polynomial fit to the data.

sources G339.88–1.26, G309.92+0.48, G336.01–0.82, G340.79–0.10 and G344.23–0.57 appeared to show very little variation but did show common behaviour at the 5 per cent level in their time-series (Fig. 1). This can be characterized by a slow third-order variation probably caused by uncalibrated system changes. An additional gain correction based upon a least-squares fit to these time-series was applied to the data. The large sample size as well as the presence of independently varying features towards the same source provided an effective means of cross-checking the amplitude calibration.

3 SOURCE SELECTION

The initial source list mainly consisted of those identified as variable by Caswell et al. (1995) or van der Walt et al. (1996). G351.78–0.54 had been monitored on a regular basis from 1993 to 1995 by MacLeod & Gaylard (1996) and was found to be highly variable on time-scales of a few months. Other sources were selected because comparison of the fluxes reported by Caswell et al. (1995) and those reported by Menten (1991) showed that the peak fluxes had changed. Sources reported to be variable at 12.2 GHz (Moscadelli & Catarzi 1996) were also selected. Some sources were dropped after the initial test observations because they were too weak or because of confusion with a neighbouring source. The final source list is given in Table 2.

4 OVERVIEW OF RESULTS

Seven sources, viz. G188.95+0.89, 196.45–1.68, G328.237–0.548, G331.13–0.24, G338.92–0.06, G339.62–0.12 and G9.62+0.20, show strong evidence of periodicity. Rigorous analysis of the periodicity is beyond the scope of this paper and will be presented in Goedhart, Gaylard & van der Walt (in preparation). The following sections describe the variability seen in the entire source sample.

4.1 Variability index

Each maser spectrum consists of a number of peaks, corresponding to emission from maser spots at different velocities. Channels with no maser emission show the maxima and minima of the noise in the spectra. Velocity channels at the maximum of each peak were selected for the following analysis. Because the relation of the spatial structure of the maser to the velocity structure is not known in many cases, it was decided not to average the channels in each peak (to

Table 2. Sources monitored at 6.7 GHz. The $V_{\rm lsr}$ (velocity relative to the local standard of rest) on which the receiver band was centred is given, plus the number of observations of each source.

Source	RA (B1950) ($^{\rm h}$ $^{\rm m}$ $^{\rm s}$)	Dec (B1950) ($^\circ$ $'$ $''$)	$V_{\rm lsr}$ (km s^{-1})	Num. Obs.
G174.20–0.08	05 : 27 : 32.4	33 : 45 : 52.0	2.5	205
G213.71–12.60	06 : 05 : 21.7	−06 : 22 : 28.0	11.0	372
G189.03+0.79	06 : 05 : 40.9	21 : 31 : 37.6	11.0	152
G188.95+0.89	06 : 05 : 53.5	21 : 39 : 02.0	10.0	386
G192.60–0.05	06 : 09 : 59.1	18 : 00 : 10.0	3.5	181
G196.45–1.68	06 : 11 : 47.1	13 : 50 : 34.0	14.0	198
G287.36+0.64	10 : 46 : 03.4	−58 : 10 : 58.0	−2.0	193
G291.27–0.71	11 : 09 : 44.7	−61 : 02 : 17.2	−26.9	166
G294.52–1.62	11 : 33 : 15.0	−62 : 58 : 13.0	−11.5	172
G298.26+0.74	12 : 09 : 08.4	−61 : 29 : 37.5	−30.0	161
G305.21+0.21	13 : 08 : 01.7	−62 : 18 : 45.3	−38.0	171
G308.92+0.12	13 : 39 : 37.0	−61 : 53 : 44.0	−54.0	177
G309.92+0.48	13 : 47 : 11.9	−61 : 20 : 18.8	−59.0	126
G312.11+0.26	14 : 05 : 02.2	−60 : 58 : 48.0	−50.0	179
G316.64–0.09	14 : 40 : 31.6	−59 : 42 : 40.0	−19.5	131
G318.95–0.20	14 : 57 : 03.8	−58 : 47 : 01.2	−35.0	176
G320.23–0.29	15 : 06 : 00.5	−58 : 14 : 14.0	−64.5	122
G322.16+0.64	15 : 14 : 45.7	−56 : 27 : 28.0	−58.5	133
G323.77–0.21	15 : 27 : 49.8	−56 : 20 : 15.0	−50.5	178
G328.81+0.63	15 : 52 : 00.3	−52 : 34 : 22.2	−44.5	168
G328.24–0.55	15 : 54 : 06.1	−53 : 50 : 47.0	−39.0	136
G331.13–0.24	16 : 07 : 10.8	−51 : 42 : 29.0	−86.5	136
G331.28–0.19	16 : 07 : 37.9	−51 : 34 : 12.2	−82.5	171
G335.55–0.31	16 : 27 : 11.3	−48 : 39 : 28.0	−114.5	121
G336.01–0.82	16 : 31 : 21.8	−48 : 40 : 51.0	−47.0	131
G336.99–0.03	16 : 31 : 51.9	−47 : 25 : 03.0	−121.5	126
G337.92–0.46	16 : 37 : 25.0	−47 : 01 : 21.0	−38.5	166
G338.93–0.06	16 : 39 : 36.5	−46 : 00 : 05.0	−43.0	182
G339.62–0.12	16 : 42 : 26.5	−45 : 31 : 18.0	−34.5	134
G339.88–1.26	16 : 48 : 24.8	−46 : 03 : 33.9	−36.0	127
G340.79–0.10	16 : 46 : 38.4	−44 : 37 : 18.5	−100.0	148
G344.23–0.57	17 : 00 : 35.0	−42 : 14 : 29.0	−24.5	130
G345.00–0.22	17 : 01 : 38.5	−41 : 24 : 59.0	−26.0	129
G345.50+0.35	17 : 00 : 54.2	−40 : 40 : 18.0	−17.0	162
G351.42+0.64	17 : 17 : 32.3	−35 : 44 : 04.0	−7.0	135
G351.58–0.35	17 : 22 : 03.2	−36 : 10 : 09.0	−93.5	143
G351.78–0.54	17 : 23 : 20.7	−36 : 06 : 45.4	1.5	217
G354.61+0.47	17 : 26 : 59.8	−33 : 11 : 34.0	−20.0	135
G359.61–0.24	17 : 42 : 27.2	−29 : 22 : 18.0	20.5	126
G9.62+0.20	18 : 03 : 15.9	−20 : 31 : 52.9	2.5	278
G10.33–0.17	18 : 06 : 06.7	−20 : 05 : 34.0	10.5	152
G10.47+0.03	18 : 05 : 40.5	−19 : 52 : 23.0	69.0	116
G12.89+0.49	18 : 08 : 56.4	−17 : 32 : 14.0	35.0	170
G12.68–0.18	18 : 10 : 59.3	−18 : 02 : 40.0	55.5	130
G12.91–0.26	18 : 11 : 44.2	−17 : 52 : 58.0	38.0	168
G23.01–0.41	18 : 31 : 56.7	−09 : 03 : 18.0	77.0	115
G23.44–0.18	18 : 31 : 55.3	−08 : 34 : 01.0	103.5	116
G35.20–1.74	18 : 59 : 13.1	01 : 09 : 07.0	43.0	113
G45.07+0.13	19 : 11 : 00.5	10 : 45 : 41.0	58.5	171
G52.67–1.09	19 : 30 : 20.2	16 : 51 : 04.0	66.0	139
G59.78+0.06	19 : 41 : 03.6	23 : 36 : 51.0	25.0	121
G78.12+3.63	20 : 12 : 40.0	41 : 04 : 20.0	−6.0	80
G81.88+0.78	20 : 36 : 50.4	42 : 27 : 23.0	6.5	124

reduce the noise) in order to minimize the chance of combining data from multiple maser spots.

While it is easy to judge the degree of variability of a source by eye, a more objective method is needed to deal with a large number of sources. The following formula for a variability index I is an adaptation of that developed by Stetson (1996) for automated searches for Cepheid variables:

$$I = \frac{\sum_{i=1}^{N} (m(t_i) - \bar{m})^2 - \sum_{i=1}^{N} [n(t_i) - \bar{n}]^2}{\bar{m}}, \quad (1)$$

where N is the total number of observations, $m(t_i)$ is the observed flux density at a given velocity channel, $n(t_i)$ is the flux density at a noise channel (the noise time-series channel is any channel in the spectrum in which there is no maser emission) and $\bar{m}$ and $\bar{n}$ are the average flux densities. The variability index is normalized by dividing by the average maser flux density, which is taken over the entire time-series. Thus, a non-varying maser will have an index tending towards zero. Note that the index can go negative for time-series with a poor signal-to-noise ratio (S/N). Therefore the average flux as well as the S/N has to be taken into account when interpreting the variability index.

Table 3 gives the statistics and variability index for the peak channels for each identifiable feature. The average rms noise is given as well as the average uncertainty $\sigma_{\rm m}$ for each maser peak taking into account the rms noise as well as calibration error. This is given by

$$\sigma_{\rm m} = \sqrt{{\sigma_{\rm rms}}^2 + \left(\frac{\delta T_{\rm sys}}{T_{\rm sys}} * T_{\rm m}\right)^2}, \quad (2)$$

where $T_{\rm sys}$ is the average system temperature, $\delta T_{\rm sys}$ is the uncertainty in the system temperature, $T_{\rm m}$ is the antenna temperature at the maser peak and $\sigma_{\rm rms}$ is the rms noise. The rms noise is calculated using the radiometer equation (Kraus 1986):

$$\sigma_{\rm rms} = \frac{K * T_{\rm sys}}{\sqrt{\Delta\nu * \tau * f}}, \quad (3)$$

where K is the correlator quantization factor ($K = 1.235$ for the HartRAO correlator), $\Delta\nu$ is the bandwidth per channel in Hz, τ is the total integration time, $f = 1$ if the observations were position-switched and $f = 2$ if frequency switching was used.

Fig. 2 shows histograms of the variability indices for all the maser peaks. The majority of the maser features have $I < 5$ but masers undergoing strong flares can have much higher indices. The ranges corresponding to descriptions such as 'highly variable' and 'significantly variable' are difficult to define, but for ease of discussion divisions have been selected after visual examination of the data set. The most variable maser feature in the sample is an otherwise insignificant feature in G351.42+0.64 (Fig. 3) with a variability index of 112.3. This peak increased from below the detection limit of 1.5 to 250 Jy in two months. It stayed at this level for about a month and then gradually subsided to below the detection limit over the next 10 months. For comparison, Fig. 4 shows the time-series of four maser features with low variability indices. The features with $I = 2.80$ and even $I = 1.00$ show moderate variability. A variability index below 0.5 generally suggests that little significant variability occurred, but as noted previously, this has to be considered in conjunction with the S/N of the feature.

There does not appear to be any correlation between the average flux density of a maser peak and its degree of variability, as can be seen in Fig. 5. Masers with an average flux density below 5 Jy were generally too weak to determine a reliable variability index, unless the maser feature underwent a flare.

4.2 Notes on individual sources

Upper and lower envelopes were calculated by finding the maxima and minima in the time-series at each velocity channel. They serve as a useful visual indication of the range of variability of a source. These envelopes, as well as time-series for selected velocity channels are

Table 3. Statistics of the time-series of the maser peaks.

Source	maser velocity (km s^{-1})	ave flux (Jy)	σ_m (Jy)	σ_{rms} (Jy)	S/N	I
G174.20–1.68	0.37	3.69	0.548	0.548	7	4.17
	1.66	57.36	0.550	0.548	104	4.58
	2.16	5.66	0.552	0.548	10	0.31
	3.62	6.33	0.560	0.548	11	0.97
	4.02	8.94	0.563	0.548	16	0.97
	4.41	6.16	0.566	0.548	11	0.98
G213.71–12.60	10.49	68.69	0.762	0.693	90	4.77
	10.94	343.96	0.768	0.693	448	53.42
	11.96	42.25	0.782	0.693	54	4.67
	12.24	23.50	0.786	0.693	30	1.56
	13.02	18.09	0.797	0.693	23	1.07
G189.03+0.79	8.87	14.09	0.647	0.587	22	0.13
	9.65	8.00	0.657	0.587	12	−0.09
	10.55	4.56	0.670	0.587	7	0.94
	10.78	3.86	0.673	0.587	6	0.82
G188.95+0.89	8.48	11.10	0.611	0.563	18	0.08
	9.72	26.82	0.625	0.563	43	0.37
	10.51	530.38	0.635	0.563	835	2.02
	10.79	437.97	0.639	0.563	686	2.14
	11.46	107.95	0.648	0.563	167	0.61
G192.60–0.05	1.81	2.90	0.400	0.397	7	1.02
	4.12	19.11	0.413	0.397	46	0.10
	4.62	60.01	0.417	0.397	144	2.39
	5.41	34.12	0.424	0.397	80	0.61
G196.45–1.68	14.73	7.83	0.526	0.354	15	0.46
	15.18	32.27	0.535	0.354	60	1.22
	15.91	4.88	0.550	0.354	9	1.44
G287.36+0.64	−2.45	13.62	0.373	0.367	36	0.09
	−2.23	27.00	0.372	0.367	73	0.11
	−1.89	86.10	0.371	0.367	232	0.43
	−1.05	11.23	0.368	0.367	30	0.58
	−0.65	3.61	0.368	0.367	10	0.23
G291.27–0.71	−30.43	45.80	1.042	0.679	44	0.31
	−29.64	75.33	1.026	0.679	73	0.99
	−29.14	40.18	1.016	0.679	40	0.03
G294.52–1.62	−11.90	12.86	0.476	0.351	27	2.78
	−11.51	4.13	0.468	0.351	9	0.09
	−11.00	6.28	0.460	0.351	14	0.11
	−10.21	8.58	0.446	0.351	19	0.31
	−8.92	0.69	0.425	0.351	2	3.02
G298.26+0.74	−30.06	12.60	0.862	0.343	15	0.05
G305.21+0.21	−43.90	39.74	1.312	0.734	30	0.56
	−38.39	400.22	1.202	0.734	333	1.94
	−36.03	49.79	1.156	0.734	43	0.35
G308.92+0.12	−55.41	11.41	1.469	0.382	8	0.04
	−54.79	40.72	1.453	0.382	28	0.12
	−54.56	28.71	1.448	0.382	20	0.18
	−54.34	29.10	1.442	0.382	20	0.29
	−53.55	9.02	1.423	0.382	6	0.14
	−52.71	9.47	1.402	0.382	7	0.13
G309.92+0.48	−62.93	81.42	1.595	0.603	51	0.18
	−62.37	187.22	1.582	0.603	118	0.46
	−61.70	100.66	1.568	0.603	64	0.26
	−60.91	113.78	1.551	0.603	73	0.39
	−59.79	800.00	1.526	0.603	524	1.91
	−58.89	173.87	1.507	0.603	115	0.45
	−58.55	302.38	1.500	0.603	202	1.11
	−57.99	186.55	1.488	0.603	125	0.56
G312.11+0.26	−51.52	4.18	1.351	0.375	3	0.04
	−50.90	5.99	1.336	0.375	4	0.12
	−49.94	17.89	1.313	0.375	14	0.40
G316.64–0.09	−24.00	4.14	0.848	0.610	5	0.13
	−23.55	4.96	0.841	0.610	6	0.17
	−22.76	3.20	0.827	0.610	4	0.28
	−22.31	33.34	0.820	0.610	41	1.00
	−21.75	14.00	0.811	0.610	17	0.56
	−21.19	18.62	0.802	0.610	23	0.37
	−20.29	73.54	0.788	0.610	93	0.32
	−19.84	80.64	0.781	0.610	103	2.55
	−18.49	9.56	0.760	0.610	13	0.19
	−17.93	13.97	0.752	0.610	19	0.41
	−17.03	4.44	0.739	0.610	6	0.62
G318.95–0.20	−38.09	13.96	1.143	0.703	12	0.38
	−37.25	46.91	1.127	0.703	42	0.77
	−36.80	118.93	1.119	0.703	106	1.69
	−36.24	65.17	1.108	0.703	59	0.20
	−35.28	95.33	1.091	0.703	87	0.24
	−34.61	545.16	1.079	0.703	505	0.91
	−33.60	29.80	1.061	0.703	28	0.26
	−32.92	37.87	1.049	0.703	36	0.39
G320.23–0.29	−70.34	5.07	1.815	0.429	3	0.28
	−62.25	28.53	1.618	0.429	18	0.67
	−61.92	26.42	1.610	0.429	16	0.42
	−61.47	17.20	1.599	0.429	11	0.55
	−60.79	7.80	1.583	0.429	5	0.31
	−59.33	8.07	1.548	0.429	5	0.59
	−58.77	5.21	1.534	0.429	3	1.18
G322.16+0.64	−64.01	164.51	1.656	0.748	99	16.51
	−63.33	258.86	1.642	0.748	158	27.51
	−63.00	250.32	1.635	0.748	153	3.09
	−62.43	77.96	1.624	0.748	48	0.80
	−62.10	115.15	1.617	0.748	71	3.09
	−61.87	68.55	1.612	0.748	43	1.25
	−60.07	26.47	1.575	0.748	17	4.15
	−59.62	10.11	1.566	0.748	6	1.49
	−57.60	20.20	1.525	0.748	13	25.61
	−56.81	59.85	1.510	0.748	40	10.37
	−56.37	102.73	1.501	0.748	68	10.56
	−55.13	51.47	1.476	0.748	35	1.45
	−54.57	80.77	1.465	0.748	55	7.54
	−53.78	40.56	1.449	0.748	28	0.37
	−53.22	53.03	1.438	0.748	37	1.38
G323.77–0.21	−53.09	203.38	1.890	0.907	108	10.92
	−51.07	3433.27	1.834	0.907	1872	41.01
	−50.56	2670.50	1.821	0.907	1467	43.76
	−49.55	1155.88	1.793	0.907	645	11.84
	−49.10	803.47	1.781	0.907	451	5.72
	−48.54	977.17	1.766	0.907	553	4.37
	−48.15	473.93	1.756	0.907	270	4.95
G328.81+0.63	−46.64	74.47	1.227	0.625	61	0.12
	−46.25	133.48	1.220	0.625	109	0.44
	−45.24	60.31	1.200	0.625	50	0.06
	−44.45	241.19	1.185	0.625	204	1.57
	−43.83	247.62	1.173	0.625	211	0.52

Table 3 – *continued*

Source	maser velocity (km s^{-1})	ave flux (Jy)	σ_m (Jy)	σ_{rms} (Jy)	S/N	I
G328.24–0.55	−49.56	50.46	1.480	1.141	34	0.69
	−45.41	60.22	1.566	1.141	38	0.38
	−44.73	670.79	1.556	1.141	431	4.37
	−44.28	186.12	1.548	1.141	120	5.35
	−43.27	107.32	1.532	1.141	70	0.54
	−38.66	58.23	1.462	1.141	40	0.47
	−37.99	141.45	1.452	1.141	97	0.99
	−37.43	292.10	1.444	1.141	202	1.62
	−37.09	156.40	1.439	1.141	109	1.06
	−36.42	34.76	1.429	1.141	24	1.08
	−35.07	21.18	1.410	1.141	15	0.90
	−34.73	9.77	1.406	1.141	7	0.55
G331.13–0.24	−90.77	6.45	2.334	0.414	3	5.27
	−85.60	13.37	2.205	0.414	6	7.18
	−84.93	9.11	2.189	0.414	4	1.52
	−84.25	18.89	2.172	0.414	9	3.42
G331.28–0.19	−85.43	17.12	2.041	0.678	8	0.19
	−85.09	31.37	2.033	0.678	15	0.92
	−84.30	8.20	2.017	0.678	4	0.14
	−83.80	10.12	2.006	0.678	5	0.16
	−83.74	10.29	2.005	0.678	5	0.32
	−82.45	14.69	1.977	0.678	7	0.85
	−81.49	41.27	1.957	0.678	21	0.14
	−81.05	18.65	1.948	0.678	10	0.13
	−80.31	14.98	1.932	0.678	8	0.18
	−79.58	7.29	1.917	0.678	4	0.25
	−78.85	45.97	1.902	0.678	24	0.89
	−78.07	116.89	1.885	0.678	62	0.40
	−77.67	40.60	1.877	0.678	22	0.20
G335.55–0.31	−116.75	14.39	3.141	0.414	5	0.08
	−113.15	10.41	3.046	0.414	3	0.09
G336.01–0.82	−53.41	312.36	1.465	0.797	213	1.37
	−52.28	21.34	1.443	0.797	15	0.50
	−48.46	22.16	1.371	0.797	16	0.20
	−48.01	13.16	1.362	0.797	10	0.41
	−45.09	29.15	1.308	0.797	22	0.22
	−44.42	3.89	1.296	0.797	3	0.07
	−43.40	3.74	1.278	0.797	3	−0.08
	−42.73	5.56	1.266	0.797	4	0.39
	−41.94	17.24	1.252	0.797	14	0.61
	−41.38	41.67	1.242	0.797	34	0.30
G336.99–0.03	−125.88	23.69	3.212	0.394	7	0.31
G337.92–0.46	−38.73	29.74	1.046	0.442	28	0.85
	−37.83	21.81	1.026	0.442	21	0.06
	−37.50	4.75	1.019	0.442	5	0.05
	−36.43	3.31	0.995	0.442	3	0.08
G338.93–0.06	−41.99	22.98	1.093	0.365	21	0.69
	−41.37	8.76	1.079	0.365	8	0.35
G339.62–0.12	−37.76	38.92	1.017	0.418	38	0.09
	−37.31	28.49	1.007	0.418	28	2.85
	−36.97	31.43	1.000	0.418	31	1.22
	−35.74	96.06	0.972	0.418	99	18.42
	−34.84	4.39	0.952	0.418	5	0.70
	−33.49	44.16	0.923	0.418	48	2.87
	−32.93	81.52	0.910	0.418	90	0.64
	−32.25	37.19	0.896	0.418	42	1.23
	−31.24	2.30	0.874	0.418	3	0.65
	−30.57	3.39	0.859	0.418	4	0.31

Table 3 – *continued*

Source	maser velocity (km s^{-1})	ave flux (Jy)	σ_m (Jy)	σ_{rms} (Jy)	S/N	I
G339.88–1.26	−39.82	21.20	1.110	0.579	19	0.03
	−38.81	1563.23	1.089	0.579	1435	2.44
	−38.14	502.65	1.076	0.579	467	0.40
	−37.57	673.56	1.065	0.579	633	0.87
	−36.67	650.32	1.047	0.579	621	0.69
	−35.66	428.03	1.027	0.579	417	0.69
	−35.21	650.93	1.018	0.579	639	4.65
	−34.54	271.65	1.005	0.579	270	0.43
	−33.87	352.50	0.992	0.579	355	0.69
	−33.19	111.68	0.979	0.579	114	4.24
	−32.29	66.94	0.962	0.579	70	6.81
	−30.16	8.14	0.922	0.579	9	1.95
G340.79–0.10	−108.43	25.43	2.651	0.577	10	14.65
	−107.76	12.68	2.635	0.577	5	12.53
	−107.09	38.31	2.619	0.577	15	41.69
	−106.64	17.03	2.609	0.577	7	6.66
	−106.07	39.61	2.596	0.577	15	0.06
	−105.17	108.76	2.575	0.577	42	0.24
	−104.72	52.83	2.564	0.577	21	0.19
	−104.05	50.33	2.549	0.577	20	0.24
	−102.14	9.44	2.504	0.577	4	0.04
	−101.69	13.43	2.494	0.577	5	0.08
	−99.22	17.36	2.436	0.577	7	0.28
	−98.66	6.35	2.423	0.577	3	0.09
G344.23–0.57	−26.41	34.12	0.980	0.771	35	1.45
	−24.50	16.40	0.954	0.771	17	0.18
	−23.49	3.65	0.941	0.771	4	0.67
	−22.70	9.47	0.930	0.771	10	0.54
	−21.13	9.59	0.911	0.771	11	0.25
	−20.45	9.58	0.902	0.771	11	0.12
	−19.78	94.88	0.895	0.771	106	0.21
G345.00–0.22	−30.38	23.72	0.811	0.414	29	7.96
	−29.93	10.62	0.802	0.414	13	0.16
	−29.37	6.10	0.791	0.414	8	−0.11
	−29.04	7.58	0.785	0.414	10	0.07
	−28.25	26.73	0.769	0.414	35	1.01
	−27.69	17.26	0.758	0.414	23	0.28
	−26.79	68.59	0.741	0.414	93	12.01
	−26.11	79.93	0.729	0.414	110	0.17
	−25.78	16.52	0.722	0.414	23	0.11
	−23.75	52.12	0.685	0.414	76	4.06
	−22.97	85.27	0.670	0.414	127	14.61
	−22.52	130.27	0.662	0.414	197	10.97
	−21.50	4.72	0.644	0.414	7	0.18
G345.50+0.35	−22.73	3.57	0.679	0.461	5	0.01
	−20.93	4.56	0.651	0.461	7	1.43
	−19.70	49.14	0.632	0.461	78	4.43
	−19.14	49.84	0.623	0.461	80	2.14
	−18.46	113.39	0.613	0.461	185	3.06
	−17.67	182.09	0.602	0.461	302	5.80
	−16.66	80.05	0.588	0.461	136	2.35
	−16.55	80.56	0.587	0.461	137	2.80
	−15.65	139.99	0.575	0.461	244	1.68
	−14.53	159.02	0.560	0.461	284	2.07
	−14.30	175.76	0.557	0.461	315	2.08
	−12.95	3.49	0.541	0.461	6	1.05
	−11.04	2.44	0.520	0.461	5	1.38

Table 3 – *continued*

Source	maser velocity (km s^{-1})	ave flux (Jy)	$\sigma_{\rm m}$ (Jy)	$\sigma_{\rm rms}$ (Jy)	S/N	I
G351.42+0.64	−11.16	1911.15	0.614	0.558	3111	3.68
	−10.37	3337.34	0.607	0.558	5498	10.37
	−9.92	401.28	0.603	0.558	665	2.63
	−8.57	114.23	0.592	0.558	193	1.48
	−7.90	67.38	0.587	0.558	115	2.60
	−7.34	195.37	0.583	0.558	335	9.56
	−6.89	88.12	0.580	0.558	152	0.96
	−6.55	120.71	0.578	0.558	209	0.47
	−5.88	21.45	0.574	0.558	37	112.29
	−2.62	30.17	0.562	0.558	54	1.41
G351.58–0.35	−95.97	7.55	2.135	0.340	4	0.01
	−95.52	17.59	2.125	0.340	8	0.05
	−95.07	10.51	2.116	0.340	5	0.01
	−94.28	46.97	2.099	0.340	22	0.05
	−93.72	10.06	2.086	0.340	5	−0.01
G351.78–0.54	1.28	160.76	0.341	0.340	472	14.00
	1.73	176.42	0.342	0.340	516	9.32
G354.61+0.47	−25.40	14.39	0.729	0.518	20	0.66
	−24.38	133.29	0.715	0.518	186	1.10
	−23.15	123.75	0.698	0.518	177	0.51
	−21.91	12.04	0.681	0.518	18	0.25
	−21.01	7.63	0.670	0.518	11	0.17
	−20.23	4.57	0.660	0.518	7	0.43
	−18.09	14.24	0.634	0.518	22	0.35
	−16.97	59.63	0.621	0.518	96	0.17
	−16.18	36.08	0.612	0.518	59	0.64
	−14.72	5.43	0.597	0.518	9	0.22
G359.61–0.24	18.37	4.94	0.492	0.308	10	1.72
	19.15	23.10	0.505	0.308	46	0.71
	19.94	21.05	0.519	0.308	41	3.54
	20.84	3.27	0.534	0.308	6	0.29
	21.85	4.77	0.551	0.308	9	0.42
	22.41	43.08	0.561	0.308	77	0.98
	22.75	48.22	0.567	0.308	85	6.67
	23.98	12.01	0.589	0.308	20	0.59
G9.62+0.20	−1.88	19.00	0.767	0.765	25	0.17
	−1.21	29.57	0.766	0.765	39	0.12
	−0.76	40.77	0.765	0.765	53	1.08
	−0.42	34.21	0.765	0.765	45	0.19
	−0.14	423.48	0.765	0.765	554	19.94
	1.26	4374.75	0.766	0.765	5712	28.95
	1.94	121.33	0.767	0.765	158	1.68
	3.12	68.07	0.771	0.765	88	1.04
	5.31	62.19	0.782	0.765	80	0.22
	6.43	12.71	0.790	0.765	16	0.47
G10.33–0.17	4.66	13.04	0.517	0.508	25	0.66
	4.99	8.88	0.519	0.508	17	3.04
	6.12	3.48	0.524	0.508	7	0.44
	6.57	1.59	0.526	0.508	3	0.82
	7.24	5.74	0.530	0.508	11	0.21
	8.14	3.50	0.536	0.508	7	0.39
	8.93	2.79	0.541	0.508	5	0.17
	9.94	109.01	0.549	0.508	199	3.04
	10.73	20.30	0.555	0.508	37	0.31
	11.62	89.56	0.563	0.508	159	1.41
	12.41	32.02	0.570	0.508	56	1.53
	13.09	3.35	0.577	0.508	6	0.50
	13.98	3.25	0.586	0.508	6	0.41
	14.66	10.05	0.593	0.508	17	0.59
	15.45	4.97	0.602	0.508	8	1.49
	15.67	5.24	0.604	0.508	9	0.64

Table 3 – *continued*

Source	maser velocity (km s^{-1})	ave flux (Jy)	$\sigma_{\rm m}$ (Jy)	$\sigma_{\rm rms}$ (Jy)	S/N	I
G10.47+0.03	59.45	15.52	1.400	0.309	11	0.05
	61.58	4.33	1.447	0.309	3	−0.13
	64.62	8.91	1.516	0.309	6	−0.01
	65.29	10.09	1.531	0.309	7	−0.04
	68.21	5.98	1.597	0.309	4	0.06
	72.37	24.03	1.690	0.309	14	0.08
	73.38	16.69	1.713	0.309	10	0.15
	74.06	14.06	1.728	0.309	8	0.00
	75.07	27.73	1.751	0.309	16	0.29
	76.31	9.63	1.779	0.309	5	−0.03
G12.68−0.18	51.17	105.55	1.444	0.736	73	3.36
	52.24	274.96	1.467	0.736	187	1.83
	54.32	26.96	1.511	0.736	18	1.69
	54.94	27.20	1.524	0.736	18	2.89
	55.50	12.69	1.536	0.736	8	0.64
	57.02	133.21	1.568	0.736	85	1.29
	57.58	362.28	1.580	0.736	229	2.66
	58.42	138.03	1.599	0.736	86	0.93
	58.14	90.58	1.592	0.736	57	1.47
	59.04	56.34	1.612	0.736	35	3.21
	59.15	63.76	1.614	0.736	39	4.83
	59.83	92.01	1.629	0.736	56	8.98
	60.73	9.60	1.648	0.736	6	0.79
G12.89+0.49	30.17	3.87	0.840	0.528	5	0.32
	31.74	3.78	0.867	0.528	4	0.44
	32.75	8.09	0.885	0.528	9	1.12
	33.76	41.77	0.902	0.528	46	0.29
	34.66	7.59	0.918	0.528	8	0.70
	36.57	3.62	0.952	0.528	4	0.99
	37.81	6.69	0.975	0.528	7	3.03
	38.71	24.86	0.991	0.528	25	1.62
	39.27	54.72	1.001	0.528	55	1.46
G12.91–0.26	35.42	5.41	0.983	0.542	5	0.18
	35.87	15.37	0.992	0.542	15	0.36
	36.20	6.81	0.999	0.542	7	0.31
	37.27	6.58	1.020	0.542	6	0.38
	38.62	46.68	1.046	0.542	45	0.10
	39.35	244.82	1.061	0.542	231	0.85
	39.80	276.82	1.070	0.542	259	0.54
G23.01–0.41	72.62	46.27	1.564	0.449	30	0.49
	74.19	283.88	1.595	0.449	178	1.09
	74.75	281.86	1.606	0.449	175	1.72
	75.09	311.02	1.613	0.449	193	1.28
	76.55	27.17	1.642	0.449	17	0.31
	78.69	8.46	1.684	0.449	5	0.13
	79.25	11.73	1.696	0.449	7	0.11
	80.60	37.39	1.723	0.449	22	0.28
	81.16	55.09	1.734	0.449	32	0.65
	81.72	44.67	1.745	0.449	26	0.26
	82.40	33.24	1.758	0.449	19	0.79
G23.44–0.18	95.86	16.88	2.043	0.636	8	0.81
	96.64	33.53	2.058	0.636	16	0.39
	97.43	18.72	2.073	0.636	9	0.17
	98.11	17.18	2.086	0.636	8	0.27
	102.60	16.26	2.173	0.636	7	0.50
	102.94	54.85	2.180	0.636	25	1.00
	104.51	10.10	2.210	0.636	5	0.29
	104.85	6.78	2.217	0.636	3	0.16
	106.98	6.84	2.258	0.636	3	0.25

Table 3 – *continued*

Source	maser velocity (km s^{-1})	ave flux (Jy)	σ_m (Jy)	σ_{rms} (Jy)	S/N	I
G35.20–1.74	40.98	172.35	1.019	0.407	169	1.00
	41.43	251.71	1.029	0.407	245	0.78
	42.44	796.83	1.050	0.407	759	7.56
	43.23	66.72	1.066	0.407	63	21.91
	43.56	53.42	1.073	0.407	50	4.75
	44.12	62.98	1.085	0.407	58	0.88
	44.69	220.19	1.097	0.407	201	8.86
	46.03	16.14	1.126	0.407	14	0.46
G45.07+0.13	57.77	43.64	1.496	0.530	29	0.11
G52.67–1.09	64.60	6.68	1.863	0.505	4	3.18
G59.78+0.06	26.91	14.45	0.860	0.438	17	0.00
G78.12+3.63	−8.47	2.40	0.422	0.379	6	−0.07
	−7.24	8.46	0.411	0.379	21	1.24
	−6.56	23.22	0.405	0.379	57	1.86
	−6.11	40.72	0.402	0.379	101	3.49
	−4.99	2.33	0.394	0.379	6	1.03
G81.88+0.78	3.47	53.10	1.031	1.026	51	3.52
	4.03	160.92	1.033	1.026	156	14.43
	4.59	231.59	1.035	1.026	224	1.92
	5.15	104.33	1.037	1.026	101	1.04
	5.77	102.13	1.040	1.026	98	0.56
	7.12	543.06	1.047	1.026	519	13.41
	9.25	21.22	1.061	1.026	20	2.62

given in Figs 6–60. Intensity contour plots for sources of particular interest are given in Figs 61–77, which are available online at http://www.blackwellpublishing.com/products/journals/suppmat/MNR/MNR8340/MNR8340sm.htm. The data for the contour plots were gridded using Barnes smoothing (Kelley 2003) with length scales of 5 d for the time-axis and 0.05 km s^{-1} for the velocity. This reduced the noise in the contour plots, compared to the unsmoothed data shown in the time-series plots. Significant gaps in the data can cause spurious features in the contour plots, and where these occur they are blanked out to prevent misinterpretation.

Where maser spot maps are available, we give a summary of the observed morphology.

G174.20–0.08/AFGL5142 (Figs 6 and 61). The peak at 1.66 km s^{-1} remained constant at approximately 70 Jy for several years before before decreasing to about 30 Jy. The feature appears to have started increasing in flux density towards the end of the period covered in this paper. Cross-correlation of the time-series at 4.02 and 1.66 km s^{-1} shows a time delay of 98 d. The peak at 0.37 km s^{-1} flared up to 20 Jy at the same time that the main peak reached its minimum level. There is no significant activity from the other features. The contour plot suggests that the intensity variations in the main peak vary back and forth across the line profile.

G213.71–12.60/MonR2 (Figs 7, 8 and 62). This source shows the most noticeable changes in spectral line profile. The 10.94 km s^{-1} feature increased in flux density from 150 to 700 Jy over three years. The behaviour in this feature is correlated with that of the weaker feature at 10.49 km s^{-1}. Fig. 8 shows the time-series and range of variation in the spectrum for observations taken from 1997 August to 1998 August. The observing parameters for this data set are the same as described in MacLeod & Gaylard (1996). The spectrum is markedly different from that seen in later years, with the maser feature at 12.24 km s^{-1} dominant. The contour plot shows that the flares drift across the maser features. Smits et al. (1998) noted a similar phenomenon in the 4.765 GHz hydroxyl masers in this source. The spot maps of Minier, Booth & Conway (2000) show a linear structure 170 mas (130 au at 830 pc) in extent.

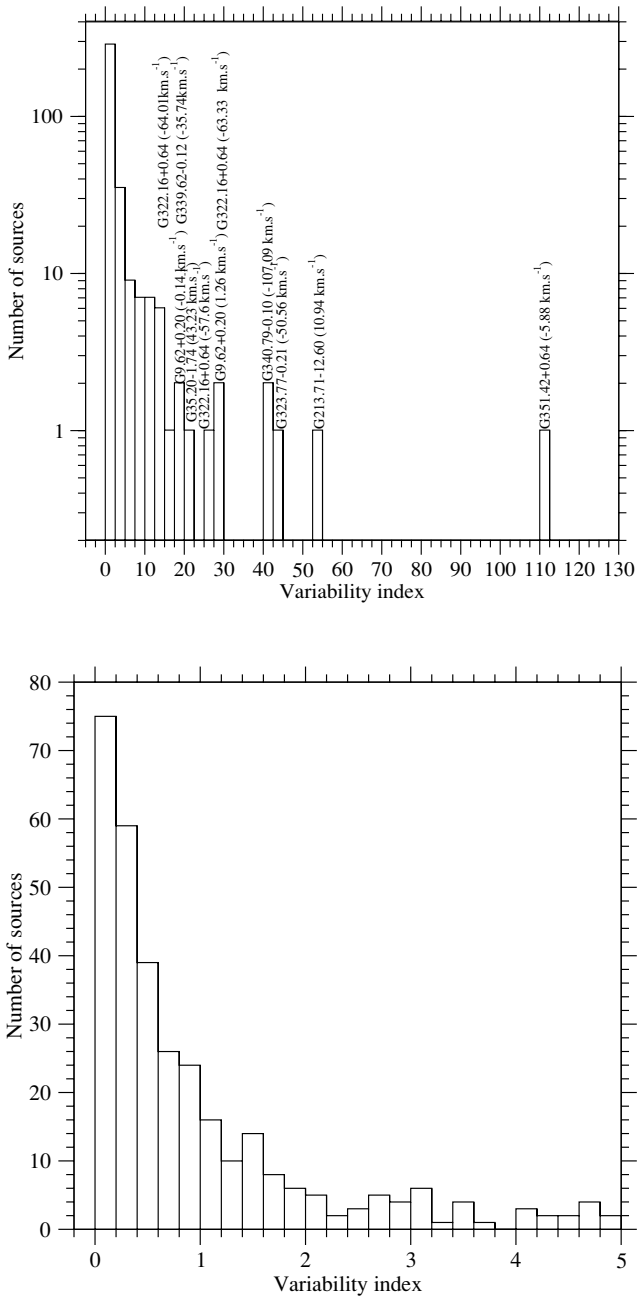

Figure 2. Histogram of the variability indices. The top panel shows the full range of variability indices. The binning interval is 2.5. The most variable maser features are identified on this histogram. The bottom panel shows the lower end of the distribution in more detail. The binning interval is 0.2.

G188.95+0.89/S252 (Figs 9 and 63). All the features in this source show a simultaneous sinusoidal modulation with a period of 416 d. The masers spots have a linear arrangement 110 mas (300 au at 2.2 kpc) in extent, but the position–velocity distribution is not consistent with a Keplerian disc (Minier et al. 2000). The contour plot indicates that the range of velocities at which emission is detectable is expanding at 9.5 to 10 km s^{-1}, possibly owing to the general slow increase in brightness of the emission.

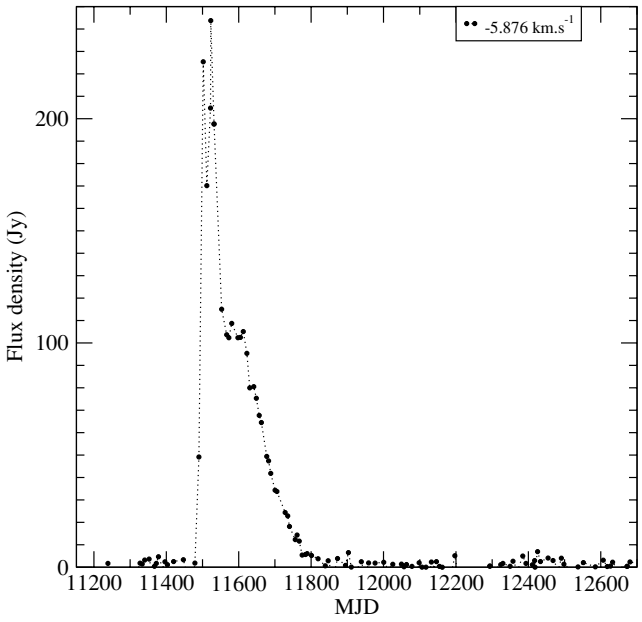

Figure 3. Time-series of the −5.88 km s^{-1} feature in G351.42+0.64. This feature has the highest variability index in the sample.

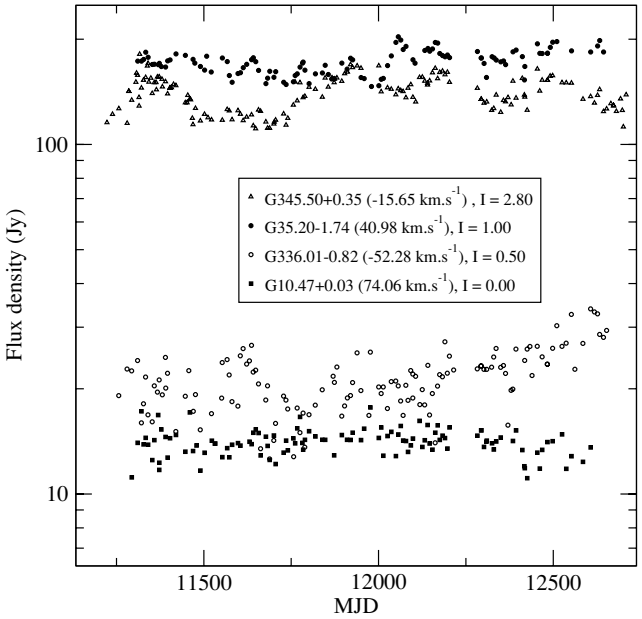

Figure 4. Time-series of a moderately variable feature in G345.50+0.35 with other time-series showing progressively less significant variations above the noise.

G189.03+0.79 (Fig. 10). This source is very weak and the changes in the time-series are dominated by the noise. No significant variations are seen.

G192.60–0.05/S255 (Fig. 11). In contrast to the non-varying 4.12 km s^{-1} feature, those at 1.81, 4.62 and 5.41 km s^{-1} are moderately variable on time-scales of a few months to a year. None of the features show correlated variations. The spot maps of Minier et al. (2000) show that the feature at 1.81 km s^{-1} is offset by 180 mas (500 au at 2.5 kpc) from the rest of the features, which are clustered within 70 mas (200 au) of each other.

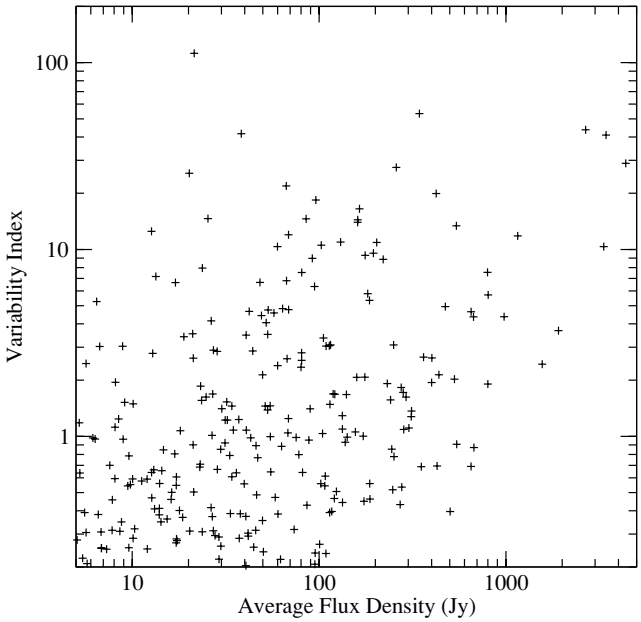

Figure 5. Variability index plotted against average flux density. Note that the scales are logarithmic.

G196.45–1.68/S269 (Figs 12 and 64). There appears to be a low amplitude sinusoidal variation at all features, with a period of 668 d. However, the time-series is not long enough to confirm the trend. The spotmaps of Minier et al. (2000) show two groups of masers separated by 60 mas (240 au at 4 kpc). The most variable feature at 15.91 km s^{-1} is not visible in these observations. Extrapolation of the sinusoidal behaviour back to the time of the European VLBI Network (EVN) observations in 1998 November shows that this feature would have been at its minimum intensity.

G287.36+0.64 (Fig. 13). All the features appear to be slowly increasing in strength. The Australia Telescope Compact Array (ATCA) observations of Walsh et al. (1998) show that all the features are clustered within 0.04 arcsec.

G291.27–0.71 (Fig. 14). The peaks at −30.43 and −29.64 km s^{-1} shows a monotonic decrease in flux density. The peak at −29.14 is not significantly variable.

G294.52–1.62 (Fig. 15). The peak at −11.90 km s^{-1} is moderately variable with an overall decrease in flux density, and may be quasi-periodic, but more data are required to confirm this. The maser at −8.92 km s^{-1} flared above the detection limit for a few weeks. The peak at −10.21 km s^{-1} showed a systematic decrease in flux density then started increasing in flux density. A maser at −8.92 km s^{-1} flared above the detection limit to a maximum flux density of 9.7 Jy at JD 2452149. It stayed above 2 Jy for about 300 d before dropping below our detection limit.

G298.26+0.74 (Fig. 16). This single-peaked source is weak and not significantly variable to within the noise.

G305.21+0.21 (Fig. 17). The peak at −38.94 km s^{-1} shows a gradual increase in flux density. The other features have a low variability index but also show a slow monotonic increase in flux density. None of the variations appear to be correlated across different features. The spot maps of Phillips et al. (1998) show a complex distribution. The features at −45 to −43 km s^{-1} are 22 arcsec away from the cluster in the range −40 to −35 km s^{-1}, which are clustered within 0.4 arcsec (300 au at 8 kpc).

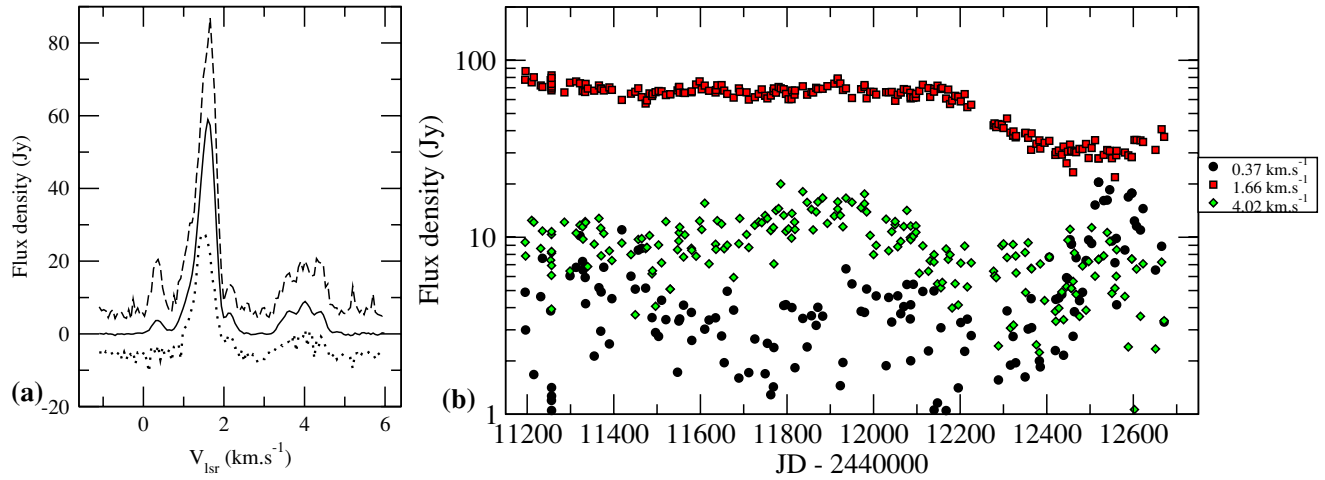

Figure 6. (a) Range of variation in spectrum of G174.20–1.68. The solid, dashed and dotted lines are the averaged spectrum, the upper envelope and the lower envelope, respectively. (b) Time-series for selected velocity channels.

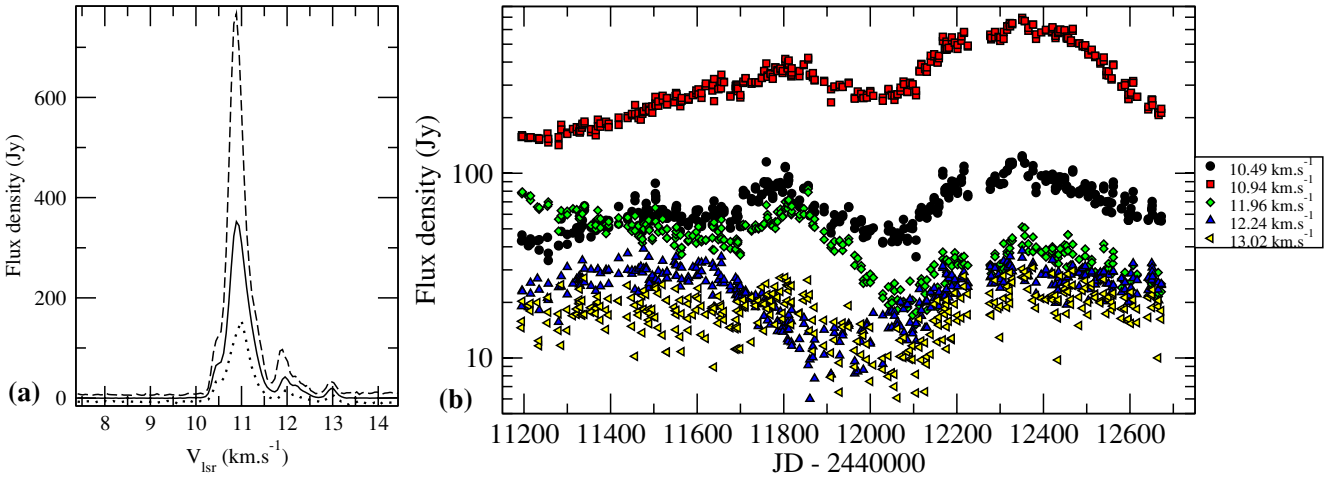

Figure 7. (a) Range of variation in spectrum of G213.71–12.60. The solid, dashed and dotted lines are the averaged spectrum, the upper envelope and the lower envelope, respectively. (b) Time-series for selected velocity channels.

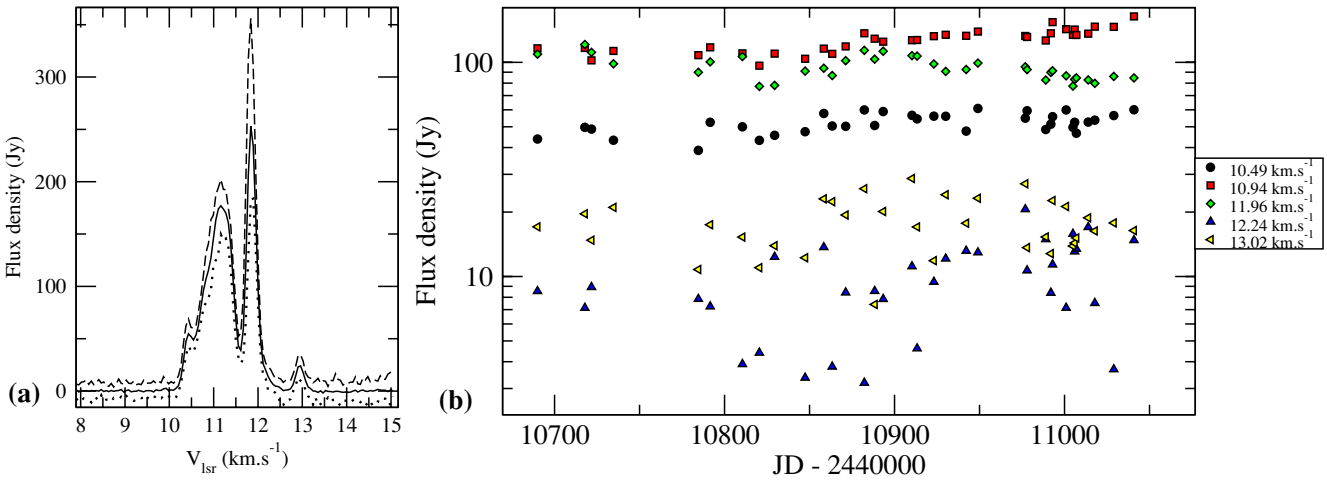

Figure 8. Monitoring data for G213.71–12.60 in the years 1997 to 1998. (a) Range of variation in the spectrum. The solid, dashed and dotted lines are the averaged spectrum, the upper envelope and the lower envelope, respectively. (b) Time-series for selected velocity channels.

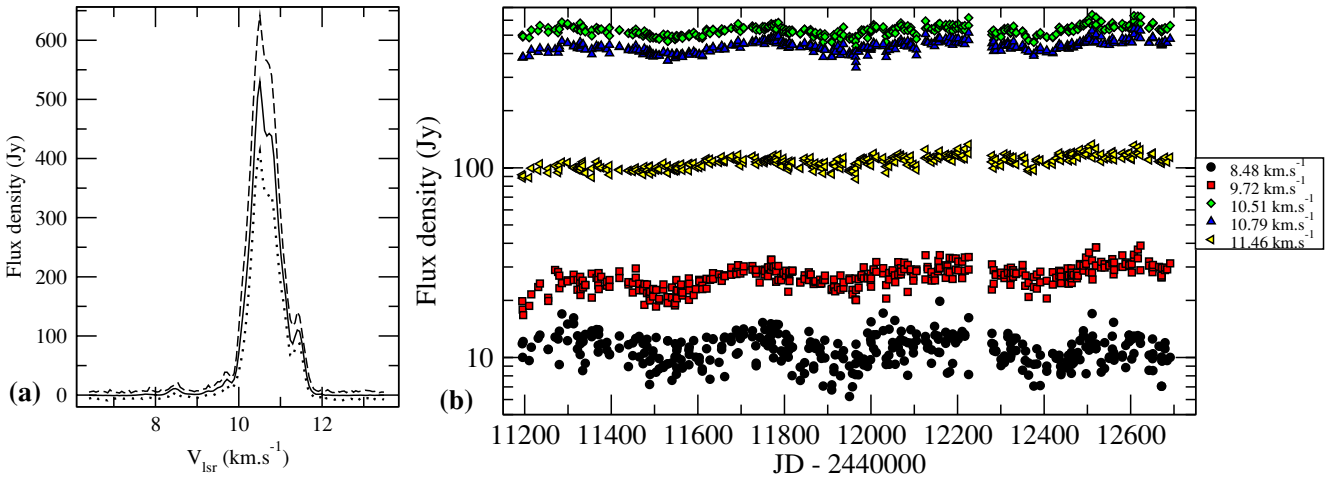

Figure 9. (a) Range of variation in spectrum of G188.95+0.89. The solid, dashed and dotted lines are the averaged spectrum, the upper envelope and the lower envelope, respectively. (b) Time-series for selected velocity channels.

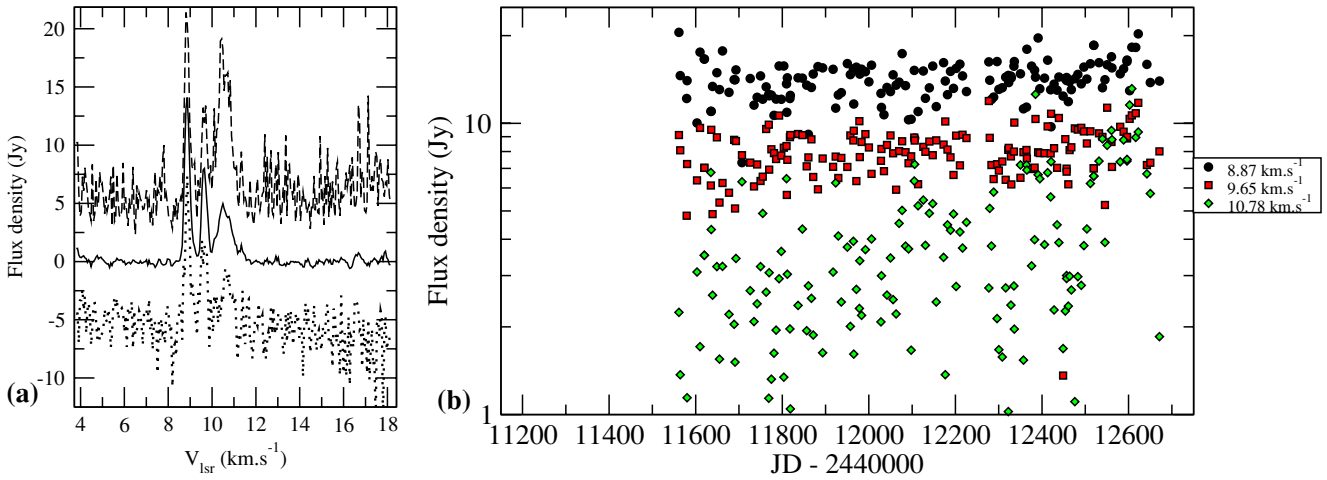

Figure 10. (a) Range of variation in spectrum of G189.03+0.79. The solid, dashed and dotted lines are the averaged spectrum, the upper envelope and the lower envelope, respectively. (b) Time-series for selected velocity channels.

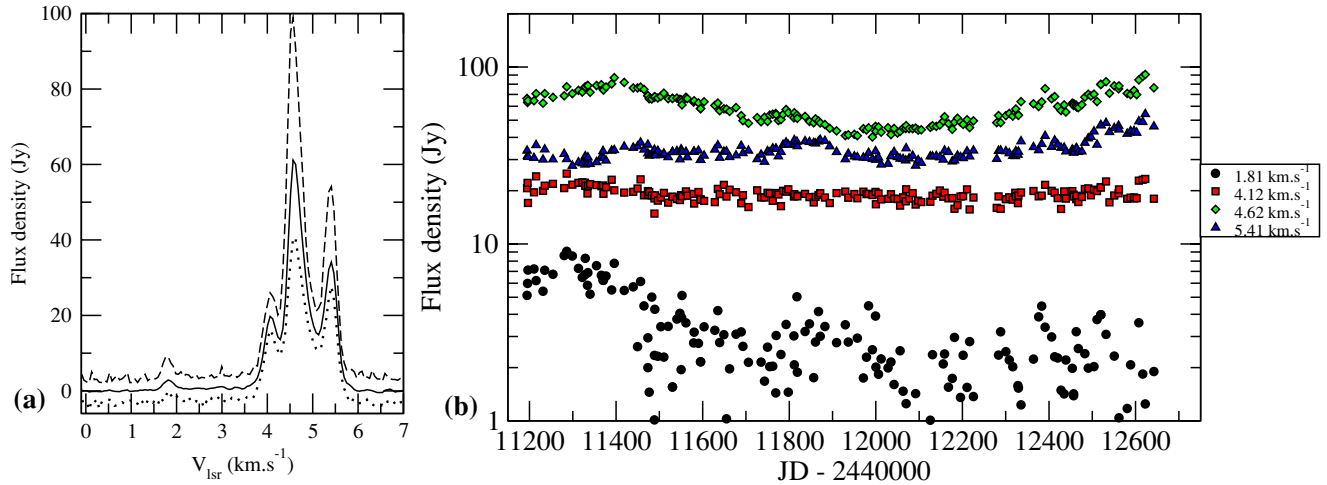

Figure 11. (a) Range of variation in spectrum of G192.60–0.05. The solid, dashed and dotted lines are the averaged spectrum, the upper envelope and the lower envelope, respectively. (b) Time-series for selected velocity channels.

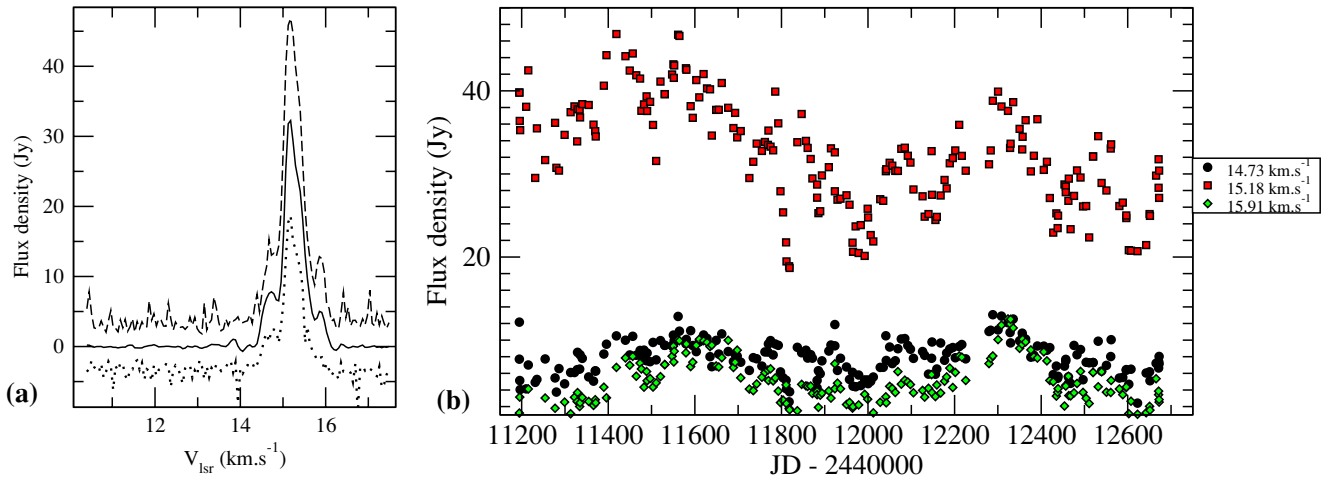

Figure 12. (a) Range of variation in spectrum of G196.45–1.68. The solid, dashed and dotted lines are the averaged spectrum, the upper envelope and the lower envelope, respectively. (b) Time-series for selected velocity channels.

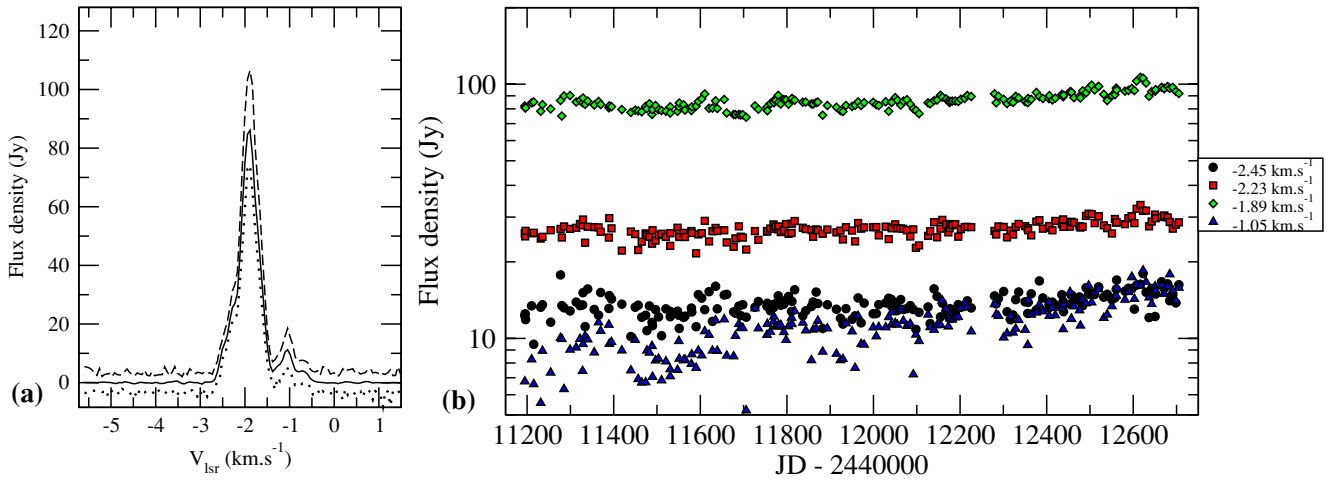

Figure 13. (a) Range of variation in spectrum of G287.36+0.64. The solid, dashed and dotted lines are the averaged spectrum, the upper envelope and the lower envelope, respectively. (b) Time-series for selected velocity channels.

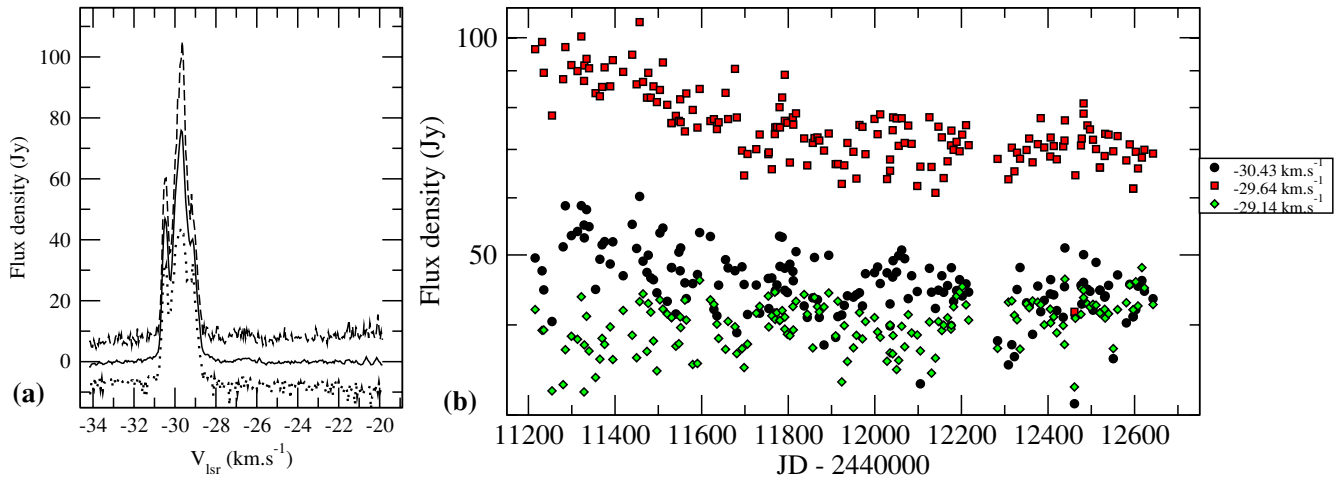

Figure 14. (a) Range of variation in spectrum of G291.27–0.71. The solid, dashed and dotted lines are the averaged spectrum, the upper envelope and the lower envelope, respectively. (b) Time-series for selected velocity channels.

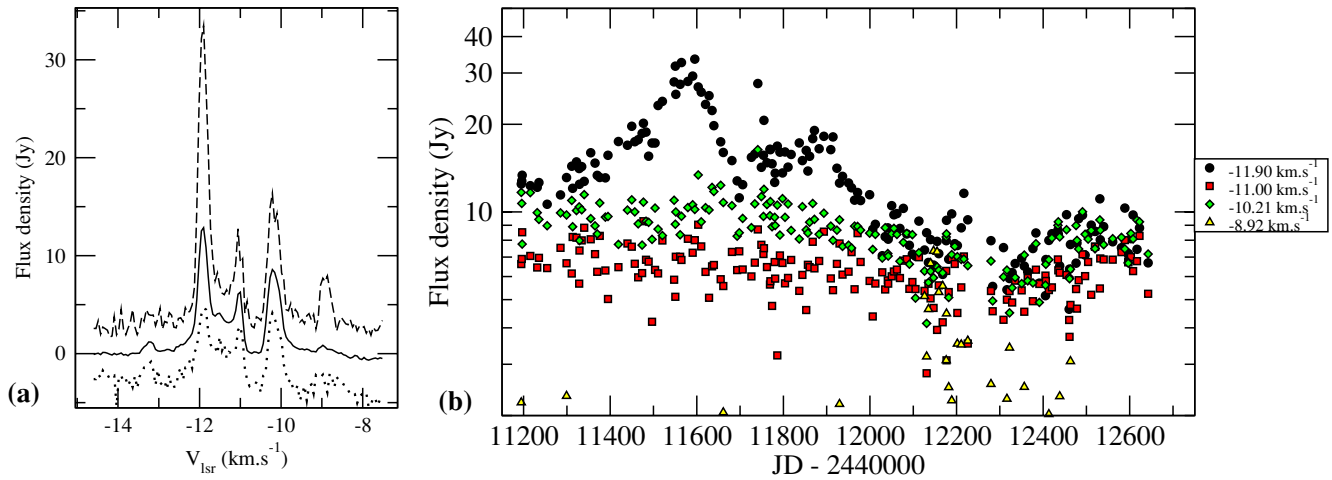

Figure 15. (a) Range of variation in spectrum of G294.52–1.62. The solid, dashed and dotted lines are the averaged spectrum, the upper envelope and the lower envelope, respectively. (b) Time-series for selected velocity channels.

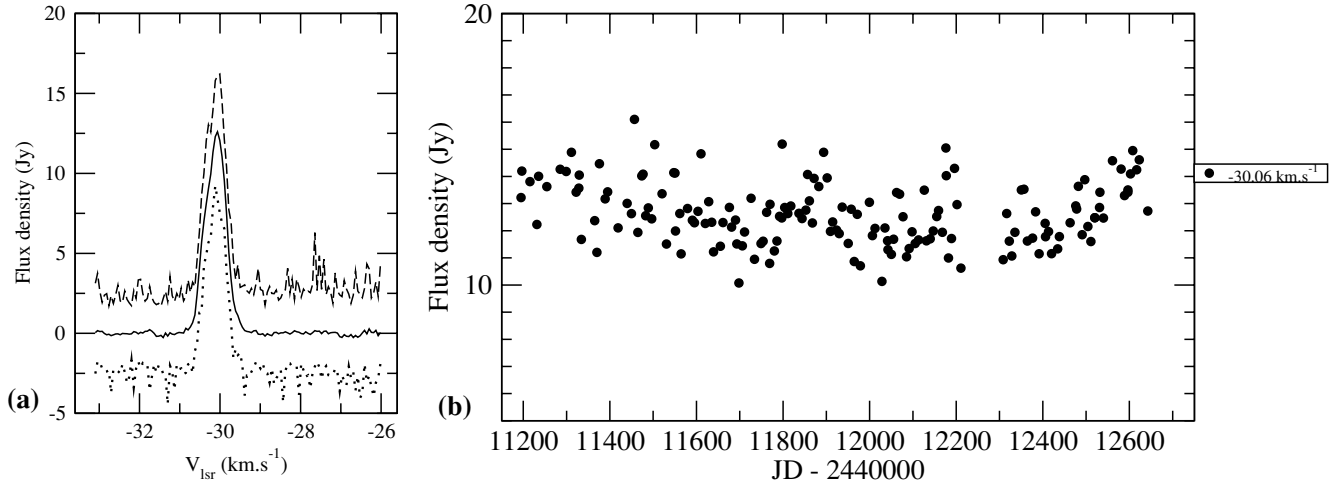

Figure 16. (a) Range of variation in spectrum of G298.26+0.74. The solid, dashed and dotted lines are the averaged spectrum, the upper envelope and the lower envelope, respectively. (b) Time-series for selected velocity channels.

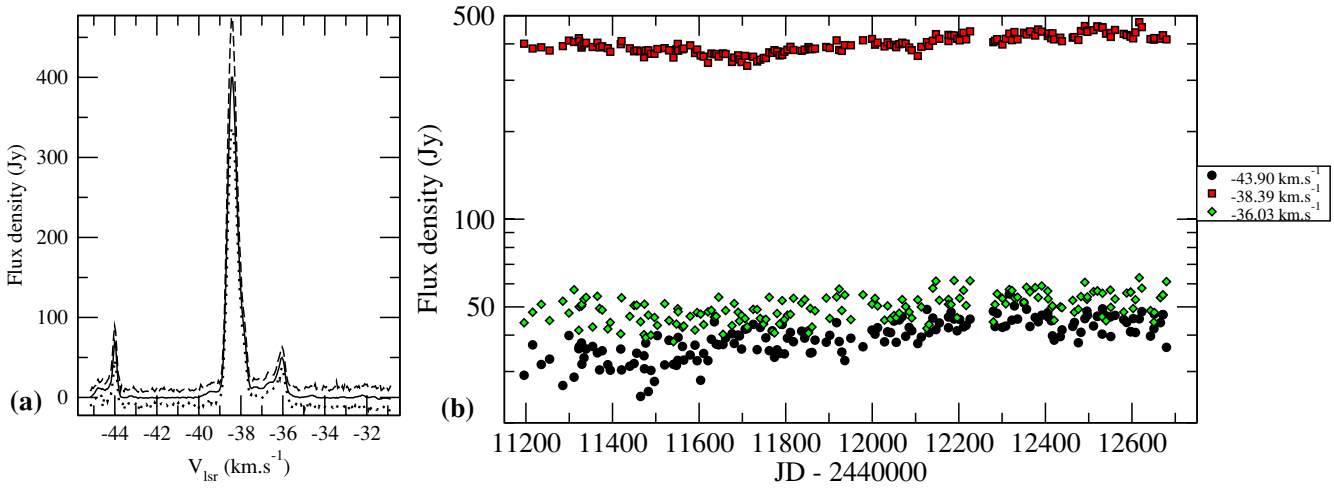

Figure 17. (a) Range of variation in spectrum of G305.21+0.21. The solid, dashed and dotted lines are the averaged spectrum, the upper envelope and the lower envelope, respectively. (b) Time-series for selected velocity channels.

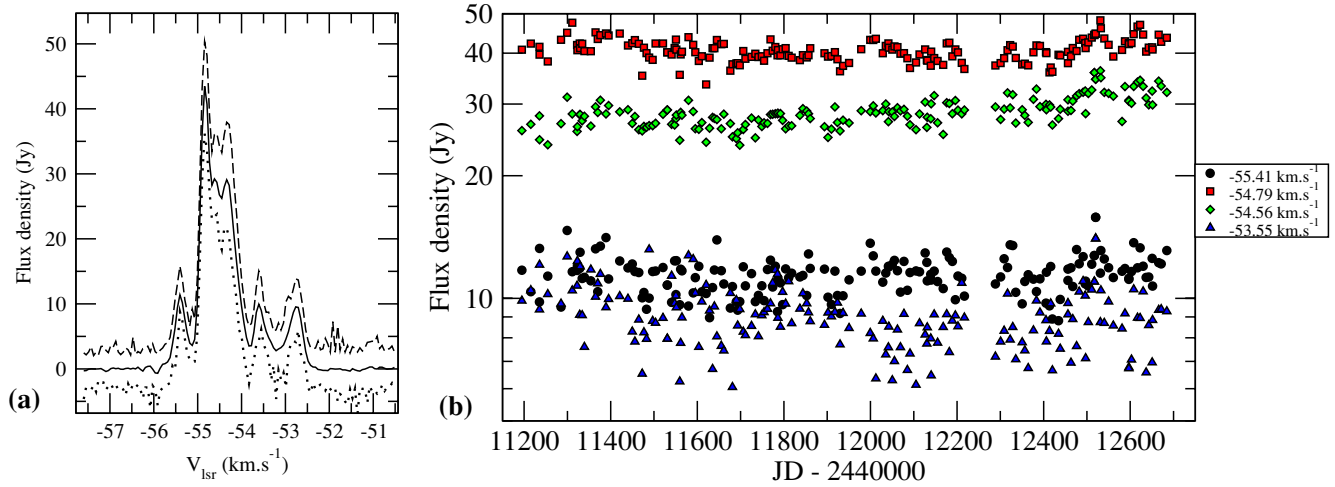

Figure 18. (a) Range of variation in spectrum of G308.92+0.12. The solid, dashed and dotted lines are the averaged spectrum, the upper envelope and the lower envelope, respectively. (b) Time-series for selected velocity channels.

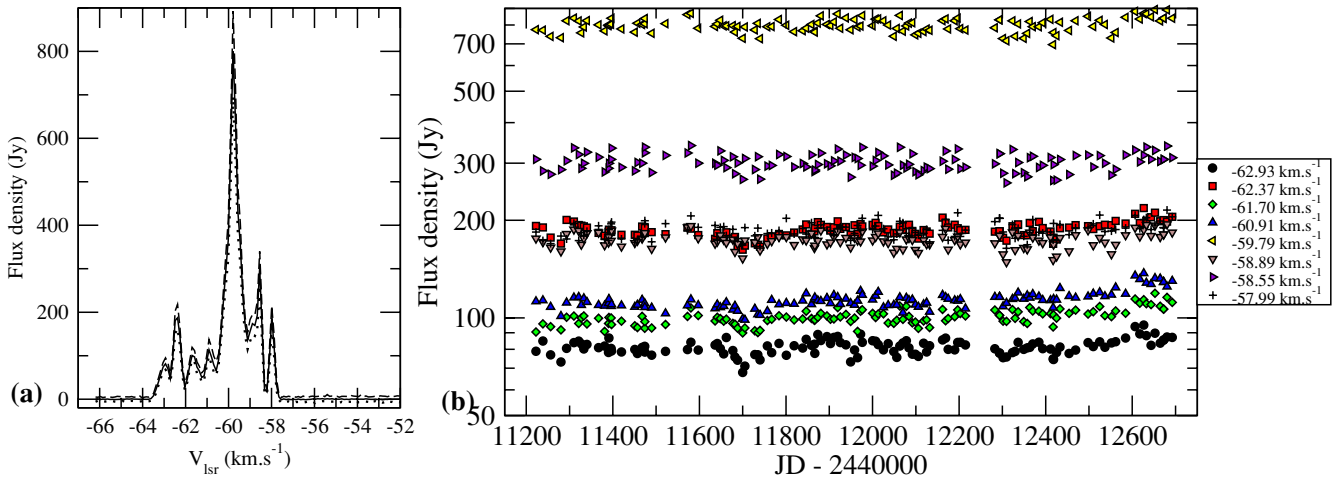

Figure 19. (a) Range of variation in spectrum of G309.92+0.48. The solid, dashed and dotted lines are the averaged spectrum, the upper envelope and the lower envelope, respectively. (b) Time-series for selected velocity channels.

G308.92+0.12 (Fig. 18). This source is not significantly variable above the noise. The maser spots have a linear distribution (Phillips et al. 1998) over 0.3 arcsec (1500 au at 5.3 kpc).

G309.92+0.48 (Fig. 19). This source does not show any significant variability, except for a slight dip in flux density seen at most of the features at JD 2451700. The maser spots are in an arc 0.8 arcsec (4000 au at 5.3 kpc) in extent and show a linear velocity gradient (Phillips et al. 1998).

G312.11+0.26 (Fig. 20). This source is very weak, with the dominant feature at −49.94 km s^{-1} being only slightly variable above the noise.

G316.64–0.09 (Figs 21 and 65). The features in the spectrum are labelled to show the corresponding spots in the maps of Phillips et al. (1998). Some of the features show a quasi-periodic variation with a mean period of 321 ± 48 d. The contour plot shows clearly that there are phase lags between different peaks, that at −22.31 km s^{-1} (I) lagging the brightest peak at −19.84 km s^{-1} (F) by 42 d, for example. The spot I is offset by 0.1 arcsec (130 au at 1.3 kpc) from the cluster of spots D, E, F and H, which are separated by less than 0.05 arcsec (65 au). Features A, B, C and G form another cluster about 0.1 arcsec south of the aforementioned cluster. The variations seen are therefore consistent with the spatial distribution of the masers.

G318.95–0.20 (Fig. 22). The features in the spectrum are labelled to show the corresponding spots in the maps of Norris et al. (1993). This source shows very weak simultaneous modulations superimposed on increases or decreases in brightness in different maser peaks. Features C, B, D and E show a correlated increase in intensity and are in a cluster 0.07 arcsec (140 au at 2 kpc) in extent. The other maser features are scattered over a region 4.5 arcsec (9000 au) in extent.

G320.23–0.29 (Fig. 23). The peaks at −62.26, −61.47 and −61.92 km s^{-1} show simultaneous, sporadic flares. The other features are not variable to within the noise. The spot map of Walsh et al. (1998) shows the maser spots scattered loosely over an area of 0.4 arcsec (1900 au at 4.7 kpc). The spots showing correlated variations are on the western side of the cluster and separated by less than 0.2 arcsec (900 au).

G322.16+0.64 (Figs 24 and 66). This source is complex and highly variable. The correlated flares occur in all the features, but

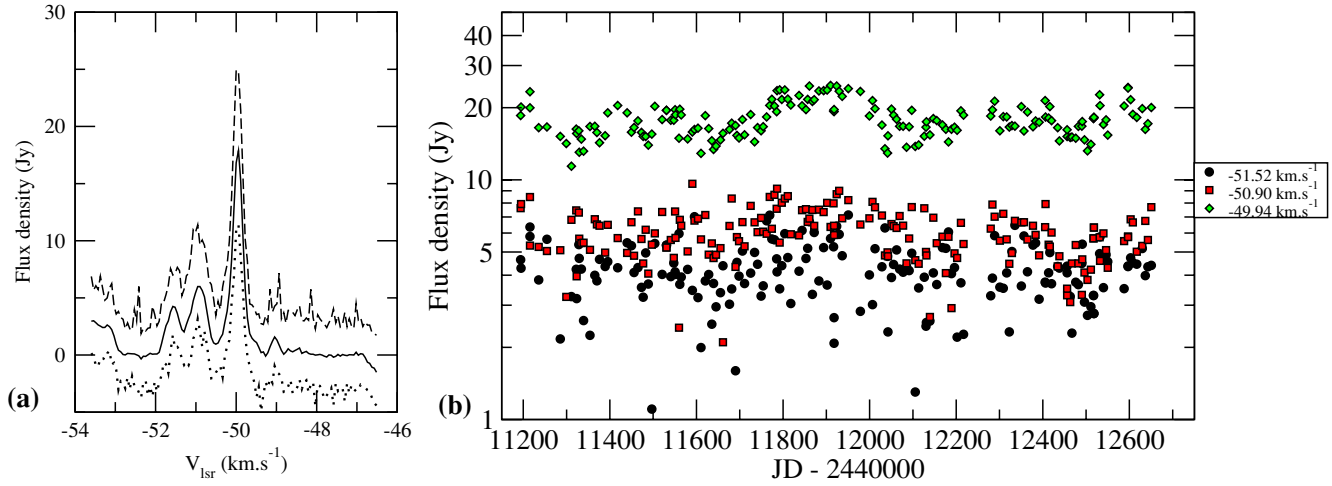

Figure 20. (a) Range of variation in spectrum of G312.11+0.26. The solid, dashed and dotted lines are the averaged spectrum, the upper envelope and the lower envelope, respectively. (b) Time-series for selected velocity channels.

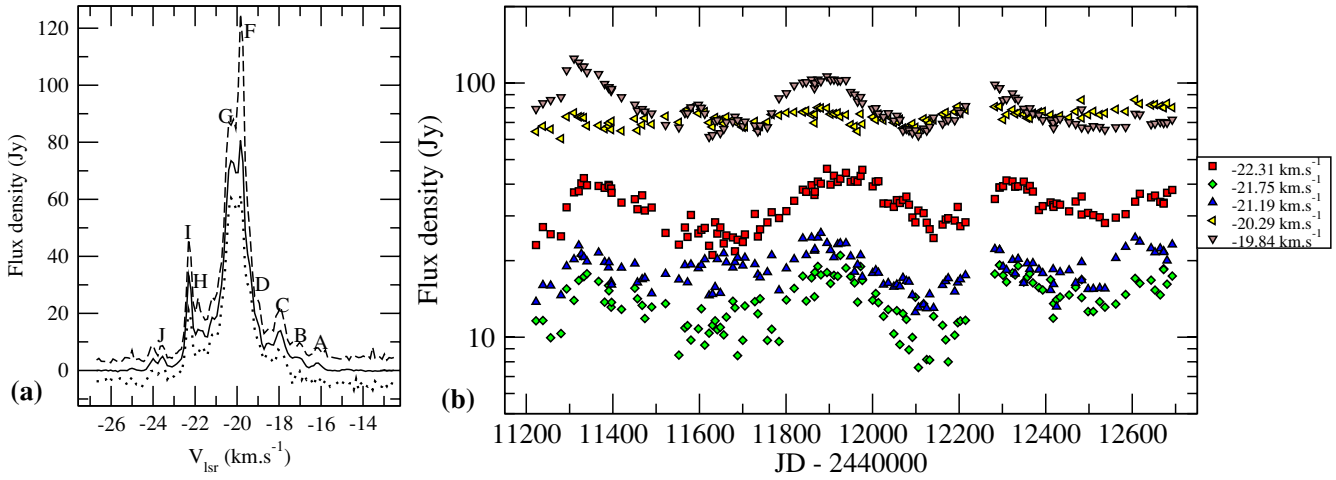

Figure 21. (a) Range of variation in spectrum of G316.64–0.09. The solid, dashed and dotted lines are the averaged spectrum, the upper envelope and the lower envelope, respectively. The spectral features are labelled following the nomenclature of Walsh et al. (1998). (b) Time-series for selected velocity channels.

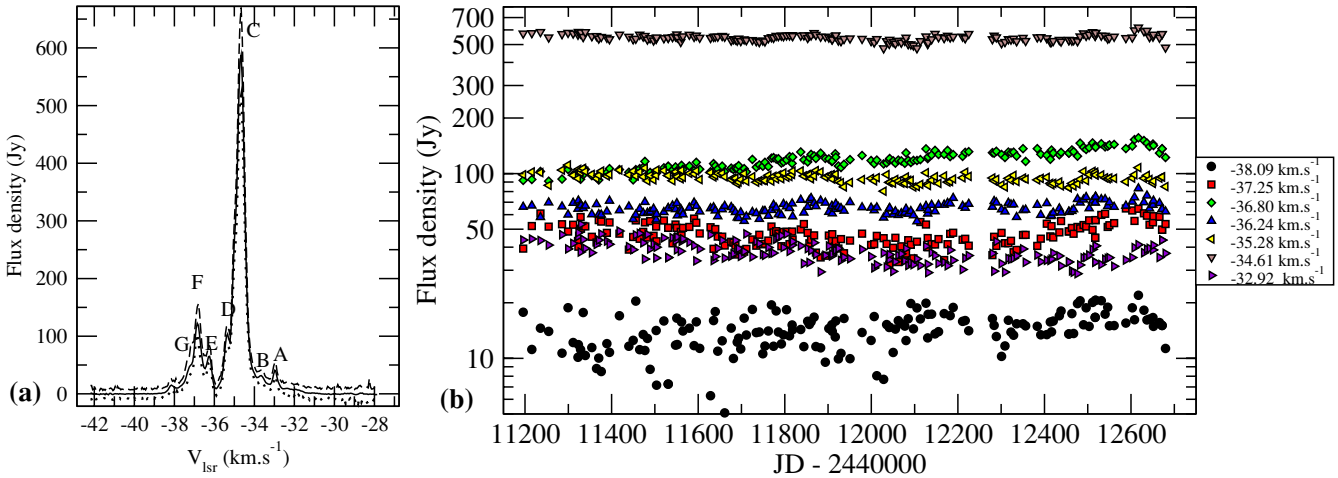

Figure 22. (a) Range of variation in spectrum of 318.95–0.20. The solid, dashed and dotted lines are the averaged spectrum, the upper envelope and the lower envelope, respectively. The spectral features are labelled following the nomenclature of Norris et al. (1993). (b) Time-series for selected velocity channels.

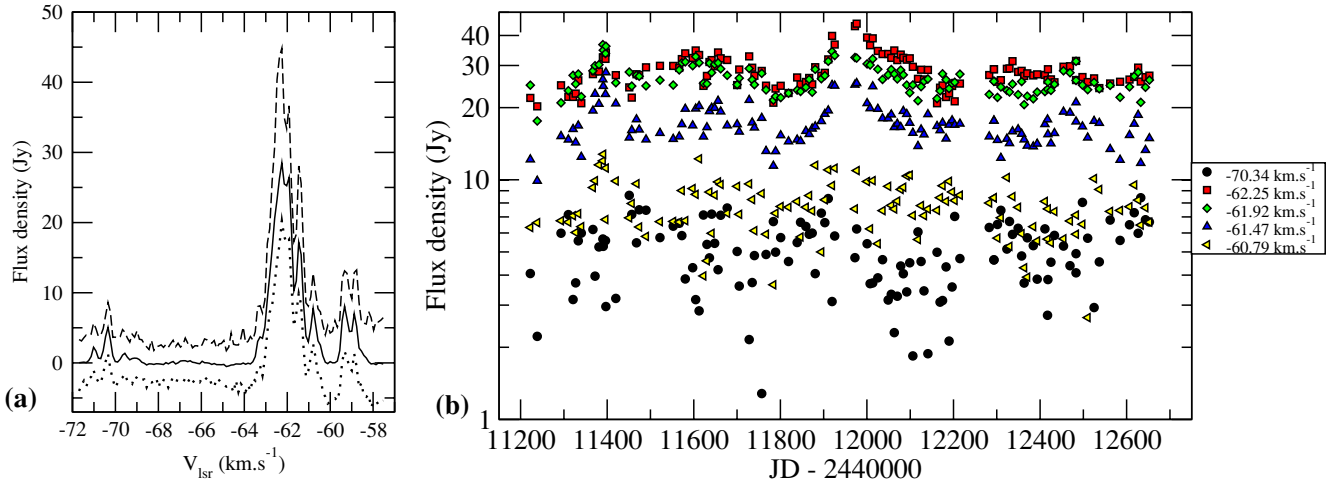

Figure 23. (a) Range of variation in spectrum of G320.23–0.29. The solid, dashed and dotted lines are the averaged spectrum, the upper envelope and the lower envelope, respectively. (b) Time-series for selected velocity channels.

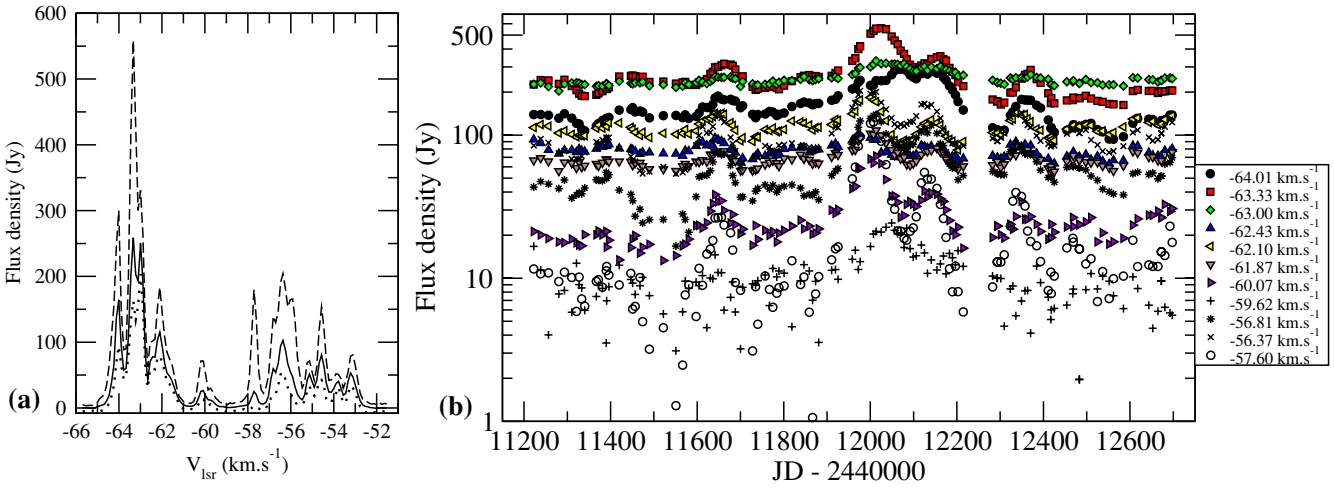

Figure 24. (a) Range of variation in spectrum of G322.16+0.64. The solid, dashed and dotted lines are the averaged spectrum, the upper envelope and the lower envelope, respectively. (b) Time-series for selected velocity channels.

the strength of the flares varies between different features. The flares are quasi-periodic with a mean interval of 176 ± 30 d between maxima. The contour plot makes phase lags in the flares in different peaks more evident than the time-series plot. This can be seen in comparing the contours for the peaks at −54.6 and −56.4 km s^{-1} and −62.1 and −63.1 km s^{-1}.

G323.77–0.21 (Fig. 25). This source is moderately variable. The variations appear to occur simultaneously and with similar percentage amplitudes at all the features. One noteworthy flare occurred around JD 2451770, when the dominant feature flared from 4000 to 5800 Jy and then decreased to its pre-flare levels. The time-series suggest that there may be a preferred interval between maxima in the variations of about 150 d. The feature at −53.09 km s^{-1} showed a slow increase in mean flux density, in addition to the correlated flares. The features from −52.5 to −47.5 km s^{-1} lie in a curve spanning 0.15 arcsec, with a linear velocity gradient, while the feature at −53.09 km s^{-1} is offset by 0.25 arcsec (750 au at 3 kpc) (Norris et al. 1993; Phillips et al. 1998).

G328.81+0.63 (Fig. 26). All the features in this source show the same trend of a slow monotonic increase in flux density, even though most of the features have a low ($I < 1$) variability index. It has a linear spot distribution covering 1 arcsec (3100 au at 3.1 kpc) but no velocity gradient (Norris et al. 1998).

G328.24–0.5 (Figs 27 and 67). Recent Australian Long Baseline Array (LBA) observations by Dodson, Ojha & Ellingsen (2004) show that there are three centres of emission are seen in the beam of the HartRAO telescope. G328.254–0.532 covers the velocity ranges from −37 to −39 km s^{-1} and −50 to −49 km s^{-1}. These masers are moderately variable. G328.237–0.548 covers the velocity range from −42 to −47 km s^{-1} and has an angular extent of 300 mas (900 au at 3 kpc). The feature at −44.28 km s^{-1} shows variations with a period of 216 d and this is seen, but less clearly, in the weaker emission from the other features in this cluster. G328.327–0.548W has emission in the range −31 to −37 km s^{-1} but is too weak to monitor with the HartRAO antenna.

G331.13–0.24 (Figs 28 and 68). The spectra are labelled to show the corresponding spots in the map of Phillips et al. (1998). There are three sets of maser features: A to F form a cluster 0.2 arcsec (960 au at 4.8 kpc) in extent, G is 0.3 arcsec (1400 au) south of the

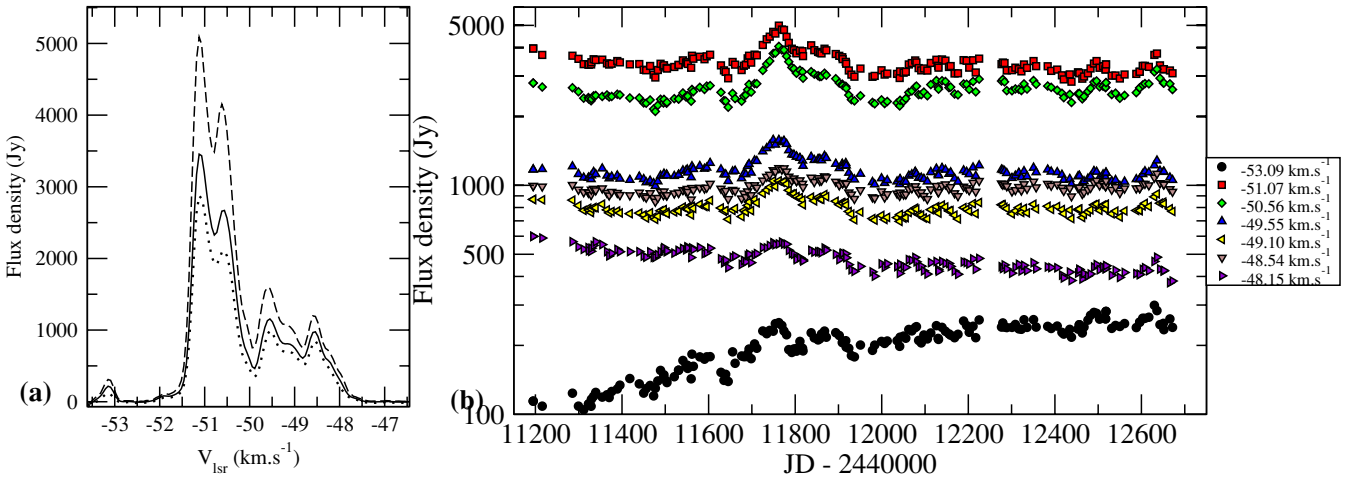

Figure 25. (a) Range of variation in spectrum of G323.77–0.21. The solid, dashed and dotted lines are the averaged spectrum, the upper envelope and the lower envelope, respectively. (b) Time-series for selected velocity channels.

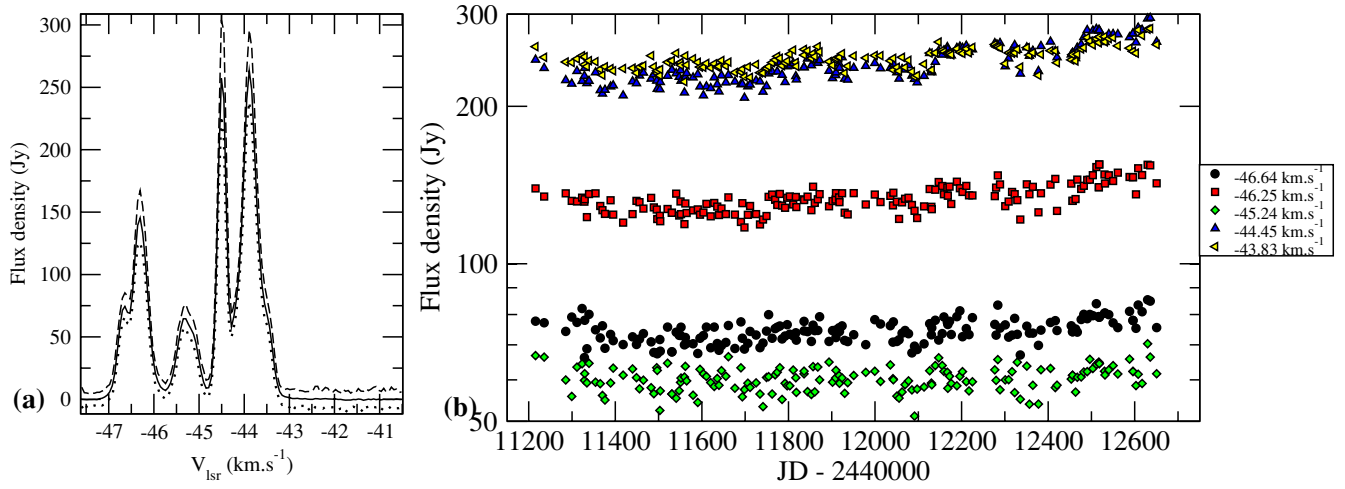

Figure 26. (a) Range of variation in spectrum of G328.81+0.63. The solid, dashed and dotted lines are the averaged spectrum, the upper envelope and the lower envelope, respectively. (b) Time-series for selected velocity channels.

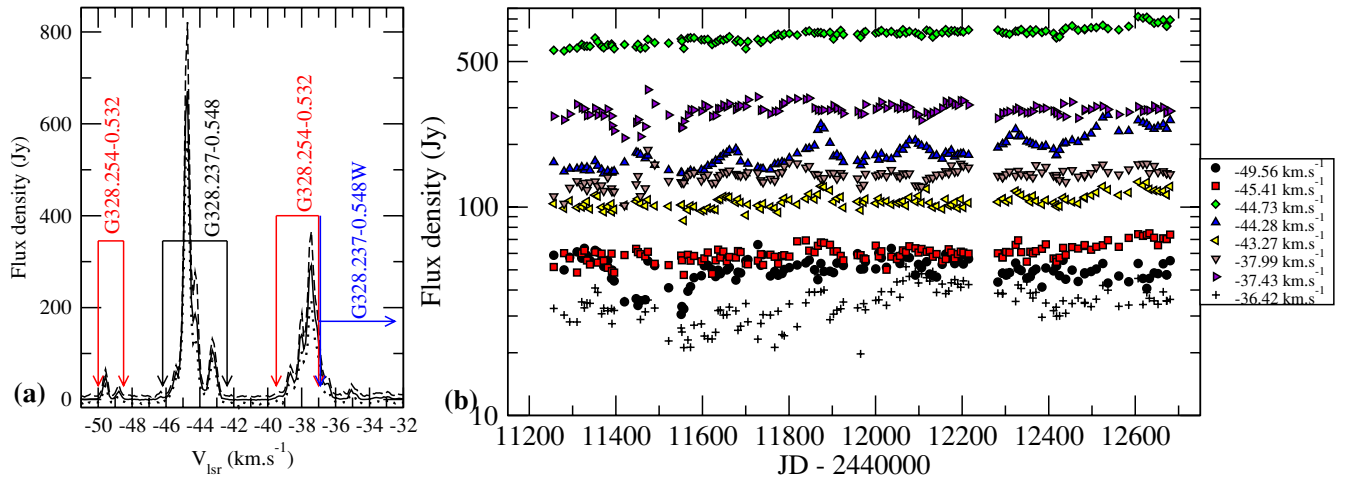

Figure 27. (a) Range of variation in spectrum of G328.24–0.5. The velocity ranges of the three centres of emission identified by Dodson et al. (2004) are indicated. The solid, dashed and dotted lines are the averaged spectrum, the upper envelope and the lower envelope, respectively. (b) Time-series for selected velocity channels.

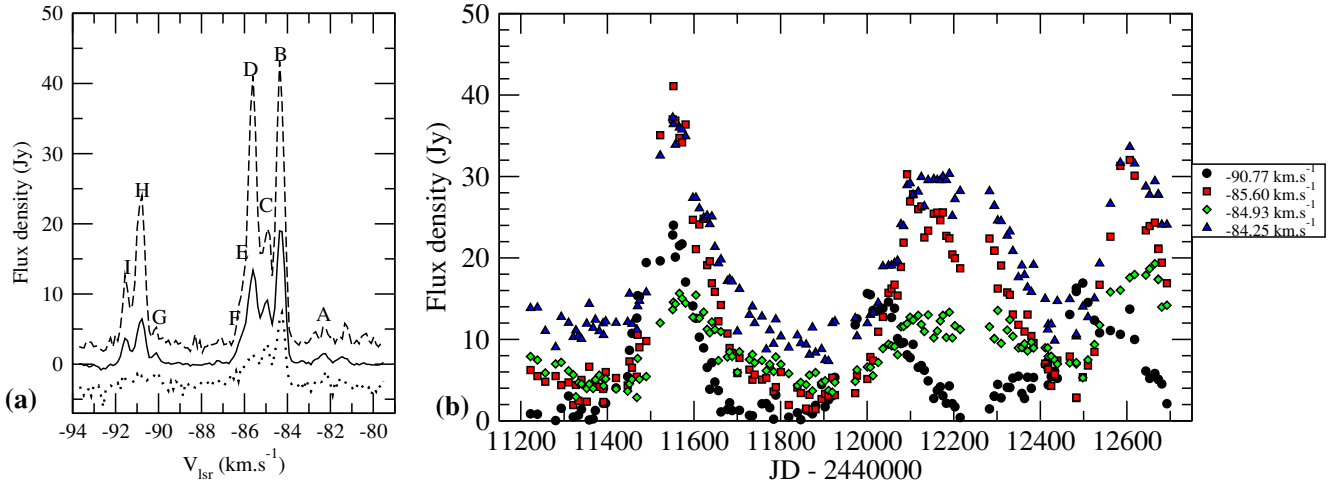

Figure 28. (a) Range of variation in spectrum of G331.13–0.24. The solid, dashed and dotted lines are the averaged spectrum, the upper envelope and the lower envelope, respectively. The spectral features are labelled following the nomenclature of Phillips et al. (1998) b. Time-series for selected velocity channels.

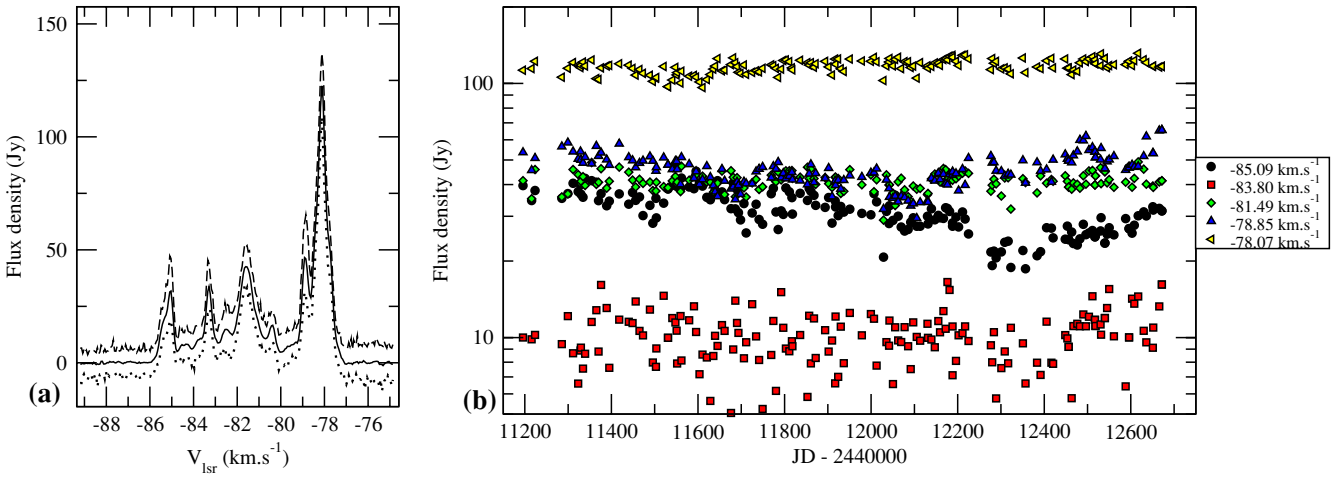

Figure 29. (a) Range of variation in spectrum of G331.28–0.19. The solid, dashed and dotted lines are the averaged spectrum, the upper envelope and the lower envelope, respectively. (b) Time-series for selected velocity channels.

main cluster while H and I are at 0.5 arcsec (2400 au) to the west of the main cluster. This source is highly variable. The features B to F show simultaneous periodic flares with an apparent period of 572 d, while G and I show similar behaviour but with a period of 472 d. The other maser features are too weak to monitor. The contour plot shows the behaviour very clearly. The features at −91.56 and −90.77 km s^{-1} are below the detection limit for almost 50 per cent of the cycle.

G331.28–0.19 (Fig. 29). Most of the features are not significantly variable, except for the feature at −85.09 km s^{-1}, which had been gradually decreasing in flux density since the start of the monitoring program. However, the maser feature started increasing in flux density towards the end of the observing period. The spots form an elongated cluster spanning 0.1 arcsec (500 au) on the long axis (Phillips et al. 1998). The variable feature does not appear to be offset from the other maser spots.

G335.55–0.31 (Fig. 30). This source is very weak and shows no variability to within the noise.

G336.01–0.82 (Fig. 31). The features are not significantly variable, except for the feature at −53.41 km s^{-1}, which has shown an overall decline in intensity coupled with small amplitude, irregular variations throughout the monitoring period. This maser spot is at the northern edge of a loosely scattered cluster of spots and 0.05 arcsec from the nearest maser spot (Walsh et al. 1998).

G336.99–0.03 (Fig. 32). The feature at −125.88 km s^{-1} shows sporadic flares at intervals of 200 to 400 d, causing changes in intensity of up to 50 per cent. The other features are very weak and show no variation to within the noise.

G337.92–0.46 (Fig. 33). The peak at −38.73 km s^{-1} increased from 20 to 50 Jy and then decreased back to 20 Jy after about 1.5 yr. In contrast, the −37.83 km s^{-1} feature showed only slight variations during this period. The spot map of Walsh et al. (1998) shows these maser spots separated by 0.16 arcsec (500 au at 3 kpc).

G338.92–0.06 (Figs 34 and 69). The −41.99 km s^{-1} feature shows remarkable, high-amplitude variations with a period of 132 d, which are well visualized in the contour plot. The time-range of the observations covers 12 cycles. The weaker maser feature at −41.37 km s^{-1} shows only slight indications of this periodicity.

G339.62–0.12 (Figs 35 and 70). The spectrum is labelled to show the corresponding spots in the map of Walsh et al. (1998). The

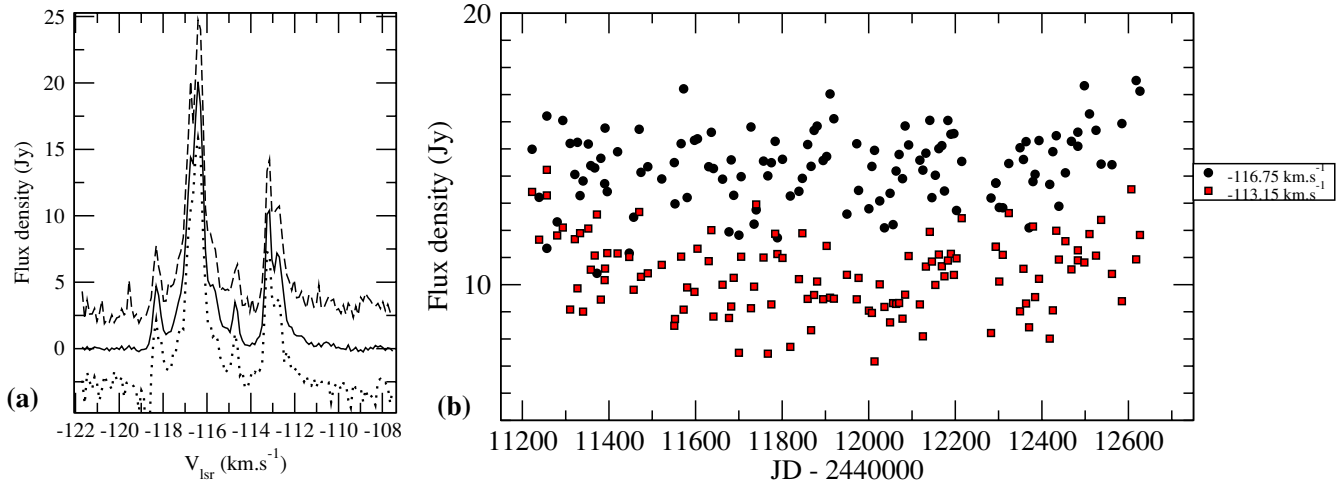

Figure 30. (a) Range of variation in spectrum of G335.55–0.31. The solid, dashed and dotted lines are the averaged spectrum, the upper envelope and the lower envelope, respectively. (b) Time-series for selected velocity channels.

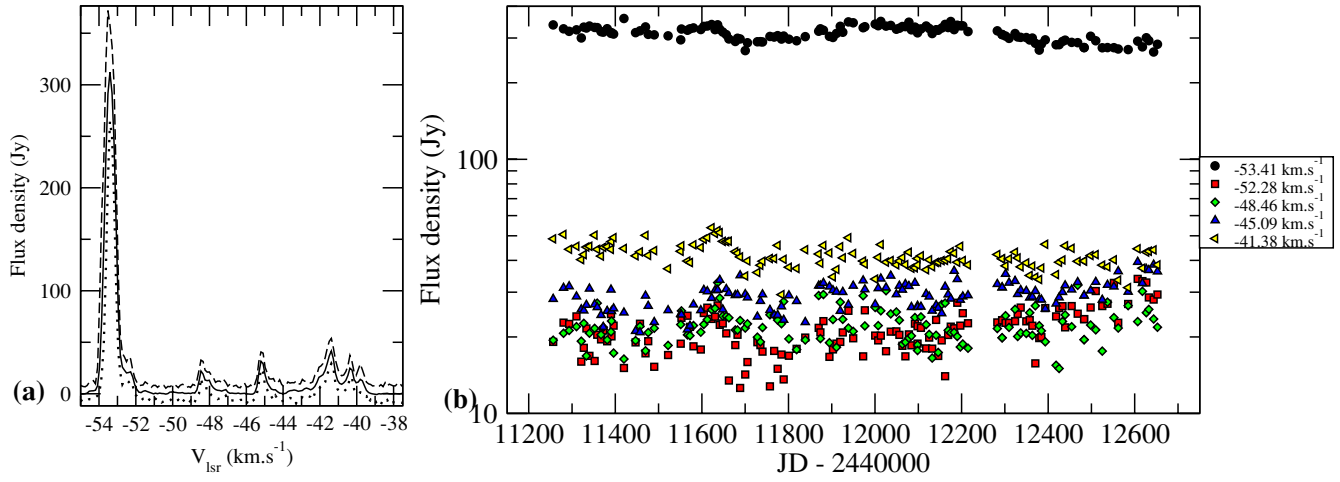

Figure 31. (a) Range of variation in spectrum of G336.01–0.82. The solid, dashed and dotted lines are the averaged spectrum, the upper envelope and the lower envelope, respectively. (b) Time-series for selected velocity channels.

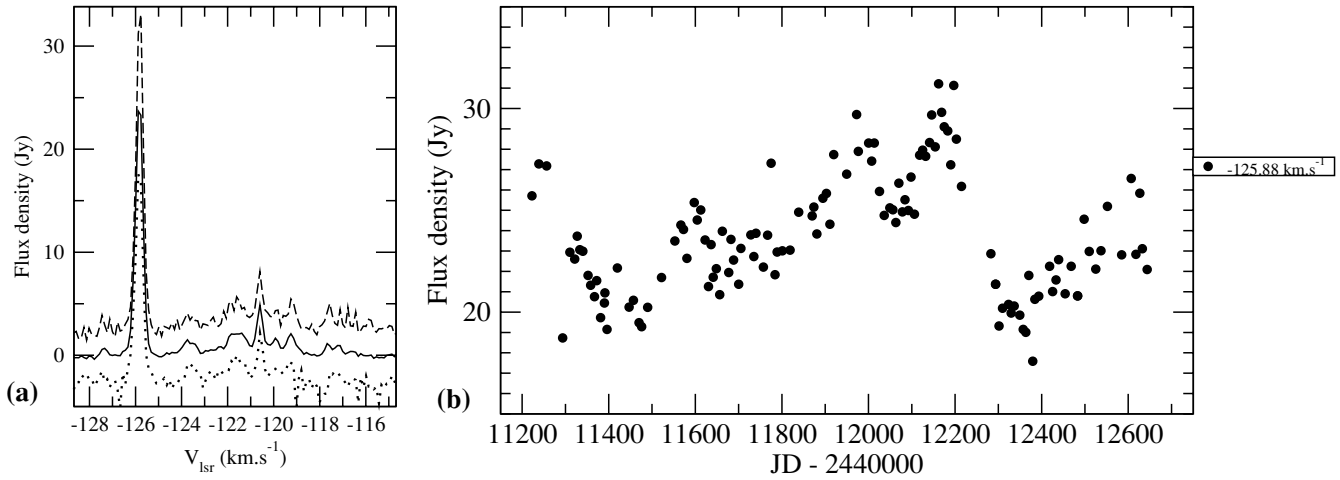

Figure 32. (a) Range of variation in spectrum of G336.99–0.03. The solid, dashed and dotted lines are the averaged spectrum, the upper envelope and the lower envelope, respectively. (b) Time-series for selected velocity channels.

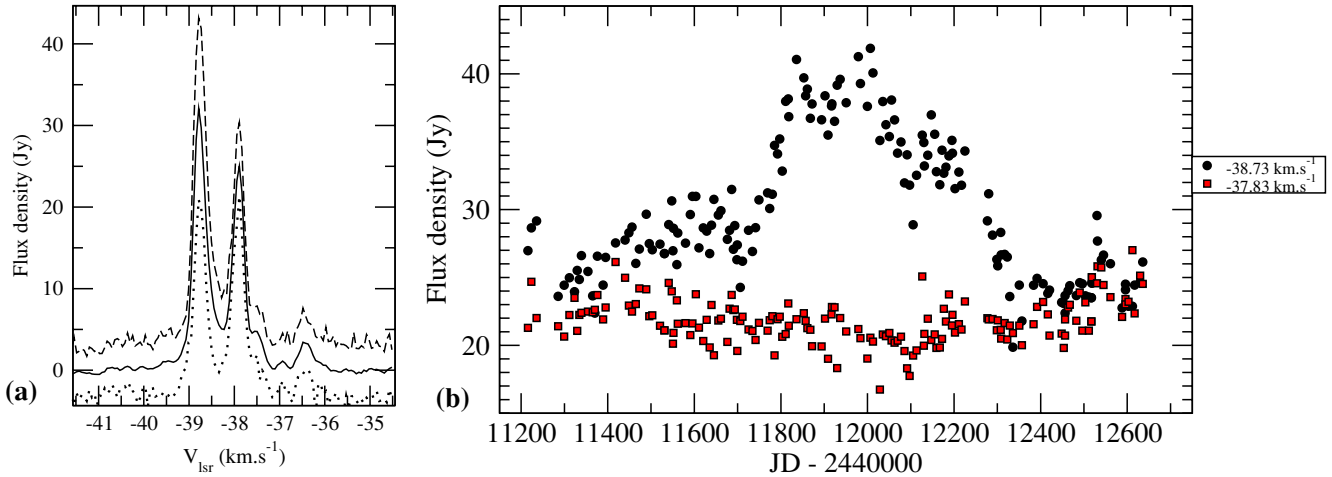

Figure 33. (a) Range of variation in spectrum of G337.92–0.46. The solid, dashed and dotted lines are the averaged spectrum, the upper envelope and the lower envelope, respectively. (b) Time-series for selected velocity channels.

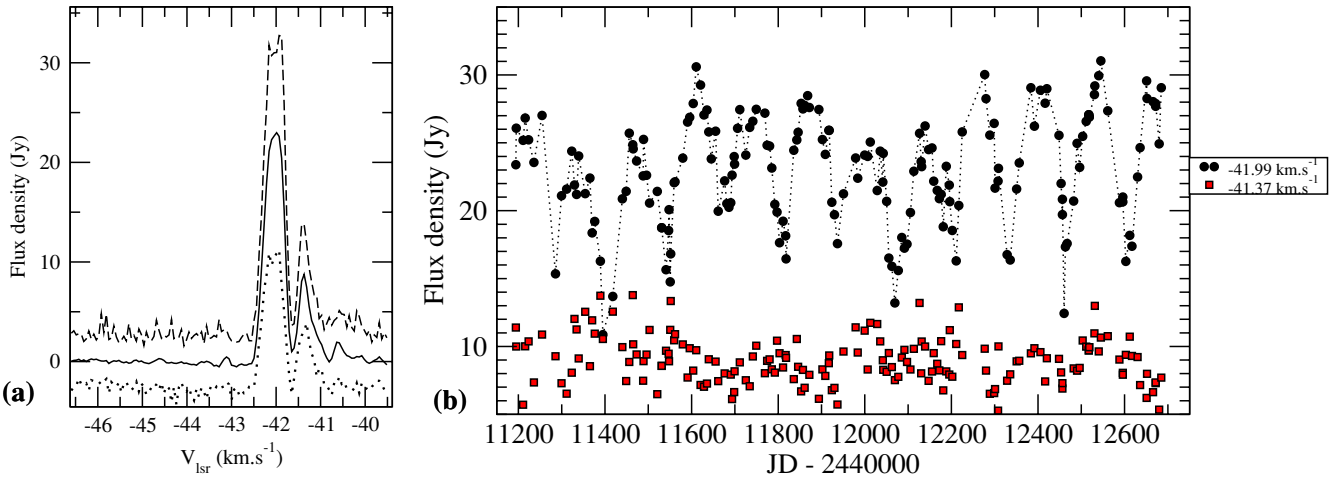

Figure 34. (a) Range of variation in spectrum of G338.92–0.06. The solid, dashed and dotted lines are the averaged spectrum, the upper envelope and the lower envelope, respectively. (b) Time-series for selected velocity channels.

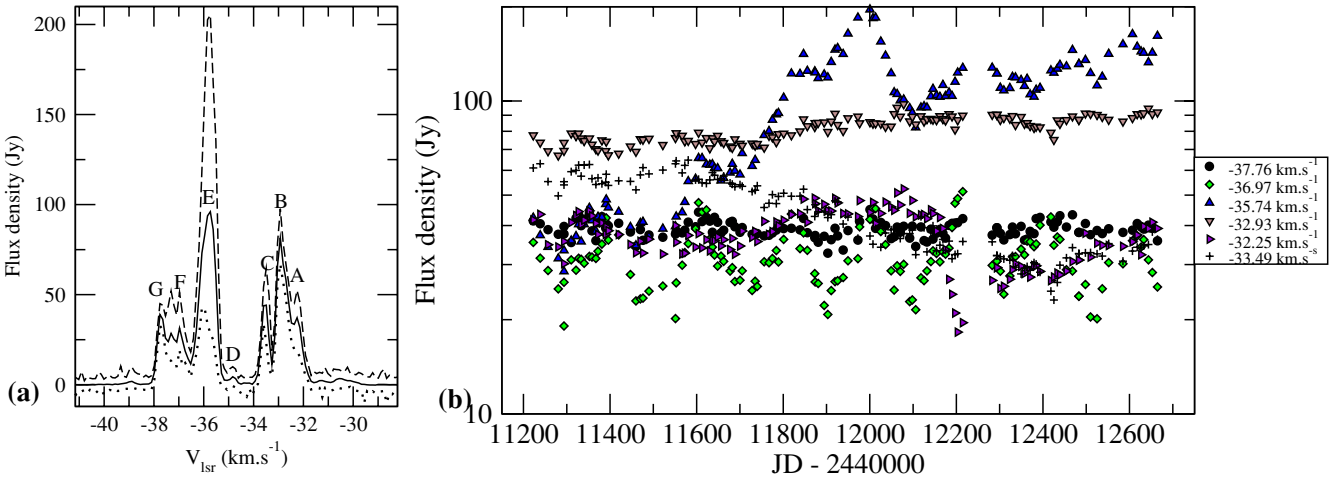

Figure 35. (a) Range of variation in spectrum of G339.62–0.12. The solid, dashed and dotted lines are the averaged spectrum, the upper envelope and the lower envelope, respectively. The spectral features have been labelled following the nomenclature of Walsh et al. (1998). (b) Time-series for selected velocity channels.

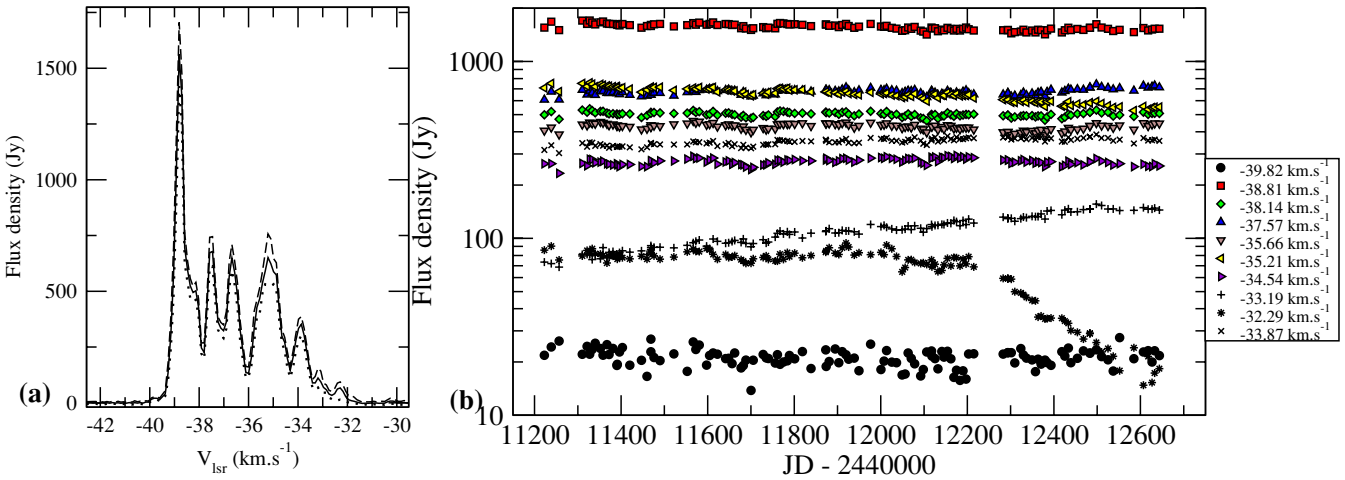

Figure 36. (a) Range of variation in spectrum of G339.88–1.26. The solid, dashed and dotted lines are the averaged spectrum, the upper envelope and the lower envelope, respectively. (b) Time-series for selected velocity channels.

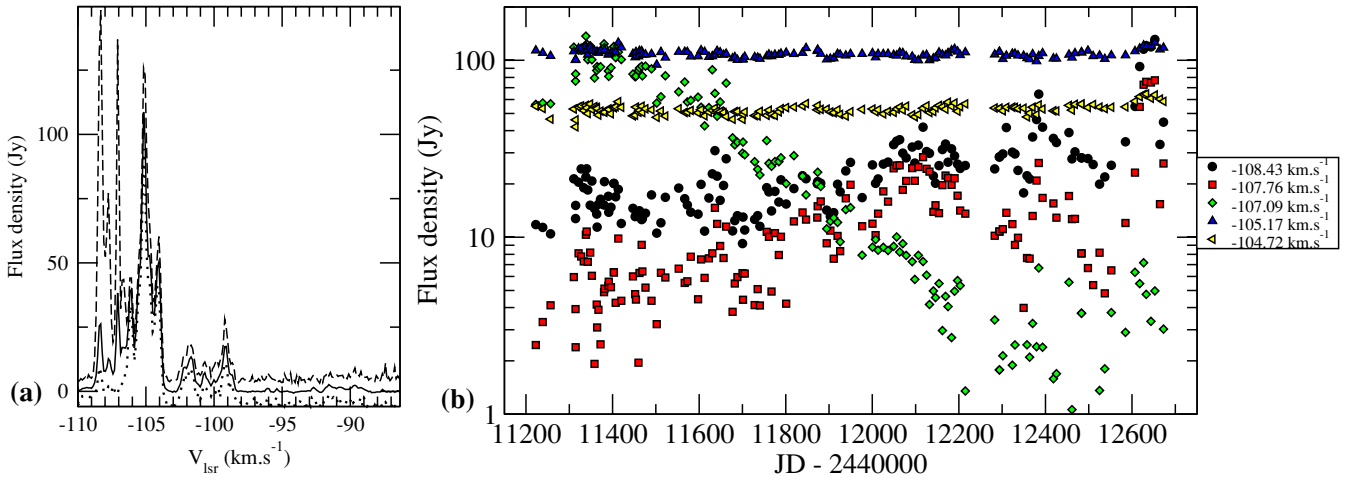

Figure 37. (a) Range of variation in spectrum of G340.79–0.10. The solid, dashed and dotted lines are the averaged spectrum, the upper envelope and the lower envelope, respectively. (b) Time-series for selected velocity channels.

majority of the peaks in this source are variable. The group of features in the velocity range from −38 to −35.5 km s^{-1} (D–G) show simultaneous periodic flares with a period of 202 d. In the peak at −35.74 km s^{-1} (E), a flare lasting from JD 2451700 to 2452100 is superimposed on this behaviour. The features from −32 to −34 km s^{-1} (A–C) show much smaller variations, which appear to lag behind those of the other group. The maser at −32.25 km s^{-1} (A) underwent a very rapid fall from 40 to 20 Jy at JD 2452200, followed by a slow recovery. The contour plot assists considerably in visualizing the variations. The spatial distribution of the maser spots is complex, but the clustering of the maser spots is consistent with the variability seen. Features A, B and C are clustered together with an angular extent less than 0.1 arcsec. Features D, E and F are 0.6 arcsec away (1800 au at 3 kpc). G is directly north of D–F and about 0.3 arcsec from both A–C and D–F. However, the position uncertainty in the ATCA spot map is of the order of 0.1 arcsec. High-resolution maps of this maser region will be needed to interpret the correlations and time-delays in the periodic flares.

G339.88–1.26 (Fig. 36). The majority of the features in this source are not significantly variable. The velocity features at −38.81 and −35.21 km s^{-1} have been showing a slow decrease in flux density over the monitoring period. The feature at −33.19 km s^{-1} shows a monotonic increase in flux density from 79 to 143 Jy. The feature at −32.29 km s^{-1} remained relatively constant at 75 Jy until about JD 2452200, after which it decayed to 15 Jy, but it may have begun to recover near the end of the monitoring period. The maser spots have a linear distribution spanning 0.7 arcsec but do not show a velocity gradient (Norris et al. 1998).

G340.79–0.10 (Fig. 37). This source has a complex spectrum in which the features in the range −110 to −106.5 km s^{-1} are highly variable, but those at less negative velocities are essentially constant. The feature at −107.09 km s^{-1} initially had a flux density of 140 Jy but decayed monotonically to about 2 Jy. The spot maps of Phillips et al. (1998) show a complex distribution covering 0.6 arcsec. Because the spectral features show strong velocity blending, high-resolution maps at each velocity channel will be necessary in order to interpret the variability.

G344.23–0.57 (Fig. 38). The feature at −26.41 km s^{-1} is moderately variable, but the remainder show little or no variation to within the noise. The maser spots lie in a curve 1 arcsec in extent but show no velocity gradient (Walsh et al. 1998). The variable feature is 0.2 arcsec from the nearest maser spot.

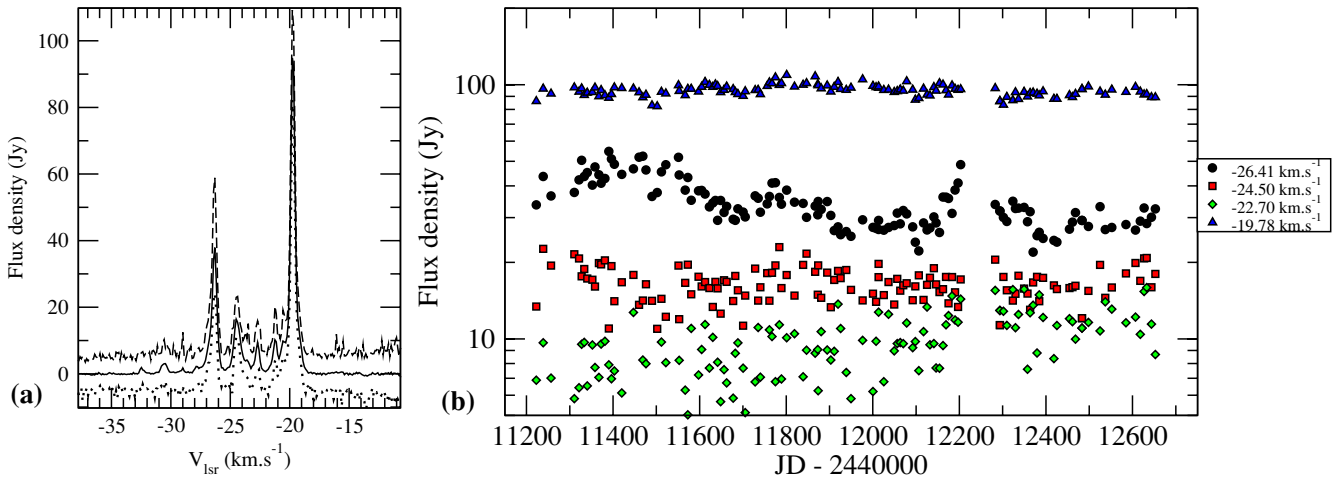

Figure 38. (a) Range of variation in spectrum of G344.23–0.57. The solid, dashed and dotted lines are the averaged spectrum, the upper envelope and the lower envelope, respectively. (b) Time-series for selected velocity channels.

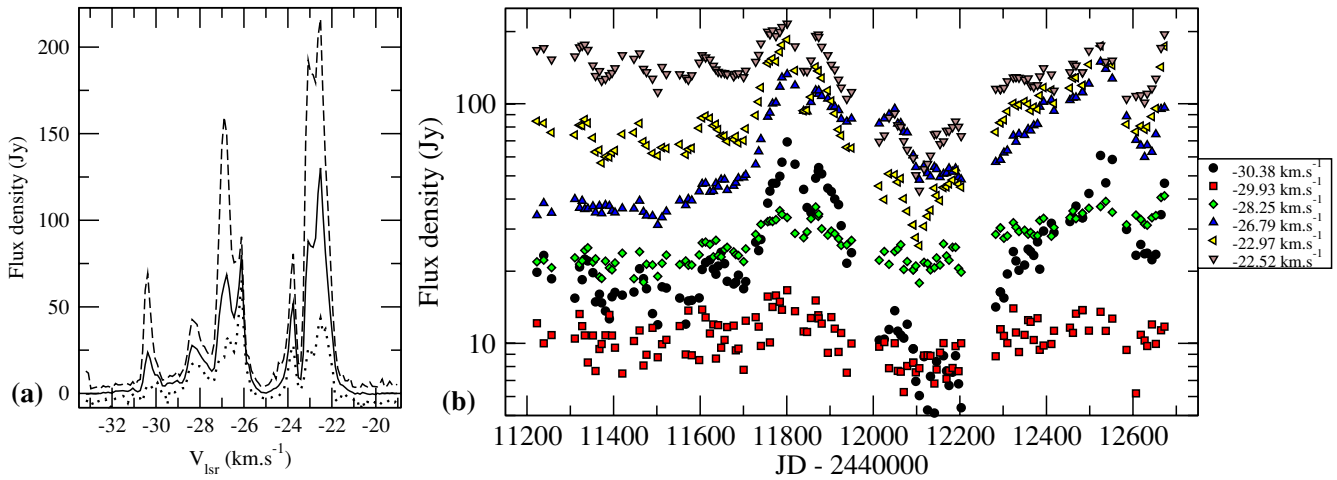

Figure 39. (a) Range of variation in spectrum of G345.00–0.22. The solid, dashed and dotted lines are the averaged spectrum, the upper envelope and the lower envelope, respectively. (b) Time-series for selected velocity channels.

G345.00–0.22 (Figs 39 and 71). The masers are highly variable, with simultaneous flares. The most extreme behaviour is seen in the feature at -30.38 km s^{-1}, which ranged from 5 to 70 Jy. By contrast with the strongly varying bright peaks, the weakest peak plotted in the time-series, at -29.93 km s^{-1}, shows the least variability. The contour plot shows that two flares across the whole spectrum stand out at JD 2451800 and 2452540. The spatial distribution of the spots is complex, with two distinct groups of spots seen (Walsh et al. 1998). However, the peak velocities listed by Walsh et al. (1998) do not correspond to those seen in the HartRAO spectra and it is not possible to identify the maser spots without a reference spectrum. It is likely that the relative intensities of the masers have changed considerably since the ATCA observations in 1994/1995. The velocity features appear to be heavily blended, thus high-resolution maps at each velocity channel are necessary to understand the structure of this maser source.

G345.50+0.35 (Figs 40 and 72). This source is highly variable. The different features show the same pattern of flares but the progression of the flares varies. There appears to be a slight time-lag in the flares across the spectrum, with the maxima occurring first at -17.67 km s^{-1}. The maser spots have a complex distribution (Walsh et al. 1998) with no obvious correlation between the spatial distribution and the time-lags. However, the uncertainty in the ATCA maps is of the same order as the separation between maser spots.

G351.42+0.64/NGC6334F (Fig. 41). The feature at -5.88 km s^{-1} has the highest variability index in the entire sample. It is below the detection limit for most of the monitoring period. The three brightest masers show a very slow increase in brightness, but with very little short term variability. The two weaker features at -7.34 and -2.62 km s^{-1} show well correlated variations. The maser spots occur in a line, but a position–velocity diagram shows two lines with opposite slopes, implying the presence of two Keplerian discs with opposite rotations (Norris et al. 1998). Higher resolution maps will be necessary for further analysis because there is a high degree of blending in the spectral features, as evidenced by differing behaviour in the time-series, but the existing spot maps only show a few features.

G351.58–0.35 (Fig. 42). The variability indices indicate that this source is not variable to within the noise. Visual inspection of the data indicates a possible weak modulation of the time-series of the -94.28 km s^{-1} feature but the amplitude would be of the order of 1 Jy, which is less than the expected calibration error of 2.1 Jy. The

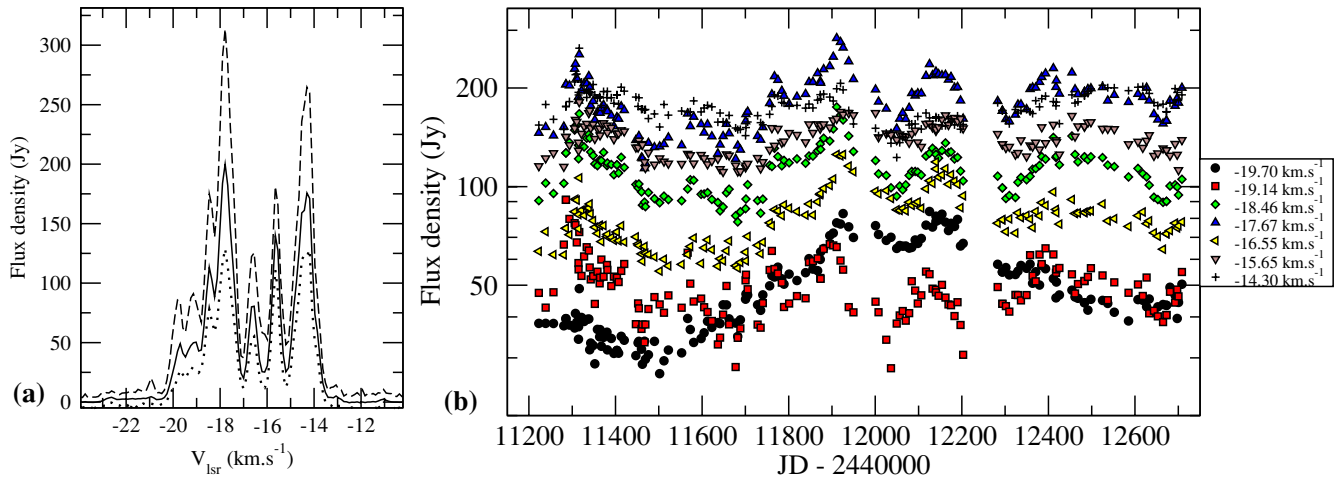

Figure 40. (a) Range of variation in spectrum of G345.50+0.35. The solid, dashed and dotted lines are the averaged spectrum, the upper envelope and the lower envelope, respectively. (b) Time-series for selected velocity channels.

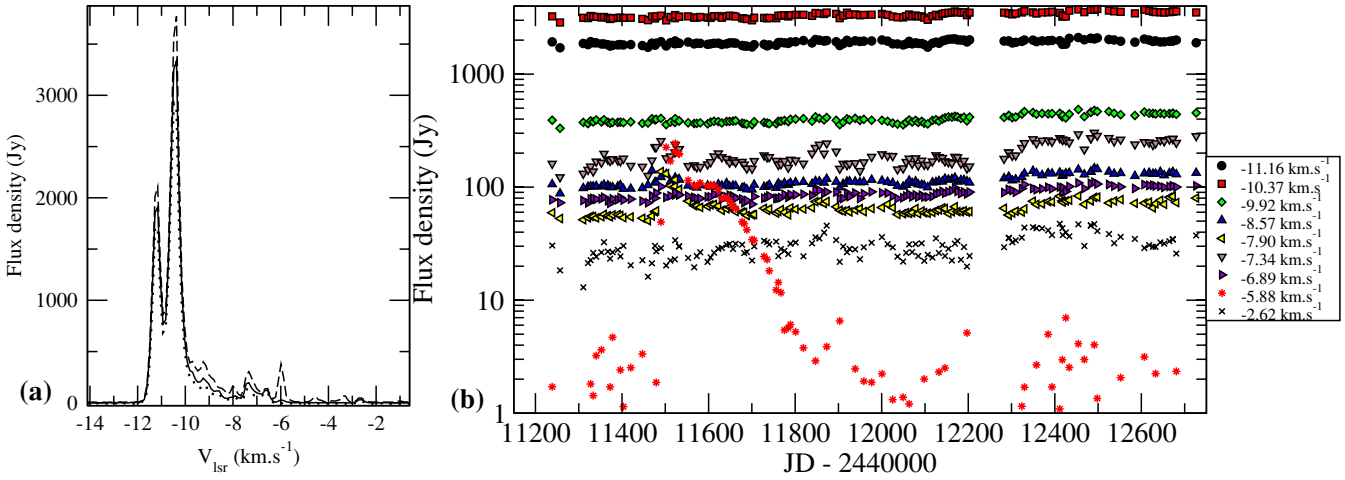

Figure 41. (a) Range of variation in spectrum of G351.42+0.64. The solid, dashed and dotted lines are the averaged spectrum, the upper envelope and the lower envelope, respectively. (b) Time-series for selected velocity channels.

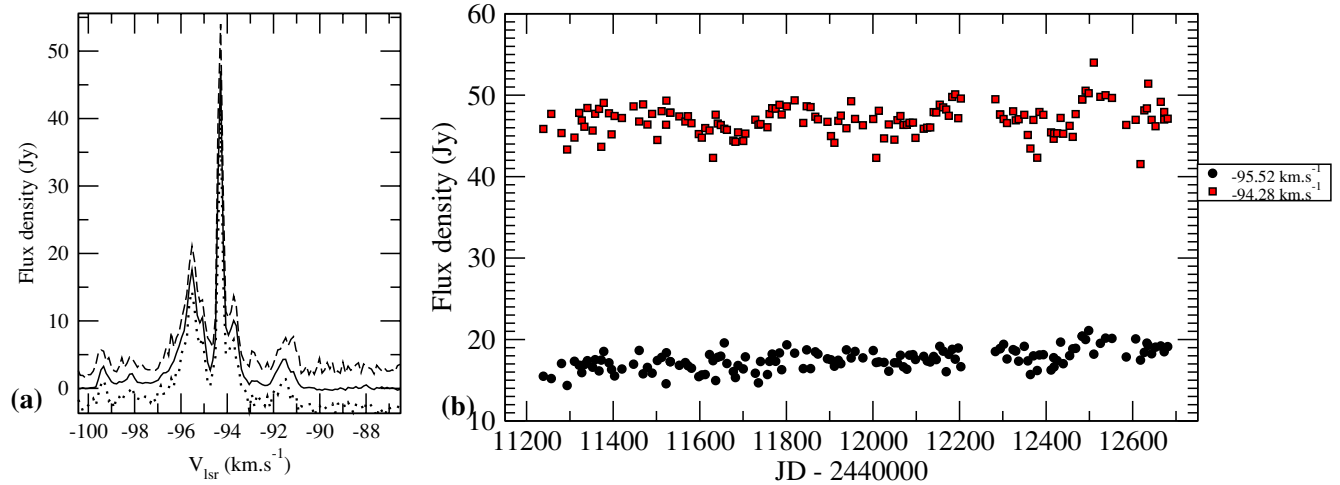

Figure 42. (a) Range of variation in spectrum of G351.58–0.35. The solid, dashed and dotted lines are the averaged spectrum, the upper envelope and the lower envelope, respectively. (b) Time-series for selected velocity channels.

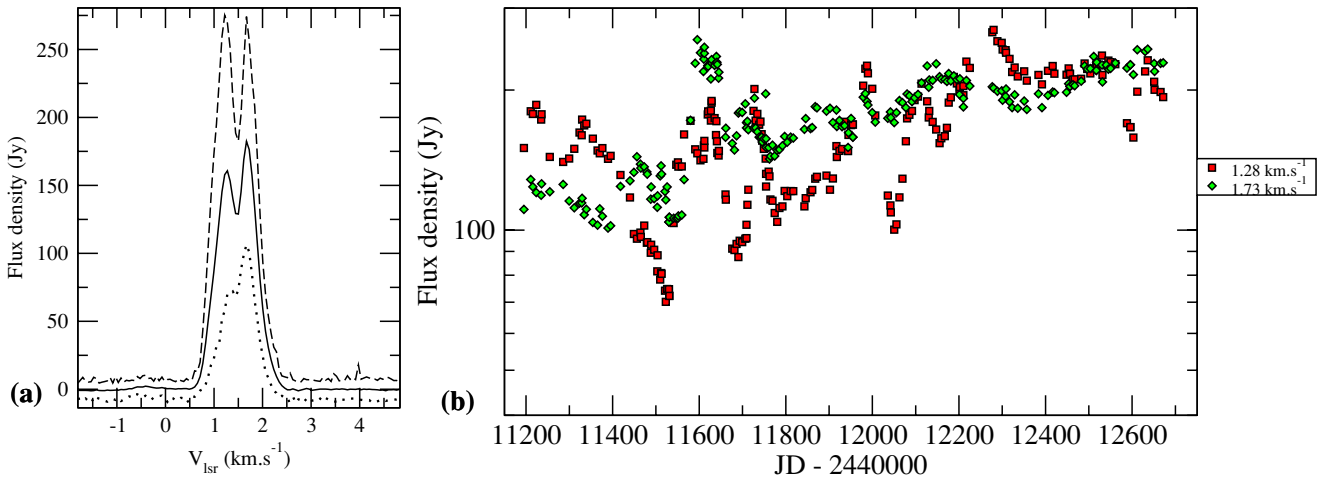

Figure 43. (a) Range of variation in spectrum of G351.78–0.54. The solid, dashed and dotted lines are the averaged spectrum, the upper envelope and the lower envelope, respectively. (b) Time-series for selected velocity channels.

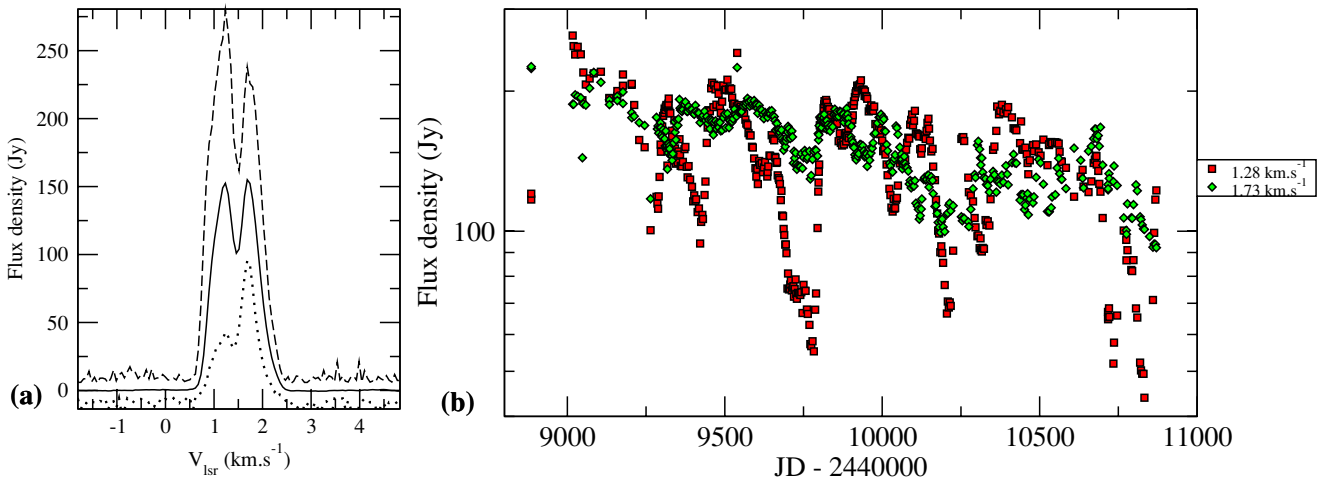

Figure 44. Monitoring data for G351.78–0.54 in the years 1992 to 1998. (a) Range of variation in the spectrum. The solid, dashed and dotted lines are the averaged spectrum, the upper envelope and the lower envelope, respectively. (b) Time-series for selected velocity channels.

maser spots have a complex distribution (Walsh et al. 1998) with an angular extent of over 2 arcsec. The variable feature is at the edge of the cluster and 0.4 arcsec (2700 au at 6.7 kpc) from any of the other maser features. It is likely that this maser is associated with a different exciting source from the other masers.

G351.78–0.54 (Figs 43, 44, 73 and 74). This source is highly variable. The two peaks show uncorrelated, cyclical behaviour with a characteristic time-scale of about three months. The flares in the peak at 1.21 km s^{-1} show a delay in the progression of the flare across this peak. The flares start at the higher velocities, with the intensities at lower velocities gradually increasing. The rate at which the flare propagates through the maser feature varies from one flare to another. This behaviour was first reported by MacLeod & Gaylard (1996), for observations from 1993 to mid-1995, and interpreted by them as being caused by a clumpy outflow passing behind an extended maser structure. The HartRAO data set for this source includes data from 1992 to 1998, with observation parameters as described in MacLeod & Gaylard (1996). The time-series shown in Fig. 44 and the intensity contour plot in Fig. 74 covers the time-range 1992 September to 1998 February. The behaviour in the two monitoring periods is essentially the same. However, the gradual overall decay in intensity in the first period was reversed in the second. The contour plots provide a clearer indication of the behaviour, and how it differs in the two peaks. The maps of Norris et al. (1998) show only two maser spots corresponding to each of the two velocity peaks. Higher resolution observations would need to be done in order to determine whether the maser features do in fact have an extended structure.

G354.61–0.47 (Fig. 45). This source is moderately variable, with simultaneous variations being most evident in the flares at JD 2451610 and 2452350. The weak blended 'shoulder' at −25.40 km s^{-1} shows the largest relative variation. The feature at −16.18 km s^{-1} nearly doubled in strength during the monitoring period, but showed the least relative change when flares occurred in the other peaks.

G359.61–0.24 (Fig. 46). The variations at different features are uncorrelated. The 22.41 km s^{-1} feature initially had a flux density of 118 Jy but has steadily decayed to about 15 Jy at the end of the monitoring period. The 18.37 km s^{-1} feature underwent one flare, but stayed unvarying to within the noise otherwise. The logarithmic scale used of necessity in the time-series plot does not make apparent the very large range in amplitude that occurred in the masers in this

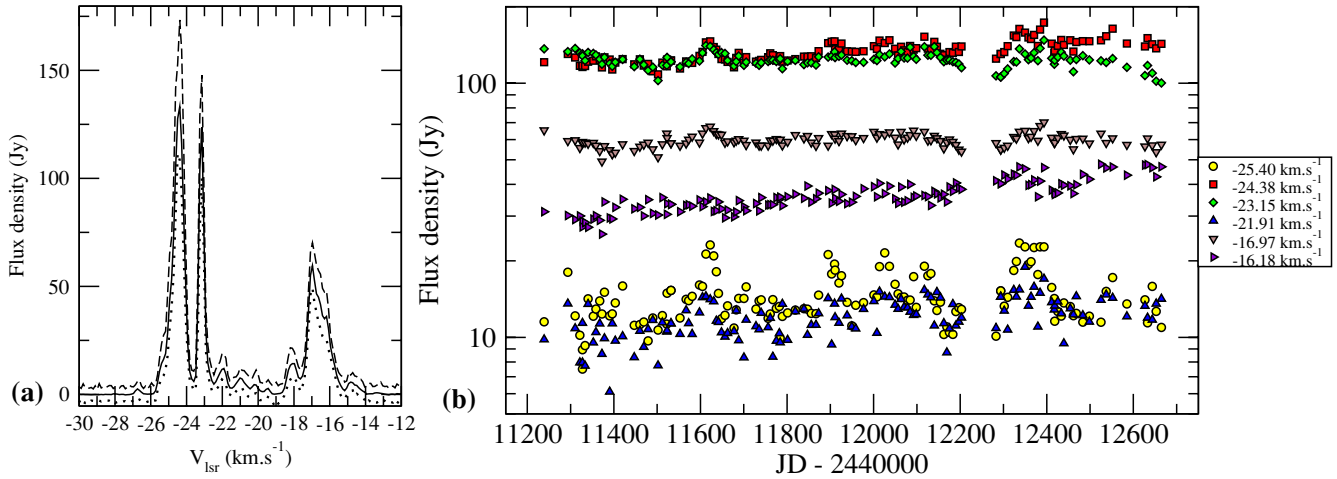

Figure 45. (a) Range of variation in spectrum of G354.61+0.47. The solid, dashed and dotted lines are the averaged spectrum, the upper envelope and the lower envelope, respectively. (b) Time-series for selected velocity channels.

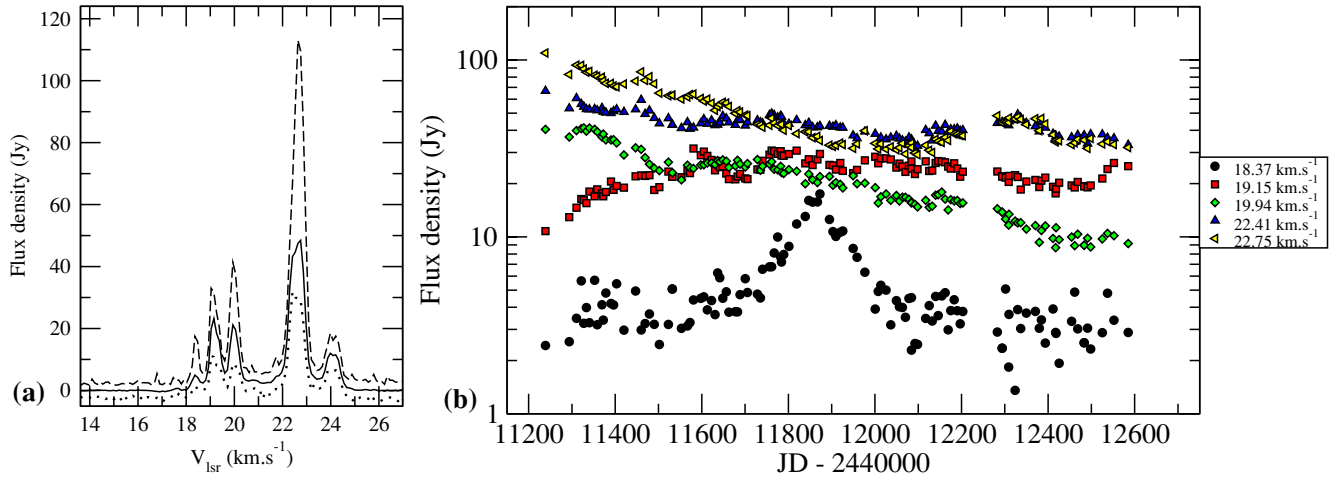

Figure 46. (a) Range of variation in spectrum of G359.61–0.24. The solid, dashed and dotted lines are the averaged spectrum, the upper envelope and the lower envelope, respectively. (b) Time-series for selected velocity channels.

source – it is more evident in the upper and lower envelopes in the plot of the spectrum.

G9.62+0.20 (Figs 47 and 75). The strongest features in the spectrum show periodic flares with a period of 246 d. Data for the first seven flares observed at both 6.7 and 12.2 GHz was presented in Goedhart, Gaylard & van der Walt (2003). A time-delay of ∼30 d can be seen in the flares at 1.21 and −0.14 km s^{-1}. The flares at 1.2 km s^{-1} are simultaneous at 6.7 and 12.2 GHz. This source has been imaged at 6.7 GHz using ATCA (Phillips et al. 1998; Walsh et al. 1998) and at 12.2 GHz using the Very Long Baseline Array (VLBA) (Minier et al. 2000). The close correlation of the flares at 6.7 and 12.2 GHz indicates that the two species of masers are probably spatially coincident. However, the existing low-resolution spot maps at 6.7 GHz show no correspondence to the high-resolution 12.2-GHz maps. The −0.14 km s^{-1} feature is offset from the 1.21 km s^{-1} feature by 90 mas (500 au at 5.7 kpc) in the 12.2-GHz maps. Comparison of the scales of the maps from the ATCA and the VLBA show that low-resolution maps may be misleading if used to interpret time-delays in maser features.

G10.33–0.17 (Fig. 48). This source is moderately variable with the three groups of features in the ranges 4–6, 9–13 and 14–16 km s^{-1} showing different behaviours. The spot maps of Walsh et al. (1998) show three complexes, corresponding to the grouping in velocity. The variability is consistent with the maser groups being in different regions of the star formation complex.

G10.47+0.03/ W31 (Fig. 49). This source exhibits only very gradual variations in the various maser peaks. However, when it was first discovered, Menten (1991) reported a peak flux of 823 Jy, yet the observations of Caswell et al. (1995) show a peak flux of 61 Jy for the 75.07 km s^{-1} feature and it has stayed at ∼30 Jy for the duration of the HartRAO monitoring program.

G12.68–0.18/W33B (Fig. 50). All the maser peaks show quasi-periodic, simultaneous variations with a time-scale of approximately 307 ± 60 d.

G12.89+0.49 (Figs 51 and 77). This source exhibits little variability above the noise except for the 39.27 km s^{-1} feature, which shows evidence of a rapid 'flickering' that has not been fully sampled with our time interval of 1–2 weeks. This variation appears not to be due to calibration errors or noise since a weaker feature at 33.76 km s^{-1} shows no evidence of this behaviour. The maser spots have a complex distribution (Walsh et al. 1998) with most of the maser spots clustered in an area less than 0.2 arcsec in extent.

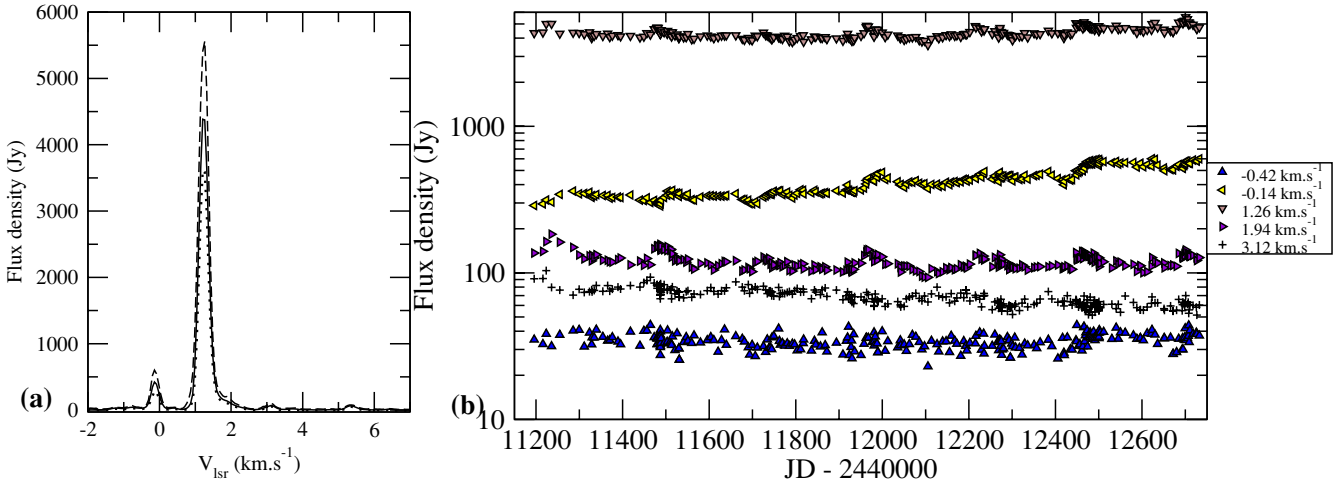

Figure 47. (a) Range of variation in spectrum of G9.62+0.20. The solid, dashed and dotted lines are the averaged spectrum, the upper envelope and the lower envelope, respectively. (b) Time-series for selected velocity channels.

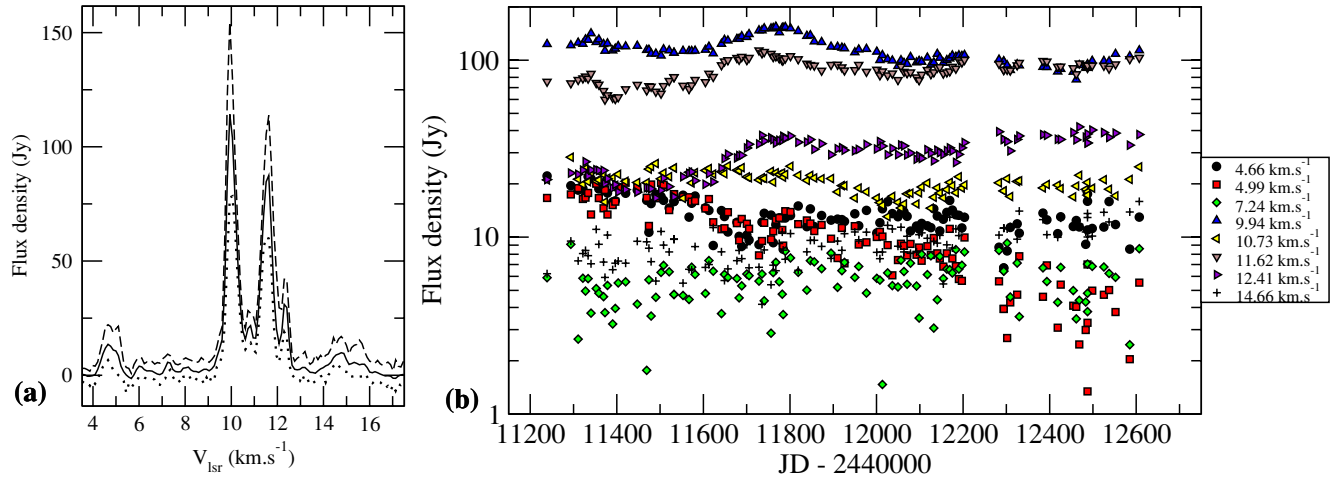

Figure 48. (a) Range of variation in spectrum of G10.33–0.17. The solid, dashed and dotted lines are the averaged spectrum, the upper envelope and the lower envelope, respectively. (b) Time-series for selected velocity channels.

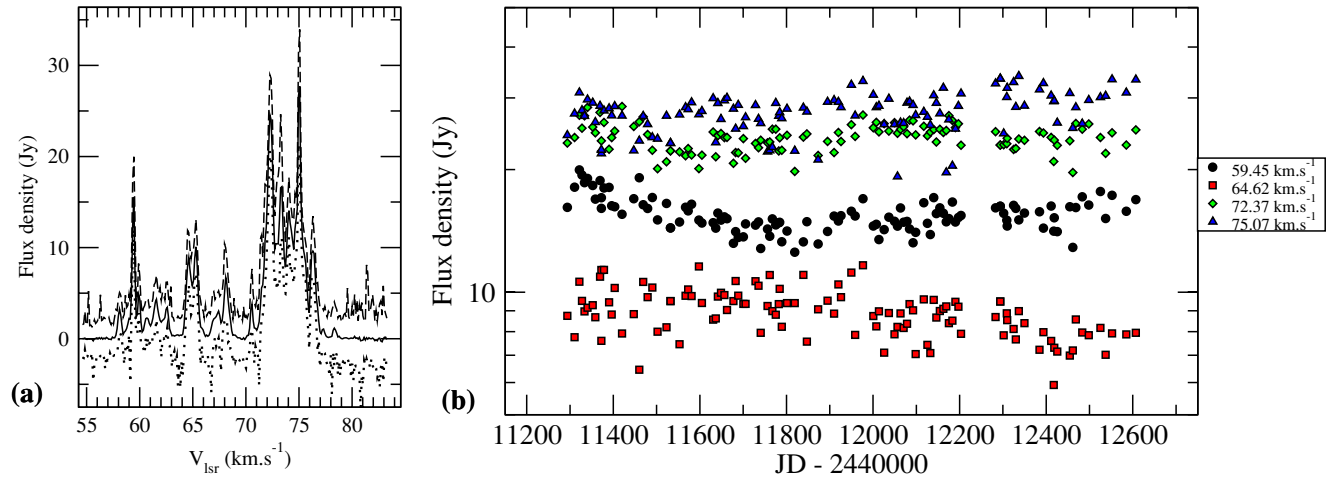

Figure 49. (a) Range of variation in spectrum of G10.47+0.03. The solid, dashed and dotted lines are the averaged spectrum, the upper envelope and the lower envelope, respectively. (b) Time-series for selected velocity channels.

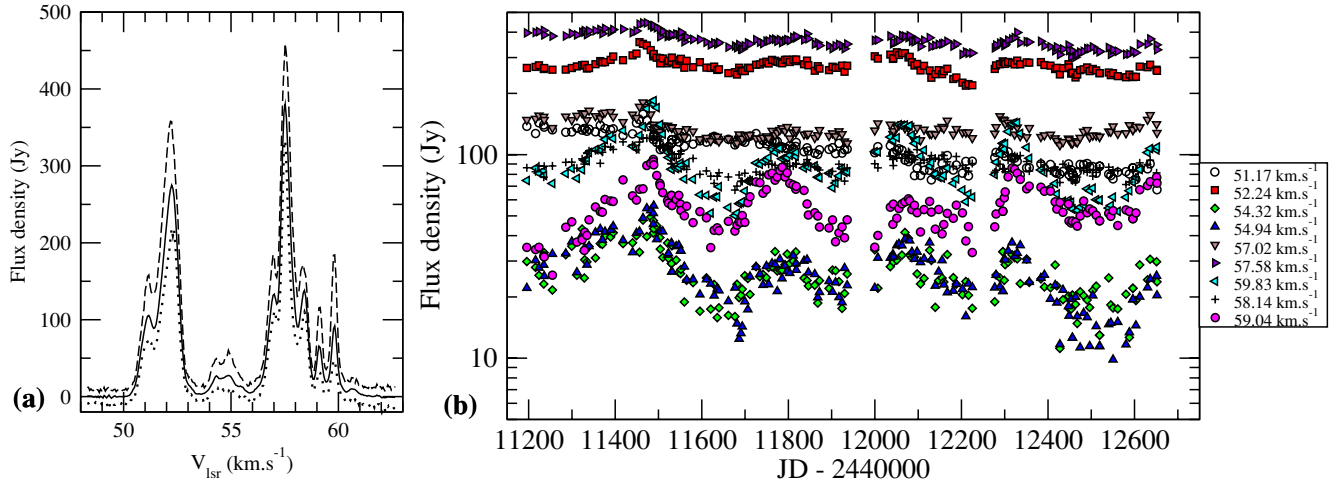

Figure 50. (a) Range of variation in spectrum of G12.68–0.18. The solid, dashed and dotted lines are the averaged spectrum, the upper envelope and the lower envelope, respectively. (b) Time-series for selected velocity channels.

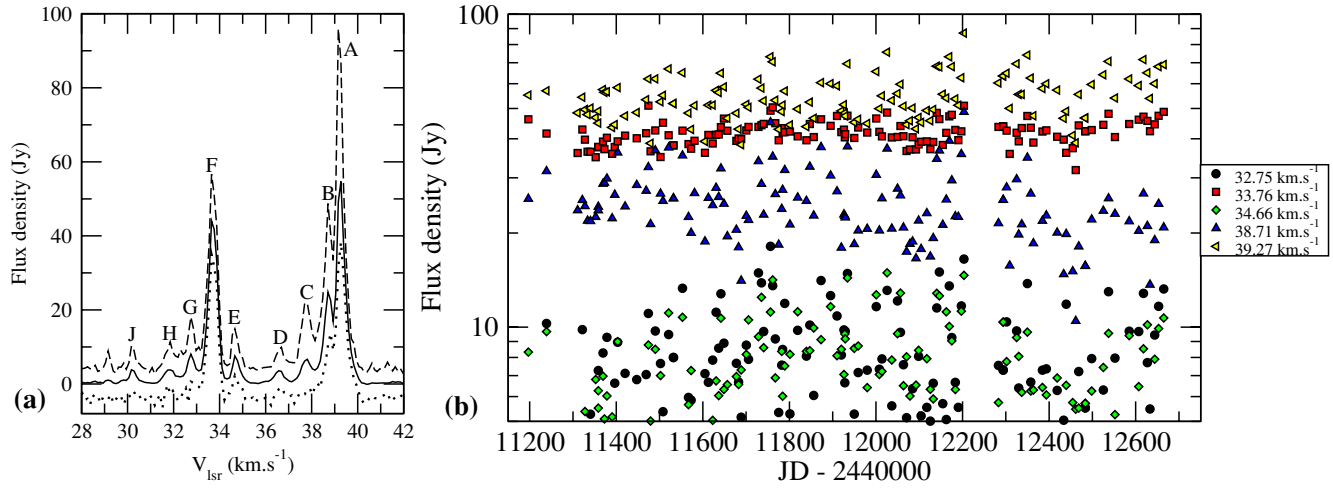

Figure 51. (a) Range of variation in spectrum of G12.89+0.49. The solid, dashed and dotted lines are the averaged spectrum, the upper envelope and the lower envelope, respectively. The spectral features have been labelled following the nomenclature of Walsh et al. (1998). (b) Time-series for selected velocity channels.

The non-varying maser feature is offset by 1.5 arcsec from the main cluster.

G12.91–0.26/W33A (Fig. 52). The two main features at 39.35 and 39.80 km s^{-1} show very little variation. The feature at 35.87 km s^{-1} increased monotonically from 12 to 20 Jy. The features from 35 to 37.5 km s^{-1} are part of a cluster less than 0.1 arcsec in extent (Walsh et al. 1998) but the error on the positions is greater than the extent of the cluster.

G23.01–0.41 (Fig. 53). The dominant features at 74.19, 74.75 and 75.09 km s^{-1} show simultaneous low-amplitude short-term variations, but different long-term trends.

G23.44–0.18 (Fig. 54). This sources shows moderate, uncorrelated variations. The peak at 102.94 km s^{-1} shows slow variations with a time-scale of about 2.5 yr. The 96.64 km s^{-1} feature shows a monotonic increase from 30 to 40 Jy, while the 95.86 km s^{-1} feature was constant at 20 Jy until JD 2452050, then decreased steadily to 8 Jy.

G35.20–1.74 (Fig. 55). The maser peaks show independent long-term changes, but the 100-d long flare peaking at JD 2452060 occurred simultaneously in several of the features. The largest variation was seen in the 43.23 km s^{-1} peak, which initially rose from 35 to ∼100 Jy then decayed monotonically to a level of 5 Jy. The maps of Minier et al. (2000) show two groups of masers with linear structures covering 400 mas (1500 au at 3.4 kpc) but neither have a velocity gradient. The highly variable feature at 43.23 km s^{-1} is not present in the spectrum of the EVN observations in 1997 May. The start of the HartRAO time-series shows this feature slowly increasing strength from a minimum of 35 Jy, so it probably was below the detection limit in 1997.

G45.07+0.13 (Fig. 56). This single-peaked source shows a low amplitude, possible sinusoidal variation. However, the period of the variation would be of the order of four years, with only one cycle observed. A longer time-series is necessary to confirm this trend.

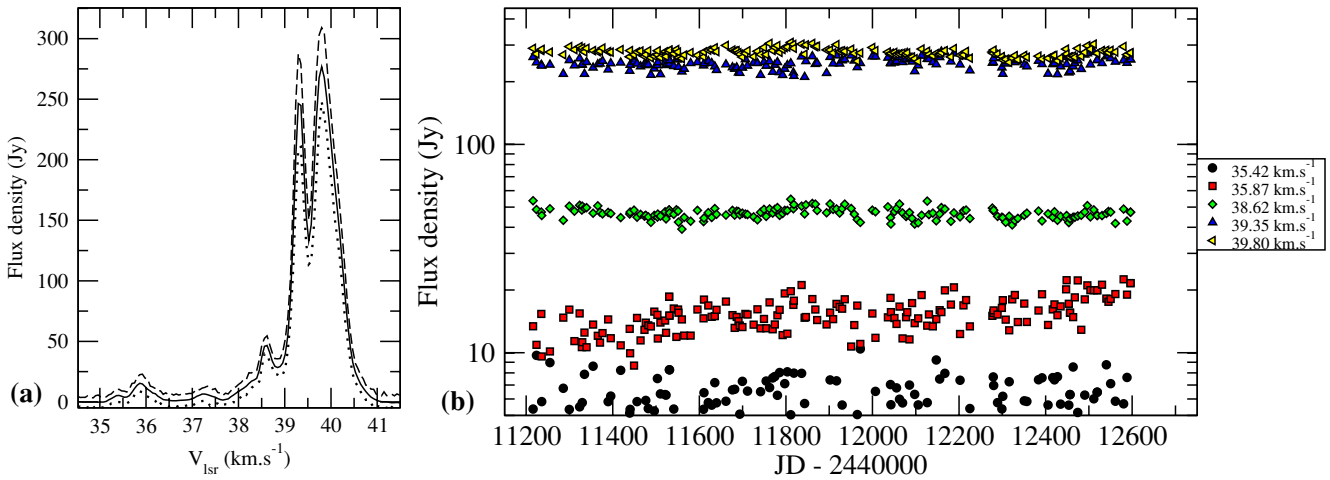

Figure 52. (a) Range of variation in spectrum of G12.91–0.26. The solid, dashed and dotted lines are the averaged spectrum, the upper envelope and the lower envelope, respectively. (b) Time-series for selected velocity channels.

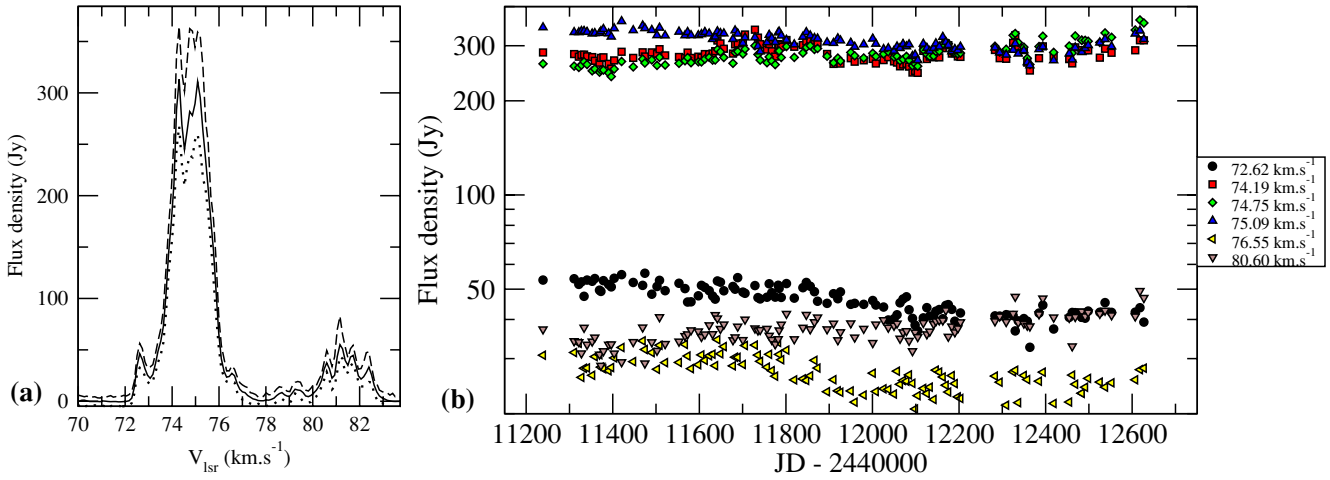

Figure 53. (a) Range of variation in spectrum of G23.01–0.41. The solid, dashed and dotted lines are the averaged spectrum, the upper envelope and the lower envelope, respectively. (b) Time-series for selected velocity channels.

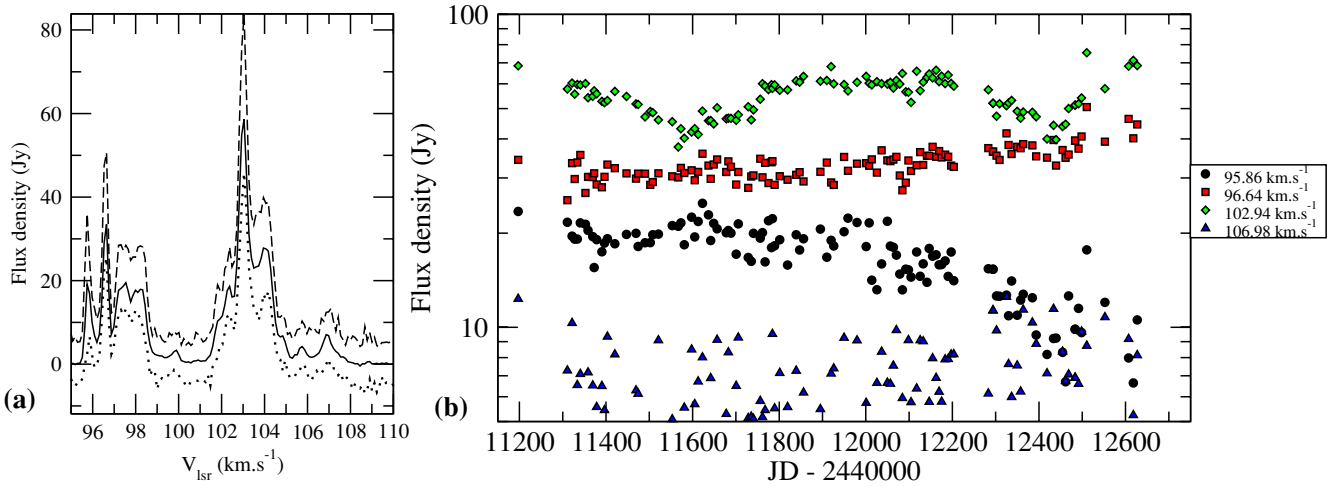

Figure 54. (a) Range of variation in spectrum of G23.44–0.18. The solid, dashed and dotted lines are the averaged spectrum, the upper envelope and the lower envelope, respectively. (b) Time-series for selected velocity channels.

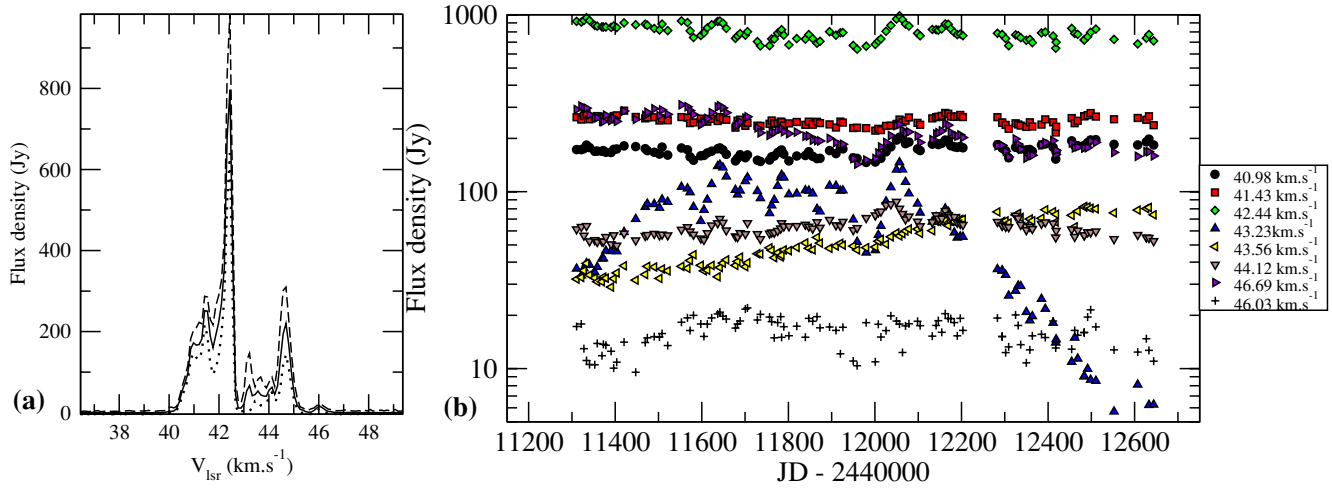

Figure 55. (a) Range of variation in spectrum of G35.20–1.74. The solid, dashed and dotted lines are the averaged spectrum, the upper envelope and the lower envelope, respectively. (b) Time-series for selected velocity channels.

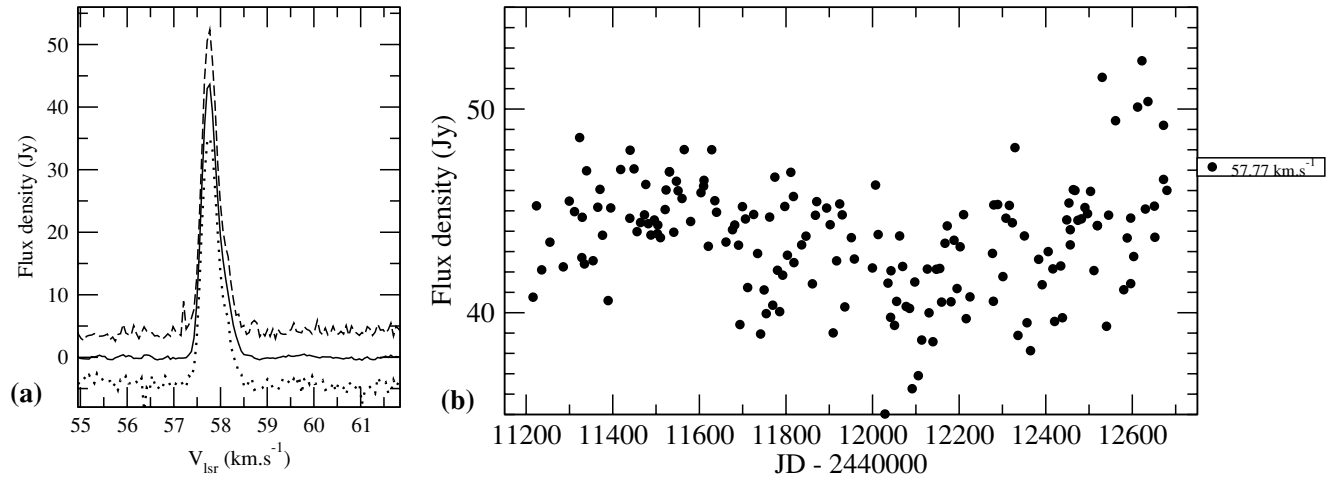

Figure 56. (a) Range of variation in spectrum of G45.07+0.13. The solid, dashed and dotted lines are the averaged spectrum, the upper envelope and the lower envelope, respectively. (b) Time-series for selected velocity channels.

G52.67–1.09 (Fig. 57). This source is moderately variable – sometimes decreasing in flux density until it is below the detection limit, but the S/N is too low to make definitive statements on the nature of the variability.

G59.78+0.06 (Fig. 58). The single feature strong enough for variations to be seen above the noise level has been increasing monotonically in flux density.

G78.12+3.63 (Fig. 59). This source may be variable but the S/N of the observations is too low to be definitive as it was always observed at a low elevation.

G81.88+0.78/W75N (Fig. 60). All of the features show simultaneous irregularly spaced flares with differing amplitudes.

4.3 Summary of results

The most significant result is the discovery of clear periodicity in the time-series of a number of maser sources in the sample. However, all the potential types of behaviour described in the introduction are seen in this sample, as follows.

(i) Non-varying masers are seen in G309.92+0.48, G318.95–0.20, G335.55–0.31, G339.88–1.26, G340.79–0.10, G344.23–0.57, G351.42+0.64 and G12.91–0.26.

(ii) Some maser features show a steady increase in flux density, e.g. in G213.71–12.60, G287.36+0.64, G305.21+0.21, G318.95–0.20, G323.77–0.21, G328.81+0.63, G328.24–0.55, G339.62–0.12, G339.88–1.26, G23.44–0.18, G35.20–1.74 and G59.78+0.06.

(iii) Conversely, a generally steady decrease in brightness occurs in maser features in G291.27–0.71 and G359.61–0.24. A feature in G340.79–0.10 nearly fitted this description, but its decay from 100 to a few Jy may have turned around during the last few hundred days of monitoring. A rapid decline was also seen in a maser in G35.20–1.74, again down to the level of detectability. The asymmetry between the number of maser peaks showing steady increases and those showing steady decreases hints that the growth phase of masers may be long and the decay phase much shorter.

(iv) Variability is seen on all time-scales that could be sampled effectively in this programme, down to the apparent variations in G12.89+0.49 on a time-scale of less than one week.

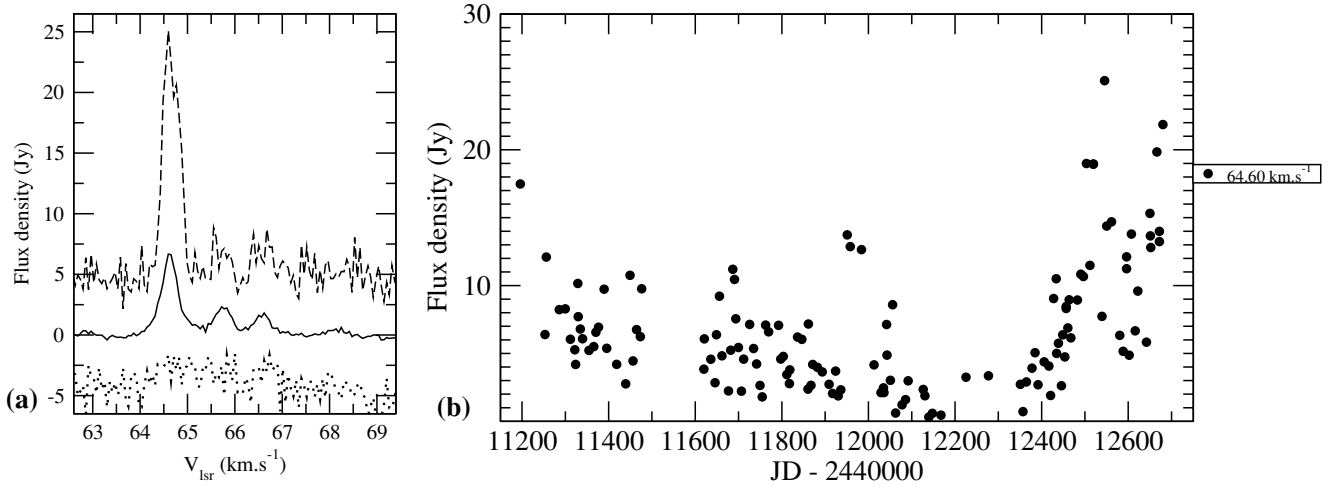

Figure 57. (a) Range of variation in spectrum of G52.67–1.09. The solid, dashed and dotted lines are the averaged spectrum, the upper envelope and the lower envelope, respectively. (b) Time-series for selected velocity channels.

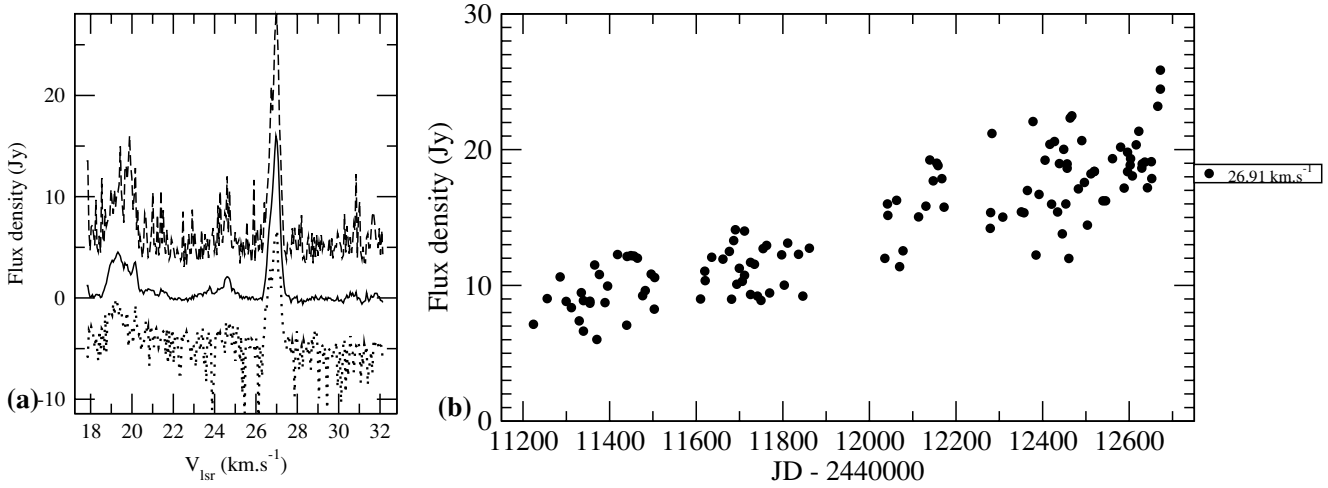

Figure 58. (a) Range of variation in spectrum of G59.78+0.06. The solid, dashed and dotted lines are the averaged spectrum, the upper envelope and the lower envelope, respectively. (b) Time-series for selected velocity channels.

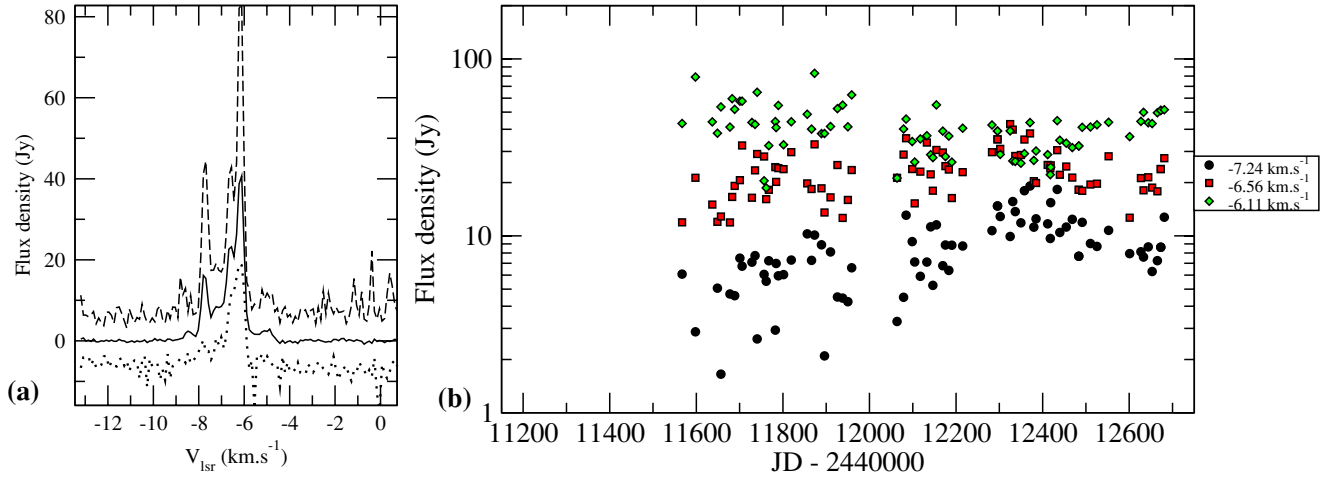

Figure 59. (a) Range of variation in spectrum of G78.12+3.63. The solid, dashed and dotted lines are the averaged spectrum, the upper envelope and the lower envelope, respectively. (b) Time-series for selected velocity channels.

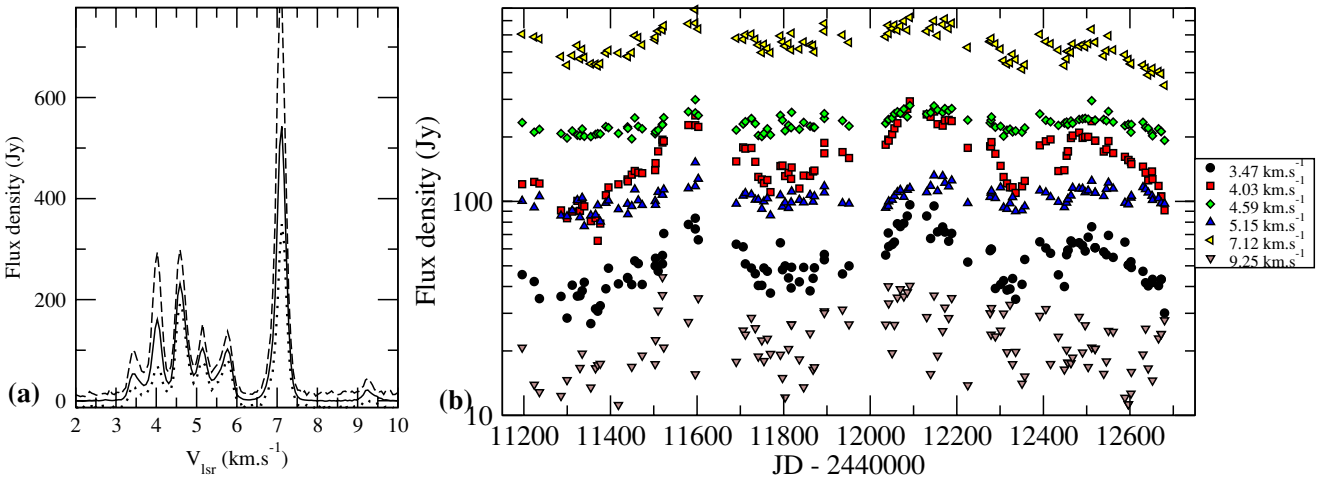

Figure 60. (a) Range of variation in spectrum of G81.88+0.78. The solid, dashed and dotted lines are the averaged spectrum, the upper envelope and the lower envelope, respectively. (b) Time-series for selected velocity channels.

(v) Much of the variability is aperiodic and it may occur independently in individual maser peaks in a given source, or be correlated across a number or all of the peaks. In some cases the variations are delayed by varying amounts in different peaks. Extremely large amplitude flares occur occasionally, the most extreme example being the -5.88 km s^{-1} feature in G351.42+0.64, and variations of a factor of two in brightness are common.

(vi) The majority of sources are significantly variable but show no predictable pattern, e.g. G213.71–12.60, G345.00–0.22 and G10.33–0.17, i.e. are aperiodic. Flares (high amplitude increases in flux density) tend to last between 2–4 months to more than a year. The time between flares ranges from weeks to years.

(vii) In several sources, the intervals between maxima in the variations appear constrained within a limited range, and we label these quasi-periodic variables. Examples are G316.6–0.09 (321 $\pm$ 48 d mean interval between maxima, 3.3 cycles observed), G12.68–0.18 (307 $\pm$ 60 d, 4.9 cycles).

(viii) Variations that appear to be strictly periodic occur in G188.95+0.89 (416 d, 3.5 cycles), G196.45–1.68 (668 d, 2.2 cycles), G328.237–0.548 (216 d, 6.8 cycles), G331.13–0.24 (470 d, 3.1 cycles and 572 d, 2.8 cycles), G338.92–0.06 (132 d, 11.4 cycles), G339.62–0.12 (202 d, 7.5 cycles), G9.62+0.20 (246 d, 6.1 cycles). In the shorter period variables in which a substantial number of cycles have been observed (e.g. 11 in G338.92–0.06), the periodicity is quite unambiguous and the period is well determined. Where only a few cycles have been monitored (e.g. two in G196.45–1.68), the possibility remains that the variations may turn out not to be strictly periodic on longer time-scales, and these may be considered probably periodic. The waveforms exhibited by this set of masers are far from uniform. For G188.95+0.89, and G196.45–1.68, the data are reasonably well modelled by a sinusoid. In G331.13–0.24 the profile is much sharper and resembles a repetitive '$\cup\cup\cup\cup$', while G338.92–0.06 has the inverse waveform, '$\cap\cap\cap\cap$'. In G9.62+0.20 quiescent intervals are punctuated by short, rapidly rising flares that decay more slowly. G328.237–0.548 appears to be intermediate between the waveforms of G331.13–0.24 and G9.62+0.20. However, a detailed analysis of the quasi-periodic and periodic masers is beyond the scope of this paper and will be discussed in Goedhart et al. (in preparation).

(ix) Visual inspection shows velocity shifts in maser peaks (as seen in some water masers) do not occur over a 4-yr time-scale. Where the emission peak does shift in velocity, the repetitive nature of the events, as in G351.78–0.54 and G213.71–12.60, suggest that it is not the maser spots themselves that are changing velocity, as noted in the former case by MacLeod & Gaylard (1996), but is more likely to be due to sequential flaring along a string of masers.

(x) There does not appear to be a correlation between types of maser variability and the linear or complex distributions of the maser spots.

5 DISCUSSION

Caswell et al. (1995) stated that about 75 per cent of the maser features in their survey sample showed no significant variability and even the most variable features did not have very high amplitude variations. They speculated that this implies that the maser gain is not very dependent on changes in the path length. From the results of the HartRAO study, it is clear that methanol maser variability may be more widespread than initially thought; 55 per cent of the 372 maser features analysed have a variability index greater than 0.5, indicating significant variability. As in the Caswell et al. (1995) sample, the ratio of minimum to maximum amplitude for most sources is less than 2, but some sources show spectacular variations with more than a 30-fold increase in flux density (as in the case of G331.13–0.24), or more than 250 times (for G351.42+0.64).

The general level of variability seen in this sample is similar to that seen in hydroxyl masers. They generally show moderate variability on long time-scales Sullivan & Kerstholt (1976), Smits (2003), with some notable exceptions such as S269, where the flux density increased by more than 260 times (Clegg & Cordes 1991; Clegg 1992). However, the remarkable periodic and quasi-periodic variations seen here have not been identified in hydroxyl masers. The behaviour labelled as periodic in several water masers has only been seen on monitoring over decades; periods of the order of a year, as seen in these methanol masers, are not recorded in water masers.

There is little similarity to other behaviour noted in water masers, which show extremely strong outbursts with increases in flux density ranging from 40 per cent to more than 1840 per cent and have gradual changes in velocity (Brand et al. 2003; Hunter et al. 1994; Liljeström et al. 1989). Water maser spectra also tend to change completely over

the years, with some features disappearing completely and new ones appearing. The only methanol maser source that showed this sort of change in its spectral profile was G213.71–12.60 (Mon R2). Interestingly, Smits (2003) reported spectacular flaring in the excited hydroxyl maser in this source, but there is apparently no correlation with the methanol maser variability (D.P. Smits, private communication). The source G351.78–0.54 also displayed high but uncorrelated variability in the main-line hydroxyl and methanol masers (MacLeod & Gaylard 1996). The similarity between the hydroxyl and methanol maser behaviour is consistent with the masers arising in similar regions. However, the lack of correlated variations is significant, as it is believed that the masers are radiatively pumped by the same mechanism (Cragg, Sobolev & Godfrey 2002). It could be that the variations are due to extremely localized changes in path length or density, or there are changes in the level of the seed photons. There is also evidence that hydroxyl masers may be prone to radiative instabilities which lead to short-term variations of the order of minutes or hours (Scappaticci & Watson 1995; Xu et al. 2000). Such rapid variations have not been seen in any of the sources observed from horizon-to-horizon during gain-curve calibration at HartRAO. However, one of the masers features in the source (G12.89+0.49) shows evidence of rapid variations with time-scales less than a week.

The time-scales of variation may shed light on the processes affecting the masers. Short-lived random flares may be due to turbulence in the molecular cloud if these variations are not correlated across different features, or changes in the stellar luminosity if all maser features in the region are affected. It is also possible that short-term correlated variations may be due to interstellar diffraction or refraction. However, interstellar scintillation can only occur when the size of the maser region is similar to the scale size of the density fluctuations in the interstellar medium. If the angular separation between maser spots is larger than the scale size, the variations due to interstellar scintillation would not be correlated between different maser spots.

Longer-lived flares, especially those which cause major changes to the spectral features, as in G213.71–12.60, indicate a far greater disturbance of the medium. These may be caused by outflows or shock waves passing through the masing region. Proper motion studies of 6.7-GHz methanol masers are still in their early stages and insufficient data is available at the moment to support any explanations of observed variability. Studies of maser variability also need to be combined with multiwavelength observations designed to probe the structure of the cloud and find the location of the star exciting the masers. Are the variations linked with outflows? Studies of northern hemisphere sources indicate that outflows can indeed be found towards newly formed massive stars (Beuther et al. 2002). However, the majority of the sources in the HartRAO sample are far south and have not been searched for outflows as yet.

Sometimes correlated variations across several different features can be seen combined with flares restricted to one feature. This indicates that there are changes taking place locally, such as turbulence, as well as more widespread changes. The correlated variations are likely to originate in changes in the radiation coming from the central region, as spatially separated features are unlikely to be affected in exactly the same way by local turbulence. Comparison with existing spotmaps shows that, in general, maser features with separations of less than 0.2 arcsec show correlated variations. The clustering seen in maser features is also consistent with correlated variability. However, it is clear from comparison of ATCA results with those from the EVN and LBA that higher resolution observations are necessary to understand uncorrelated or time-delayed variability. For example, G328.24–0.5 was initially reported by Norris et al. (1993) as being two sources separated by 1 arcmin. Phillips et al. (1998) subsequently resolved the southern source into two clumps on either side of an unresolved H II region and separated by approximately 0.4 arcsec, leading them to believe that the masers were associated with the same H II region. However, the LBA observations of Dodson et al. (2004) lead them to conclude that the two sites are unrelated. This is consistent with the observed variability, where one group of maser features is periodic.

The quasi-periodic masers indicate that there is some mechanism that is driving the variations which is repetitive, but not deterministically so. A possible mechanism might be density waves propagating in the accretion disc assumed to be present at this stage around the forming star (Durisen et al. 2001).

Masers with a strictly periodic variation must be driven by a deterministic mechanism. The possible mechanisms will be discussed in detail in Goedhart, Gaylard & van der Walt (in preparation). The range of periods is not consistent with any known type of pulsating star listed in the General Catalogue of Variable Stars (Kholopov et al. 1985). The infrared pump photons reaching the maser region could be modulated by a disc-outflow system; the simulations of Ouyed, Clarke & Pudritz (2003) show that outflow jets can develop a corkscrew structure or wobbling motion. However, high-resolution multiwavelength observations show no evidence of outflows associated with the periodic source G9.62+0.20E. Most plausible is that the system contains more than one massive object, so that orbital motion of the object(s) around high mass protostar modulates the masers. Such a system could cause modulation in either the pump or the seed photons. The stars in a very young UC H II region would be embedded in an ionized plasma. One or both of the stars could have supersonic velocities relative to the plasma, creating shock waves. Changes in the viewing angle of the shockwave during an orbit could cause periodic modulation of the emission propagated out to the maser region. While this mechanism provides the requisite period, a full explanation needs to account for the variety of waveforms observed, the fact that not all the maser peaks may be modulated with the same period, and that substantial phase lags can occur between different maser peaks.

In summary, this programme has provided four years of monitoring data containing typically 150 data points for each of 369 maser peaks in 54 6.7-GHz methanol masers. Unsuspected behaviour has been discovered in the form of periodic and quasi-periodic variations, and the general level and time-scales of variability has been quantified.

ACKNOWLEDGMENTS

The authors would like to thank all those members of staff at HartRAO who helped with starting up observations after hours.

REFERENCES

Beuther H., Schilke P., Gueth F., McCaughrean M., Andersen M., Sridharan T., Menten K., 2002, A&A, 387, 931

Brand J., Cesaroni R., Comoretto G., Felli M., Palagi F., Palla F., Valdettaro R., 2003, A&A, 407, 573

Caswell J. L., Vaile R. A., Ellingsen S. P., 1995, Pub. Astron. Soc. Aust., 12, 37

Caswell J. L., Vaile R. A., Ellingsen S. P., Whiteoak J. B., Norris R. P., 1995, MNRAS, 272, 96

Clegg A. W., 1992, in Clegg A. W., Nedoluha G. E., eds, Astrophysical Masers. Springer-Verlag, Berlin, p. 279

Clegg A. W., Cordes J. M., 1991, ApJ, 374, 150

Cragg D. M., Sobolev A. M., Godfrey P. D., 2002, MNRAS, 331, 521
Dodson R., Ojha R., Ellingsen S. P., 2004, MNRAS, 351, 779
Durisen R. H., Mejia A. C., Pickett B. K., Hartquist T. W., 2001, ApJ, 563, L157
Goedhart S., Gaylard M. J., van der Walt D. J., 2003, MNRAS, 339, L33
Hunter T. R., Taylor G. B., Felli M., Tofani G., 1994, A&A, 284, 215
Kelley D., 2003, GRI User Manual, available at http://gri.sourceforge.net
Kholopov P. N. et al., 1985, General Catalogue of Variable Stars, 4th edn. Nauka Publishing House, Moscow
Kraus J. D., 1986, Radio Astronomy 2nd edn. Cygnus-Quasar Books, Powell, OH
Lekht E. E., 1974, SvA, 18, 198
Lekht E. E., Krasnov V., 2000, Astron. Lett., 26, 38
Liljeström T., Mattila K., Toriseva M., Anttila R., 1989, A&AS, 79, 19
MacLeod G. C., Gaylard M. J., 1993, in Clegg A. W., Nedoluha G. E., eds, Astrophysical Masers. Springer-Verlag, Heidelberg, p. 195
MacLeod G. C., Gaylard M. J., 1996, MNRAS, 280, 868
Menten K. M., 1991, ApJ, 380, L75
Menten K. M., 2002, in Migenes V., Reid M., eds, Proc. IAU Symp. 206, Cosmic Masers: From Protostars to Black Holes. Astron. Soc. Pac., San Francisco, p. 125
Minier V., Booth R. S., Burton M. G., Pestalozzi M. R., 2002, in Ros E., Porcas R., Lobanov A., Zensus J., eds, Proc. 6th European VLBI Network Symp, New Developments in VLBI Science and Technology. Max-Planck-Institut fuer Radioastronomie, Bonn, p. 205
Minier V., Booth R. S., Conway J. E., 2000, A&A, 362, 1093
Minier V., Ellingsen S. P., Norris R. P., Booth R. S., 2003, A&A, 403, 1095
Moscadelli L., Catarzi M., 1996, A&AS, 116, 211
Norris R. P. et al., 1998, ApJ, 508, 275
Norris R. P., Whiteoak J. B., Caswell J. L., Wieringa M. H., Gough R. G., 1993, ApJ, 412, 222
Ott M., Witzel A., Quirrenbach A., Krichbaum T. P., Standke K. J., Schalinski C. J., Hummel C. A., 1994, A&A, 284, 331
Ouyed R., Clarke D. A., Pudritz R. E., 2003, ApJ, 582, 292
Phillips C. J., Norris R. P., Ellingsen S. P., McCulloch P. M., 1998, MNRAS, 300, 1131
Scappaticci G., Watson W. D., 1995, ApJ, 448, 862
Smits D., 1997, MNRAS, 287, 253
Smits D. P., 2003, MNRAS, 339, 1
Smits D. P., Cohen R. J., Hutawarakorn B., 1998, MNRAS, 296, L11
Stetson P. B., 1996, PASP, 108, 851
Sullivan W. T., Kerstholt J. H., 1976, A&A, 51, 427
Trinidad M. A., Rojas V., Plascencia J. C., Ricalde A., Curiel S., Rodríguez L. F., 2003, Rev. Mex. Astron. Astrofis., 39, 311
van der Walt D. J., Retief S. J. P., Gaylard M. J., MacLeod G. C., 1996, MNRAS, 282, 1085
Walsh A. J., Burton M. G., Hyland A. R., Robinson G., 1998, MNRAS, 301, 640
Weaver H., Dieter N. H., Williams D. R. W., 1968, ApJS, 16, 219
White G. J., MacDonald G. H., 1979, MNRAS, 188, 745
Xu Y., Zheng X. W., Zhang E. J., Yu Z. Y., Han P., Scalise E., Chen Y. J., 2000, A&A, 364, 232

This paper has been typeset from a TEX/LATEX file prepared by the author.